

UNIVERSIDADE DE BRASÍLIA
CAMPUS DE PLANALTINA
PROGRAMA DE PÓS-GRADUAÇÃO EM CIÊNCIAS AMBIENTAIS

João Paulo Sena Souza

**Modelos isotópicos espaciais de nitrogênio do solo nos ecossistemas naturais da
América do Sul**

Planaltina, DF

2019

UNIVERSIDADE DE BRASÍLIA
CAMPUS DE PLANALTINA
PROGRAMA DE PÓS-GRADUAÇÃO EM CIÊNCIAS AMBIENTAIS

João Paulo Sena Souza

**Modelos isotópicos espaciais de nitrogênio do solo nos ecossistemas naturais da
América do Sul**

Tese apresentada ao Programa de Pós-Graduação em Ciências Ambientais da Universidade de Brasília, para a obtenção do título de Doutor em Ciências Ambientais

Orientadora: Prof. Dra. Gabriela Bielefeld Nardoto

Planaltina, DF

2019

**Ficha catalográfica elaborada automaticamente,
com os dados fornecidos pelo(a) autor(a)**

Sm
Sena Souza, João Paulo
Modelos isotópicos espaciais de nitrogênio do solo nos
ecossistemas naturais da América do Sul / João Paulo Sena
Souza; orientador Gabriela Bielefeld Nardoto. -- Brasília,
2019.
126 p.

Tese (Doutorado - Doutorado em Ciências Ambientais) --
Universidade de Brasília, 2019.

1. isótopos estáveis. 2. floresta randômica. 3. issoscape.
4. desnitrificação. 5. lixiviação. I. Bielefeld Nardoto,
Gabriela, orient. II. Título.

UNIVERSIDADE DE BRASÍLIA
CAMPUS DE PLANALTINA
PROGRAMA DE PÓS-GRADUAÇÃO EM CIÊNCIAS AMBIENTAIS

João Paulo Sena Souza

**Modelos isotópicos espaciais de nitrogênio do solo nos ecossistemas naturais da
América do Sul**

Banca Examinadora:

Dra. Gabriela Bielefeld Nardoto / PPG CA – UnB (Presidente/Orientadora)

Dr. Edson Eyji Sano / PPG CA – UnB (Membro titular)

Dra Arminda Moreira de Carvalho / Embrapa – CPAC (Membro titular)

Dr. Jean Pierre Henry Balbaud Ometto / INPE – COCST (Membro titular)

Dr. Luiz Felipe Salemi / PPG CA – UnB (Membro suplente)

Dedico esta tese aos meus pais Fau e Peixão, que sempre me deram apoio para seguir em frente, e à minha esposa Mayanna, que foi minha fortaleza durante todo o doutorado.

Agradecimentos

À minha orientadora, Gabriela Bielefeld Nardoto, pelas orientações certeiras, por me encorajar a encarar novos desafios, pelos conselhos e ensinamentos, pela amizade e pela confiança depositada em mim!

Sempre tive sorte com orientadores, desde o início da minha caminhada acadêmica. Por isso, agradeço a todos eles: Ao Ludgero Vieira, meu primeiro orientador de iniciação científica, por ter me encorajado a seguir neste caminho apenas demonstrando o seu entusiasmo com a ciência e com a natureza. Ao Antônio Felipe, que orientou o meu TCC e seguiu orientando na vida, conseguindo a proeza de me transformar em um ser humano um pouco mais organizado. Ao Éder Martins, que orientou minha dissertação de mestrado, sempre muito sábio e com conversas enriquecedoras sobre tudo. Muito obrigado!

Tive a oportunidade de participar de dois cursos que contribuíram de forma expressiva, ensinando conceitos e técnicas empregadas nesta tese. Portanto, agradeço à todos da *School of Advanced Science on Nitrogen Cycling for Environmental Sustainability and Climate Change*, no nome do coordenador Luiz Antônio Martinelli; e do *Isotopes in Spatial Ecology and Biogeochemistry (SPATIAL)*, no nome do coordenador Gabriel Bowen.

Ao Fábio “Fafá”, ao Kisaka “Kiki”, ao Ray “Raony” e ao Glauber “das Neves” por estarem presentes em cada momento, aconselhando, compartilhando sucessos e fracassos e tornando a caminhada mais fácil e até engracada. Obrigado, amigos!

Aos meus amigos do laboratório, que agora podem trabalhar em paz: Aragonês, Gio, Jeh, Jacaré, Pedrón, Vinícius, Fabão. Obrigado pela convivência!

A todos do projeto Origem: Caparroz, Gislaine, Nina, Cássia, Ju, Soninho, Fabão, Fafá, das Neves, Gabi, Felipe, Vinícius, pelo excelente convívio nas reuniões e parceria nas viagens para coleta de amostras!

À minha esposa Mayanna, pela paciência e confiança e compreensão em tantas viagens de campo, congressos, sanduíche; pelo apoio psicológico, pelo incentivo, pelo companheirismo, pela amizade e pelo amor, que sempre foram combustíveis pra seguir na caminhada!

Ao meu pai Peixão, minha mainha Fau e meu irmão Zé, que sempre me incentivaram e me deram o apoio pra seguir em frente. Obrigado família!

Ao Benjamin Houlton por ter me acolhido com tanta simpatia em Davis, pelas orientações e contribuições para a tese durante o período de doutorado sanduíche; e pelo que tem feito para convencer os políticos do mundo sobre os perigos das mudanças climáticas com tanto entusiasmo.

Ao Programa de Pós-Graduação em Ciências Ambientais da Universidade de Brasília, pelo aperfeiçoamento profissional proporcionado!

A Coordenação de Aperfeiçoamento de Pessoal de Nível Superior (CAPES), pela concessão da bolsa de doutorado e do Programa de Doutorado Sanduíche no Exterior (PDSE).

E a todos que contribuíram direta ou indiretamente para a realização deste trabalho, reitero meu apreço e minha eterna gratidão.

Resumo

O nitrogênio (N) é um elemento limitante da produção primária dos ecossistemas terrestres. Por isso, é importante entender os padrões de perdas de N ao longo dos ecossistemas. Medidas da razão isotópica de nitrogênio ($\delta^{15}\text{N}$) no solo refletem os caminhos dominantes de entradas e saídas de N do sistema terrestre. A abordagem isotópica aparece como uma ferramenta que auxilia a modelagem de emissões e fluxos de N em modelos de balanço de massa. Para ser aplicado em modelos de ciclagem de N, o $\delta^{15}\text{N}$ do solo deve ser representado em modelos isotópicos espaciais (isoscapes). Além de serem fundamentais para modelos de ciclagem de N, isoscapes $\delta^{15}\text{N}$ do solo podem ser usadas em outras áreas, como antropologia, forense e ecologia de comunidades. Entretanto, isoscapes de $\delta^{15}\text{N}$ do solo disponíveis na escala global mascaram alguns padrões regionais do ciclo do N. Novas isoscapes em escala continental devem incorporar mais locais de amostragem e abordagens metodológicas que evidenciem as relações não lineares do $\delta^{15}\text{N}$ com as variáveis preditoras. Neste contexto, o objetivo desta tese de doutorado foi elaborar uma isoscape de $\delta^{15}\text{N}$ do solo em escala continental. A América do Sul foi escolhida como área modelo por apresentar grandes vazios amostrais em modelos globais anteriores e permitir a coleta de novas amostras. Posteriormente, a isoscape de $\delta^{15}\text{N}$ do solo foi testada em um modelo isotópico de balanço de massa para estimar as perdas de N por lixiviação e desnitrificação. No total foram consideradas 278 localidades ao longo de áreas naturais da América do Sul, com dados da literatura e novos dados de campo. Foram usadas variáveis preditoras para representar as condições pedológicas, climáticas e biológicas do ambiente. Além disso, os limites dos biomas e ecorregiões foram inseridos no modelo como variáveis discretas. Três algoritmos de *machine learning* foram testados para o modelo de $\delta^{15}\text{N}$ do solo: *Cubist*, Floresta Randômica (RF) e *Stochastic Gradient Boosting* (GBM). O melhor algoritmo foi escolhido com base na validação cruzada e aplicado na modelagem. Entre os modelos testados, a RF teve a melhor performance ($R^2 = 0,64$). A análise de importância de variável mostrou que o tipo de bioma foi a principal variável para representar a variação espacial de $\delta^{15}\text{N}$ do solo, seguido por carbono orgânico do solo. A amplitude estimada foi de -2,0 ‰ a 14,3 ‰. Os maiores valores se concentraram nas regiões de clima semi-árido e os menores nas regiões mais frias. Os padrões representados na isoscape de $\delta^{15}\text{N}$ do solo se refletiram na variação espacial da proporção do N de entrada que se perde por vias gasosas (f_{gas}). A região com maiores perdas relativas de N gasoso foi a de desertos e arbustos xéricos, seguida pelas florestas tropicais secas e florestas tropicais úmidas. As maiores perdas relativas por lixiviação ocorreram nos ecossistemas de florestas mistas temperadas, florestas de mediterrâneo e nos ecossistemas savânicos tropicais. A partir do modelo de f_{gas} , foram incorporados modelos de entrada de N por fixação biológica de N (FBN) e deposição atmosférica para calcular os fluxos de perdas de N gasoso e por lixiviação. As estimativas de fluxo de N mostraram que $1,3 \pm 1,1 \text{ g N m}^{-2}\text{ano}^{-1}$ é perdido em média pelo processo de desnitrificação nos solos naturais do continente. Perdas por lixiviação foram de $2,5 \pm 1,8 \text{ g N m}^{-2}\text{ano}^{-1}$. Foram estimados valores significativamente menores nas regiões das savanas tropicais e savanas e campos alagados da América do Sul em comparação aos modelos anteriores. Isso é reflexo do aumento da quantidade de pontos representando esses ecossistemas, visto que essas áreas foram sub-amostradas em estudos anteriores em escala global. As relações não-lineares e o uso de variáveis preditoras representando múltiplos fatores de estado dos ecossistemas evidenciaram padrões espaciais de $\delta^{15}\text{N}$ no solo coerentes com as observações empíricas, que ainda não haviam sido representados em modelos globais, principalmente das savanas tropicais.

Palavras-chave: isótopos estáveis; floresta randômica; isoscape; lixiviação; desnitrificação.

Abstract

Nitrogen (N) is a limiting element of the terrestrial ecosystems primary production. Therefore, it is essential to understand the patterns of N losses across ecosystems. The isotopic ratio of nitrogen ($\delta^{15}\text{N}$) in soil samples reflects the dominant paths of N inputs and outputs in the terrestrial system. The isotopic approach appears as a tool to estimate N emissions and fluxes in mass balance models. To be applied in N cycling models, soil $\delta^{15}\text{N}$ must be represented in isotopic landscapes (isoscapes). In addition to being central to N cycling models, Soil $\delta^{15}\text{N}$ isoscapes can be used in other scientific fields such as anthropology, forensics and community ecology. However, soil $\delta^{15}\text{N}$ isoscapes available at a global scale mask some regional patterns of the N cycle. New continental scale isoscapes should incorporate more sampling sites and methodological approaches that highlight nonlinear relationships between $\delta^{15}\text{N}$ and predictor variables. In this context, the objective of this doctoral thesis was to elaborate an isoscape soil $\delta^{15}\text{N}$ at the continental scale. South America was chosen as a model area because it presented large sample voids in previous global compilations and allowed the collection of new samples. Subsequently, the soil $\delta^{15}\text{N}$ isoscope was tested in an isotopic mass balance model to estimate the N losses by leaching and denitrification. In total, 278 geographical locations were considered in South America, with data from the literature and new field samples. The covariates represented the pedological, climatic and biological conditions of the environment. Besides, the biome boundaries and ecoregions were inserted into the model as discrete variables. Three machine learning algorithms were tested for the $\delta^{15}\text{N}$ soil model: Cubist, Random Forest (RF) and Stochastic Gradient Boosting (GBM). The best algorithm was chosen based on the 10-fold cross-validation and applied in the modeling. Among the tested models, RF had the best performance ($R^2 = 0.64$). The importance of variable analysis showed that the biome type was the main variable to represent the spatial variation of $\delta^{15}\text{N}$ of the soil, followed by soil organic carbon. The estimated amplitude was -2.0 ‰ to 14.3 ‰. The highest values are concentrated in semi-arid climate regions and the lowest in the coldest regions. The patterns represented in the isoscape of $\delta^{15}\text{N}$ of the soil were reflected in the spatial variation of the proportion of the incoming N that is lost by gaseous pathways (f_{gas}). The region with the highest relative losses of gaseous N is that of deserts and xeric shrubs, followed by dry tropical forests and humid tropical forests. The highest relative leaching losses occur in the ecosystems of temperate mixed forests and Mediterranean forests; and tropical savanna ecosystems. From the f_{gas} model, N input models were incorporated by biological N fixation (FBN) and atmospheric deposition to calculate the flow losses of gaseous N and by leaching. N flux estimates showed that $1.3 \pm 1.1 \text{ g N m}^{-2}\text{yr}^{-1}$ is lost on average by the denitrification process on the continent's natural soils. Leaching losses are $2.5 \pm 1.8 \text{ g N m}^{-2}\text{yr}^{-1}$. Significantly lower values were estimated in the tropical savannas and grassland savannas and floodplains of South America in comparison to previous models. That pattern is due to the increase in the number of points representing these ecosystems since they were underrepresented in previous studies on a global scale. Nonlinear relationships and the use of predictor variables representing multiple state factors revealed spatial patterns of $\delta^{15}\text{N}$ in soil consistent with empirical observations that had not yet been represented in global models, mainly in tropical savannas.

Keywords: stable isotope; random forest; isoscape; leaching; denitrification.

Sumário

Agradecimentos	vi
Resumo	vii
Abstract	viii
Introdução Geral	11
Objetivos e Estrutura da Tese	18
Resultados e Discussões Gerais	22
Considerações Finais	27
<i>Conclusões</i>	27
<i>Perspectivas Futuras</i>	27
Referências Bibliográficas	29
CAPÍTULO 1 - BACKGROUND AND THE USE OF ISOSCAPES IN THE BRAZILIAN CONTEXT: ESSENTIAL TOOL FOR ISOTOPE DATA INTERPRETATION AND NATURAL RESOURCES MANAGING*	35
Abstract	35
Introduction	36
Methodology	37
Key concepts and methods used in the design of isoscapes	38
<i>Describing stable isotopes and their natural variations</i>	38
<i>Scaling isoscapes</i>	40
<i>Mapping isoscapes</i>	41
Main applications of the isoscapes	43
<i>Water isoscapes</i>	43
<i>Isoscapes on ecosystem ecology approach</i>	43
<i>Isoscapes on animal movement and biological conservation studies</i>	44
<i>Isoscapes on forensic applications</i>	47
Potential use of isoscapes in Brazil	48
<i>Perspectives of using isoscapes in Brazil</i>	49
Synthesis and future	53
References	55
CAPÍTULO 2 - RECONSTRUCTING CONTINENTAL-SCALE VARIATION IN SOIL $\delta^{15}\text{N}$: A MACHINE LEARNING APPROACH IN SOUTH AMERICA*	67
Abstract	67
Introduction	68
Methods	69
<i>Study area and soil $\delta^{15}\text{N}$ dataset</i>	69
<i>Soil sampling and isotopic analysis</i>	70

<i>Auxiliary variables</i>	71
<i>Modelling</i>	72
<i>Spatial prediction of soil $\delta^{15}\text{N}$ isoscape</i>	75
Results	75
<i>Model performances and comparisons</i>	75
<i>Importance of covariates</i>	78
<i>Uncertainty of the model</i>	81
Discussion	83
<i>Source of uncertainty and model performance</i>	83
<i>Soil $\delta^{15}\text{N}$ spatial distribution in South America</i>	83
<i>Applicability of the machine-learning soil $\delta^{15}\text{N}$ isoscape model</i>	86
Literature Cited	87
CAPÍTULO 3 - ESTIMATIVAS DE PERDAS DE NITROGÊNIO POR DESNITRIFICAÇÃO E LIXIVIAÇÃO NOS ECOSISTEMAS NATURAIS DA AMÉRICA DO SUL	92
Resumo	92
Introdução	93
Material e Métodos	95
<i>Área de estudo</i>	95
<i>Abordagem metodológica</i>	96
<i>Evolução do modelo isotópico de balanço de massa</i>	96
<i>Parametrização do modelo</i>	98
<i>Isoscapes de $\delta^{15}\text{N}$ do solo e comparação entre os modelos</i>	98
Resultados	99
<i>Modelo f_{gas}</i>	99
<i>Fluxo de saída de N via lixiviação vs desnitrificação</i>	101
<i>Comparação com abordagens anteriores usando outras isoscapes de $\delta^{15}\text{N}$ do solo</i>	103
Discussão	104
Referências Bibliográficas	107
ANEXO A	111
ANEXO B	118

Introdução Geral

O nitrogênio (N) é um elemento essencial para o funcionamento dos ecossistemas terrestres por ser um dos principais responsáveis pela produtividade primária, afetando toda a teia trófica (LeBauer and Treseder, 2008). O ciclo de N em ecossistemas terrestres é complexo, com diferentes caminhos de entrada (deposição seca e úmida, fixação biológica) e saída (lixiviação, volatilização), além de diferentes processos internos microbiológicos como mineralização, nitrificação e desnitrificação (Galloway et al., 2004; Vitousek et al., 2002). Um dos produtos do processo de desnitrificação é o óxido nitroso (N_2O), que é um gás do efeito estufa (Dalal and Allen, 2008; Galloway et al., 2004). Portanto, o N influencia o sistema climático de forma direta, mas também de forma indireta pelo seu papel central no processo da fotossíntese, que leva ao sequestro e estoque de dióxido de carbono (CO_2).

A desnitrificação é um processo de redução do nitrato (NO_3^-) no solo por grupos específicos de bactérias heterotróficas que ocorrem na grande maioria dos ecossistemas. Essas bactérias usam o NO_3^- como fonte de O_2 na respiração anaeróbica, deixando como produto o N em formas gasosas (Firestone and Davidson, 1989). Em ambientes com níveis muito baixos de O, alguns microorganismos se adaptaram ao uso do nitrito e óxido nitroso como fontes alternativas de O_2 , deixando o N_2 como principal produto da respiração, conforme a seguinte ordem de redução: $NO_3 \rightarrow NO_2 \rightarrow NO \rightarrow N_2O \rightarrow N_2$. Entender essas diferenças de subproduto da desnitrificação nos ambientes é de grande interesse, principalmente porque o NO e N_2O trazem consequências ambientais negativas, enquanto o N_2 é um gás inerte abundante na atmosfera que não causa danos ao funcionamento dos ecossistemas.

Além dos impactos na atmosfera, outras formas reativas de N (Nr: amônia NH_3 ; amônio NH_4^+ ; óxidos de nitrogênio NO_x ; nitrato NO_3^-) podem causar mudanças nos ecossistemas terrestres e aquáticos. O NO_3^- , por exemplo, pode ser perdido dos ecossistemas terrestres, sendo carreado para os corpos d'água no processo de lixiviação. Quando ocorre em excesso, esse processo gera impactos nos ecossistemas aquáticos como eutrofização, poluição da água e mudanças nos padrões de biodiversidade e prejuízos à saúde humana (Galloway et al., 2004; Jones et al., 2014). Portanto, a estimativas sobre a circulação de N entre os biomas globais é de interesse de diversas áreas como

climatologia, biogeoquímica, ecologia, além de tomadores de decisão no processo de gestão de recursos naturais.

As atividades humanas têm causado alterações significativas na ciclagem do N (Galloway et al., 2008). Essas mudanças são causadas principalmente pelas atividades agrícolas que levam a um aumento do Nr nos ecossistemas devido à aplicação de fertilizantes nitrogenados e às monoculturas de espécies de leguminosas fixadoras de N (Galloway et al., 2004). A América Latina se destaca por ter cerca de 25% do Nr global entrando nos seus ecossistemas terrestres, sendo a região com maiores estimativas de fixação biológica de N no mundo (Austin et al., 2013). Somente na América do Sul, seis importantes *hotspots* de conservação da biodiversidade sofrerão com o aumento da deposição de N até o ano 2050: Mata Atlântica, Cerrado, Floresta de Valdívia, Andes Tropical e região de Tumbes-Chacó-Magdalena (Phoenix et al., 2006). No Cerrado, por exemplo, a deposição de N poderá dobrar até 2050 (Phoenix et al., 2006). O papel desses ecossistemas para o balanço de N ainda é pouco estudado em escala regional.

Estimativas globais ajudam a entender o balanço do N e suas consequências sócio-econômicas e ecossistêmicas. Entretanto, a abordagem global pode mascarar aspectos regionais do ciclo de N. Apesar da tendência em se estudar as mudanças do ciclo de N causadas por atividades humanas, a modelagem de N em ecossistemas naturais podem ajudar a entender a resposta desses ecossistemas às mudanças previstas no ciclo de N. Estima-se que solos em ambientes naturais colaboram com uma quantidade pequena na perda de N, comparando com áreas agrícolas (Barton et al., 1999; Denk et al., 2017). No entanto, conhecer o potencial de perdas em áreas naturais pode ajudar a prever as consequências de possíveis mudanças ambientais. Além disso, essas estimativas ajudam a fechar a conta do balanço global de N (Houlton and Bai, 2009).

As principais dificuldades que as estimativas de saídas e entradas de N enfrentam se devem à expressiva variabilidade espacial e temporal que envolve os fatores ambientais causadores das emissões de gases por desnitrificação (Groffman et al., 2009). Portanto, podem ocorrer picos de emissão de gases de N em curtos períodos de tempo (*hot moments*) e/ou locais específicos (*hotspots*) que são difíceis de serem previstos (Groffman et al., 2009; McClain et al., 2003). Estima-se que esses picos de desnitrificação sejam responsáveis por até 80% do total de emissão de N gasoso na escala global (Butterbach-Bahl et al., 2013; Groffman et al., 2009).

Métodos de modelagem espacial surgiram com a finalidade de quantificar o efeito cumulativo dos fatores controladores das perdas de N por vias gasosas e por lixiviação

em grandes escalas (Boyer et al., 2006). A abordagem básica dos principais modelos de N é integrar as condições ambientais favoráveis à desnitrificação, ao invés de simular explicitamente a dinâmica das bactérias desnitrificantes (Boyer et al., 2006). Os modelos de ciclagem de N se encaixam em duas abordagens metodológicas: modelos de simulação e modelos de balanço de massa (Boyer et al., 2006). Os principais modelos de simulação são o DAYCENT (Parton et al., 1998), desnitrificação-decomposição (DNDC) (Li et al., 1992), Carnegie-Ames-Stanford (CASA) (Potter et al., 1996; Wang et al., 2010), *Erosion-Productivity Impact Calculator* (EPIC) (Williams et al. 1984). Esses modelos baseiam-se nas relações entre as variáveis que controlam as taxas de desnitrificação (variáveis climáticas, pedológicas e de uso do solo) e medidas empíricas de experimentos em laboratório ou campo (Boyer et al., 2006). Essas relações são então extrapoladas para nível de ecossistemas ou em escala regional. No entanto, a extração de medidas de emissão de N gasoso em campo ou laboratório para grandes escalas gera erros expressivos que podem prejudicar as estimativas (Butterbach-Bahl et al., 2002; Galloway et al., 2004; Groffman et al., 2009; McClain et al., 2003). Isso ocorre porque as medidas empíricas dificilmente abrangem toda a variabilidade espacial de abrangência do modelo. Além disso, ao elevado número de parâmetros dos modelos de simulação dificulta a aplicação em escala continental ou global devido à falta de variáveis espacialmente explícitas disponíveis (Groffman et al., 2009).

Os modelos de balanço de massa, por sua vez, são baseados no equilíbrio entre as entradas, saídas de N dos ecossistemas. Modelos espaciais de balanço de massa dependem da interação entre modelos secundários independentes de entrada de N (fixação biológica de N, deposição atmosférica, e aplicação de fertilizantes para áreas antrópicas), saídas de N (volatilização de NH₃), e em alguns casos, de estoque de N (solo, vegetação) (Boyer et al., 2006). O principal produto dos modelos de balanço de massa é a estimativa das entradas N em um determinado ecossistema que é perdido via desnitrificação e lixiviação (Houlton et al., 2006; Howarth et al., 1996). Esses modelos são úteis para mostrar a magnitude das taxas de desnitrificação e lixiviação que ocorrem em grandes áreas (Howarth et al., 1996).

Mesmo usando dados com baixa resolução espacial para alimentar os modelos, essa abordagem tem sido eficiente nas estimativas de perdas de N por desnitrificação em diversos ecossistemas terrestres tanto em escala regional (Howarth et al., 1996; van Egmond et al., 2002; Weintraub et al., 2016; Xing and Zhu, 2002; Zheng et al., 2002), quanto em escala global (Bai et al., 2012; Galloway et al., 2004; Houlton and Bai, 2009).

De forma análoga, medidas da razão isotópica de nitrogênio ($\delta^{15}\text{N}$) (ver Box 1) no solo refletem os caminhos dominantes de entrada e saída de N do sistema terrestre (Amundson et al., 2003; Craine et al., 2015a; Handley et al., 1999; Houlton et al., 2015, 2006; Houlton and Bai, 2009; Weintraub et al., 2016). Portanto, a abordagem isotópica aparece como uma ferramenta que auxilia a modelagem de emissões e fluxos de N em modelos de balanço de massa (Hilton et al., 2013; Houlton et al., 2006; Houlton and Bai, 2009; Weintraub et al., 2016).

Neste contexto, Houlton e Bai (2009) propuseram um modelo de balanço de massa que agrega medidas de isótopos estáveis de N para estimar a transferência deste nutriente do solo de ecossistemas naturais para a atmosfera e corpos d'água. Esse modelo foi aprimorado por Bai et al. (2012) com a inclusão da fração de N perdida pela volatilização do NH_3 . A principal vantagem do modelo isotópico de balanço de massa em relação aos tradicionais é a integração implícita dos fatores ambientais que influenciam os caminhos de perdas de N (Bai et al., 2012; Houlton et al., 2015). Além disso, o $\delta^{15}\text{N}$ do solo é relativamente simples de ser medido e pode ser usado como um integrador dos processos do ciclo de N nos ecossistemas (Craine et al., 2015b). Assim, o $\delta^{15}\text{N}$ é apontado como um padrão comum por trás do qual modelos de vários graus de complexidade podem se comunicar uns com os outros (Houlton et al., 2015). Essa abordagem vêm sendo apontada

Box 1. Os Isótopos Estáveis

Isótopos são elementos que ocupam o mesmo lugar na tabela periódica, mas possuem massa atômica diferentes devido ao número maior de nêutrons no seu núcleo. Isótopos estáveis são aqueles que não sofrem decaimento radioativo. O isótopo mais leve é mais comum na natureza em relação ao mais pesado. Moléculas que contém o isótopo mais pesado são discriminadas nos processos e reações químicas. Portanto, o substrato é mais enriquecido com isótopos mais pesados em relação ao produto das reações.

No caso do N do solo, três processos se destacam pela maior discriminação isotópica:

- Nitrificação, que deixa as moléculas de NH_4^+ enriquecidas na formação de NO_3^- .
- Perda de N gasoso: volatilização de NH_3 ; nitrificação ou desnitrificação.
- Absorção do nitrogênio pelos fungos micorrízicos, que preferem o N mais leve.

O valor isotópico de uma amostra é dado na notação delta (δ):

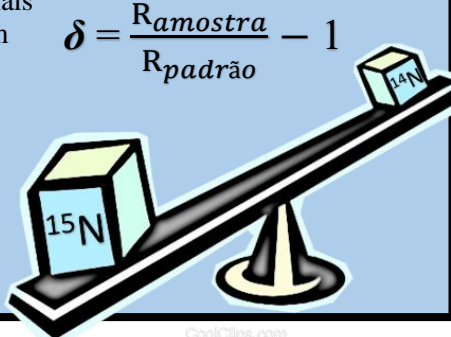
onde o R_{amostra} é a razão entre o isótopo mais raro e o mais comum da amostra; e o $R_{\text{padrão}}$ é a razão isotópica de um padrão internacional estabelecido.

$$R = {}^{15}\text{N}/{}^{14}\text{N}$$

Os valores de delta são muito próximos de zero. Para facilitar a interpretação eles são multiplicados por 1000 e expressos em per mil (‰).

O $R_{\text{padrão}}$ para o $\delta^{15}\text{N}$ é o N atmosférico:

$${}^{15}\text{N}/{}^{14}\text{N} = 0,0036765$$



CoolClips.com

como fundamental para predições de mudanças climáticas globais que devem ser inseridas nos relatórios do IPCC (Houlton et al., 2015).

De modo geral, esses modelos isotópicos de balanço de massa assumem o pressuposto do estado de equilíbrio, onde a quantidade de N que entra no ecossistema é a mesma quantidade que se perde (Bai et al., 2012; Houlton and Bai, 2009). Eles são baseados em modelos isotópicos espaciais de $\delta^{15}\text{N}$ do solo, da vegetação e do N de entrada, além de valores médios do efeito isotópico da lixiviação (ε_L) e da desnitrificação (ε_G) (Bai et al., 2012; Houlton et al., 2006; Houlton and Bai, 2009). Usando essa abordagem, alguns estudos mostram que a desnitrificação é responsável por aproximadamente 1/3 da perda total de N nos ecossistemas naturais em todo o globo, sendo que 71% dessa perda ocorre nas regiões tropicais (Bai et al., 2012).

Os resultados de Bai et al. (2012) foram coerentes com modelos globais anteriores. Porém, no modelo isotópico de balanço de massa, a desnitrificação média global pode ser extremamente sensível ao modelo isotópico espacial de $\delta^{15}\text{N}$ do solo: um aumento de 10% nos valores de $\delta^{15}\text{N}$ do solo resultou em 11.9% de variação na desnitrificação (Bai et al., 2012). Portanto, a precisão do modelo de balanço de massa com dados isotópicos depende diretamente da acurácia do modelo isotópico espacial utilizado.

Modelos isotópicos espaciais são denominados *isoscape* na literatura internacional (do inglês *isotopic* + *landscape*, ou paisagem isotópica). O conceito de isoscape surgiu da necessidade de sistematizar as abordagens de distribuição espacial e temporal da complexidade por trás do fracionamento isotópico, agregando conceitos de geoestatística e biogeoquímica (Bowen, 2010). A aplicação dessa abordagem no mapeamento dos valores de $\delta^{15}\text{N}$ para compreender a ciclagem de N ainda é pouco explorada. A isoscape de Amundson et al. (2003) é a mais utilizada em modelos de grandes escalas espaciais (Houlton et al., 2015; Vitousek et al., 2013). Essa isoscape foi elaborada a partir de regressões simples entre dados empíricos de $\delta^{15}\text{N}$ do solo – com falhas de representatividade espacial – e dados de média anual de precipitação (MAP) e média anual de temperatura (MAT) (Amundson et al., 2003). Usar apenas variáveis climáticas como *proxy* para o mapeamento de $\delta^{15}\text{N}$ do solo era coerente enquanto ainda não existiam modelos de variáveis pedológicas espacialmente explícitas disponíveis.

Embora a influência das variáveis climáticas no $\delta^{15}\text{N}$ do solo em grandes escalas tenha sido amplamente documentada para a escala global (Amundson et al., 2003; Handley et al., 1999; Martinelli et al., 1999), estudos mais recentes demonstram que essa relação é indireta (Craine et al., 2015a). Como já visto, os fatores climáticos exercem

influência direta nas condições que favorecem os diferentes caminhos pelos quais o N é perdido dos ecossistemas terrestres. A dinâmica da matéria orgânica do solo (MOS) e o tamanho das partículas do solo também estão relacionados aos valores de $\delta^{15}\text{N}$ do solo e são diretamente influenciados pelo clima (Craine et al., 2015b; Liao et al., 2006; Scott Bechtold and Naiman, 2006). De modo geral, valores de $\delta^{15}\text{N}$ da matéria orgânica associada aos minerais (MOM), mais estável, são maiores que os da matéria orgânica particulada (MOP) (Conen et al., 2008). Isso ocorre porque conforme aumenta o grau de decomposição da MOS, diminui a quantidade de carbono; e as moléculas de N que ficam no substrato da decomposição são enriquecidas em ^{15}N . Craine et al. (2015) argumentaram que em ambientes quentes e/ou secos, existe uma proporção maior de MOM em relação à MOP presente no solo, o que ajuda a explicar os maiores valores de $\delta^{15}\text{N}$ nesses ambientes. Portanto, o teor de carbono no solo aparece como uma covariável importante para a modelagem de $\delta^{15}\text{N}$ do solo (Craine et al., 2015b).

Ainda que essa abordagem geral seja eficiente para mostrar padrões de variação global, ela apresenta inconsistências na representação dos padrões regionais de $\delta^{15}\text{N}$ do solo (Chen et al., 2018; Cheng et al., 2009; Freitas et al., 2010). Isso ocorre, em parte, devido à falta de pontos amostrais em alguns ecossistemas importantes. Esse é o caso das savanas tropicais, que são sub-representadas espacialmente tanto na compilação de dados mais antiga (Amundson et al., 2003), quanto na mais recente (Craine et al., 2015a). Esses modelos generalistas acarretaram um viés na modelagem global, que atribuiu valores elevados de $\delta^{15}\text{N}$ para esses ecossistemas.

Independentemente da relação de $\delta^{15}\text{N}$ com variáveis climáticas ser direta ou indireta, MAP tende a apresentar uma relação inversa com o $\delta^{15}\text{N}$ na escala global, acentuada principalmente pelos valores elevados nas regiões de clima semi-árido (Freitas et al., 2010; Wang et al., 2013), e pelo padrão espacial de $\delta^{15}\text{N}$ do solo encontrado em florestas tropicais, onde a correlação negativa é explícita (Houlton et al., 2006; Nardoto et al., 2014). Seguindo essa lógica, regiões savânicas que apresentam valores intermediários de MAP (1000 mm a 1800 mm), entre regiões de semi-árido (300 mm a 800 mm) e de florestas tropicais (2000 mm a 5000 mm), deveriam apresentar valores de $\delta^{15}\text{N}$ do solo entre os valores encontrados nos dois outros biomas. Porém, este padrão não se confirma nas observações empíricas em ambientes de savanas tropicais, onde os valores de $\delta^{15}\text{N}$ do solo são significativamente menores em comparação com o semi-árido e as florestas tropicais (Bustamante et al., 2004; Freitas et al., 2010; Nardoto et al., 2014). Esses padrões sugerem que a escala espacial de análise tem um impacto em como os

padrões serão modelados. Por essa razão, modelos de emissões de N gasoso que se basearam no modelo de $\delta^{15}\text{N}$ do solo de Amundson et al. (2003) podem ter superestimado a quantidade de desnitrificação em algumas regiões.

Para superar essas limitações, novas isoscapes de $\delta^{15}\text{N}$ do solo devem incorporar mais covariáveis e evidenciar características regionais do ciclo do N (Pardo and Nadelhoffer, 2010). Uma maneira de considerar essas características é inserir limites de ecossistemas regionais como biomas ou ecorregiões no mapeamento. Algumas metodologias permitem incorporar variáveis contínuas e discretas na mesma análise espacial. Dentro do espectro metodológico das isoscapes, regressões regionalizadas e krigagem com média local variando seriam alternativas viáveis (Terzer et al., 2013). Terzer et al. (2013) realizaram regressões regionalizadas a partir das variáveis climáticas para elaborar isoscapes globais e continentais de $\delta^2\text{H}$ e $\delta^{18}\text{O}$ da precipitação. Contudo, o mapeamento do $\delta^{15}\text{N}$ do solo é mais complexo devido à influência de variáveis pedológicas.

Atualmente, estão disponíveis novos modelos globais de variáveis pedológicas, como textura do solo e teor de C orgânico, de alta resolução espacial (250 m) (Hengl et al., 2017). Novas isoscapes do solo podem, inclusive, se apropriar de métodos usados no mapeamento digital de solos (MDS). Nesse sentido, a abordagem *machine learning* vem sendo usada como uma alternativa robusta que permite a integração de variáveis discretas, como limites de biomas, e contínuas no MDS (Gomes et al., 2019; Hengl et al., 2017). Entre os algoritmos de *machine learning* mais usados no MDS, métodos baseados em árvore de regressão têm apresentado resultados mais precisos em comparação com redes neurais e modelos lineares (Bataille et al., 2018; Gomes et al., 2019; Hengl et al., 2017). Bataille et al. (2018) aplicaram essa abordagem para criar uma isoscape de Sr no continente europeu e mostrou que entre os algoritmos de *machine learning*, a floresta randômica teve a melhor performance, com o menor erro e o maior coeficiente de correlação entre os valores observados e preditos.

Neste contexto, é imperativo o uso desses novos algoritmos e modelos espaciais no mapeamento de isoscapes de $\delta^{15}\text{N}$ do solo. Os benefícios dessas novas isoscapes mais robustas vão além da aplicação em modelos de ciclagem de N. Estudos utilizam isoscapes de $\delta^{15}\text{N}$ para rastrear movimento de animais (Garcia-Perez and Hobson, 2014; Hobson et al., 2012) e até mesmo estudos forenses como origem de drogas ilegais apreendidas, devido à incorporação dos valores isotópicos do ambiente de origem nos tecido biológicos desse material (Mallette et al., 2016). Pelo mesmo princípio de incorporação do $\delta^{15}\text{N}$ do

ambiente nos tecidos biológicos, isoscapes de $\delta^{15}\text{N}$ do solo podem ser usadas para entender os padrões espaciais da dieta humana (Nardoto et al., no prelo). Portanto, uma isoscape de $\delta^{15}\text{N}$ do solo em escala continental é de interesse de diversas áreas do conhecimento.

Objetivos e Estrutura da Tese

O objetivo desta tese de doutorado foi elaborar um modelo isotópico espacial de nitrogênio no solo para América do Sul. Para isso, realizamos três estudos que compõem esta tese de doutorado (Figura 0.1). Cada um desses estudos tem um papel fundamental para a conclusão do trabalho. Embora eles sejam interdependentes, os estudos podem ser lidos separadamente, pois foram escritos em forma de artigo para posterior publicação em revistas científicas. O primeiro estudo representa a etapa de contextualização e apresenta lacunas do conhecimento, as principais metodologias, e as aplicações dos modelos isotópicos espaciais. O segundo estudo é a etapa de criação, onde um novo modelo isotópico é criado a partir da adaptação de métodos e análise de novos dados. O terceiro estudo corresponde à etapa de aplicação, quando a isoscape criada no estudo anterior é usada para aperfeiçoar modelos já existentes que, embora aplicado para América do Sul, gera informação de interesse global.

No **capítulo 1** foi feita uma revisão da literatura sobre modelos isotópicos

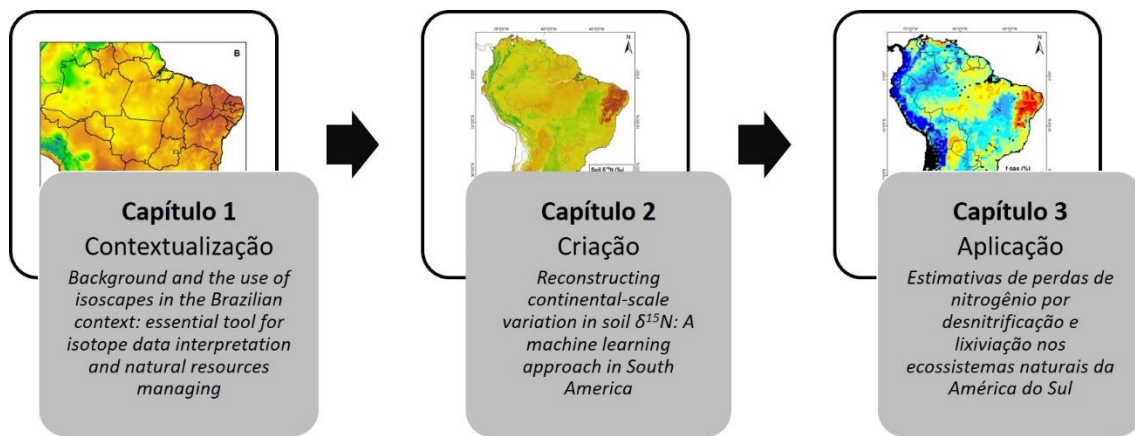


Figura 0.1. Estrutura da tese.

espaciais (isoscapes). O objetivo da revisão foi explorar os conceitos chaves e métodos usados para elaborar isoscapes, apresentando explicações sobre os mecanismos por trás da distribuição espacial dos isótopos estáveis, os maiores problemas relacionados com a definição da escala e as metodologias usadas nas modelagens. Dentro do escopo desta

tese, o capítulo 1 serve como base conceitual e identificação do contexto científico no qual este trabalho se insere.

Este estudo foi realizado por meio de um levantamento bibliográfico usando a base do *Web of Science*. A palavra “isoscap*” foi usada como termo indexador na busca. Essa busca abrangeu o período de 2006 até 2018, visto que o termo isoscape surgiu para a ciência no ano de 2006. Entretanto, antes desse período já existiam modelos isotópicos espaciais relevantes para a revisão. Por isso, uma segunda busca foi realizada com base nas listas de referências bibliográficas dos estudos encontrados na primeira parte. Os artigos encontrados foram separados em quatro grandes áreas de aplicação: ciclo hidrológico, abordagem ecossistêmica (ciclos biogeoquímicos), migração de animais e estudos forenses. Na tentativa de identificar abordagens metodológicas usadas para mapear outros isótopos estáveis, a busca não ficou restrita ao $\delta^{15}\text{N}$. Além disso, possíveis aplicações futuras dos resultados desta tese podem envolver a abordagem multi-isotópica, principalmente em estudos sobre migração de animais e forenses. Portanto, a pesquisa englobou isoscapes de $\delta^2\text{H}$, $\delta^{18}\text{O}$, $\delta^{13}\text{C}$ e $\delta^{15}\text{N}$. Por fim, a revisão aponta para aplicações no contexto brasileiro.

No **capítulo 2**, novas abordagens metodológicas foram usadas para gerar um modelo isotópico espacial de $\delta^{15}\text{N}$ do solo mais acurado usando dados da literatura em conjunto com novas amostras coletadas no campo (Figura 0.2). O objetivo foi elaborar uma isoscape de $\delta^{15}\text{N}$ do solo para América do Sul aplicando a abordagem de *machine learning* e novas variáveis preditoras espacialmente explícitas. Esta nova isoscape mostrou a distribuição espacial de $\delta^{15}\text{N}$ do solo em escala continental, e foi capaz de mapear os principais padrões espaciais em escala regional.

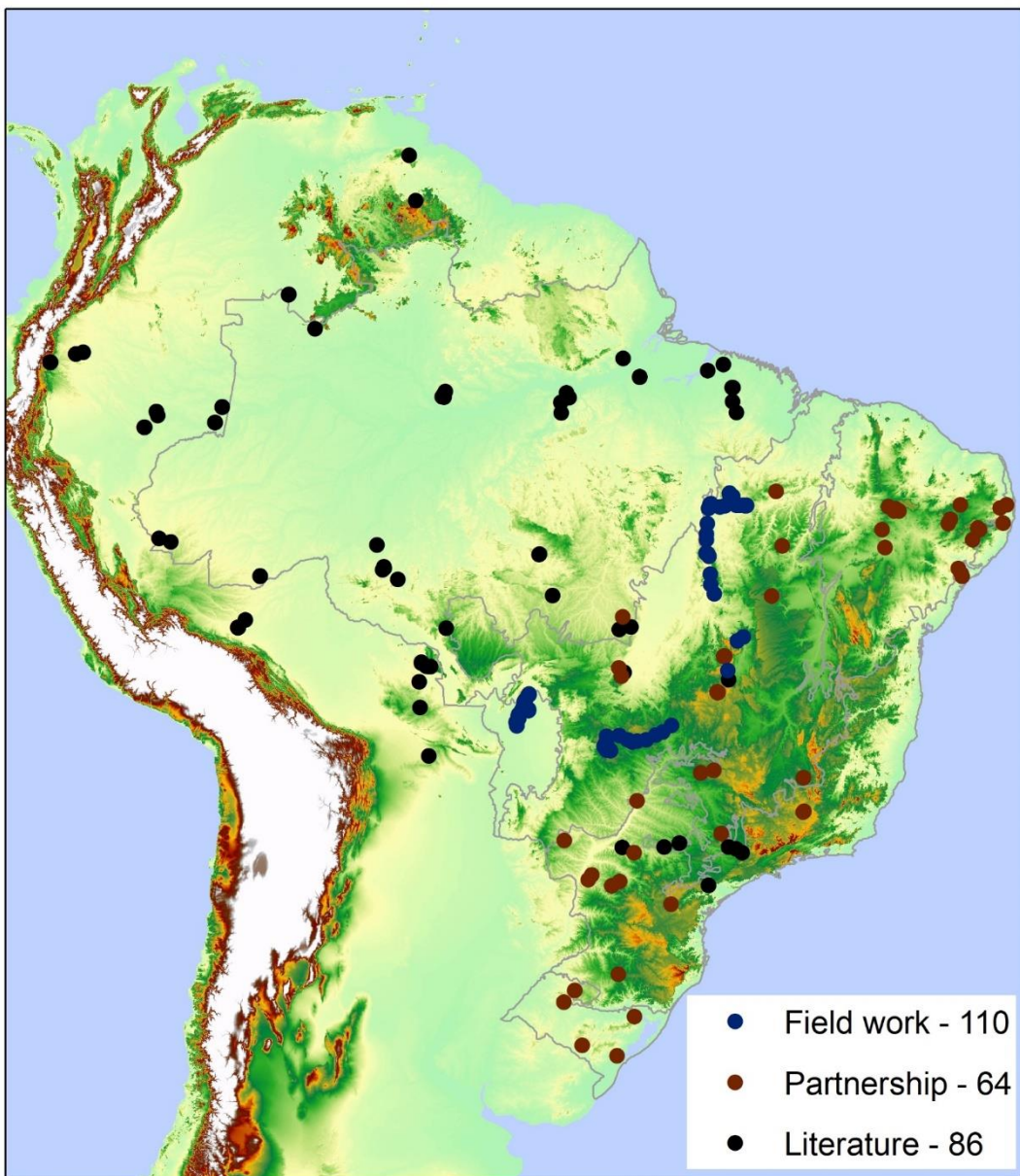


Figura 0.2. Distribuição espacial da localização geográfica dos dados usados neste estudo: círculos pretos representam dados da literatura; círculos marrons são dados de colaborações e parcerias de pesquisa; círculos azuis representam os locais amostrados nos trabalhos de campo realizados para este estudo.

Para isso foram compiladas informações georreferenciadas de $\delta^{15}\text{N}$ do solo publicadas na literatura científica. Foram identificadas áreas sub-representadas nos trabalhos anteriores onde foram coletadas novas amostras de solo, principalmente nas regiões do bioma Cerrado e Pantanal. As novas amostras foram coletadas em fragmentos de vegetação natural ao longo das estradas e em unidades de conservação (Figura 0.3).

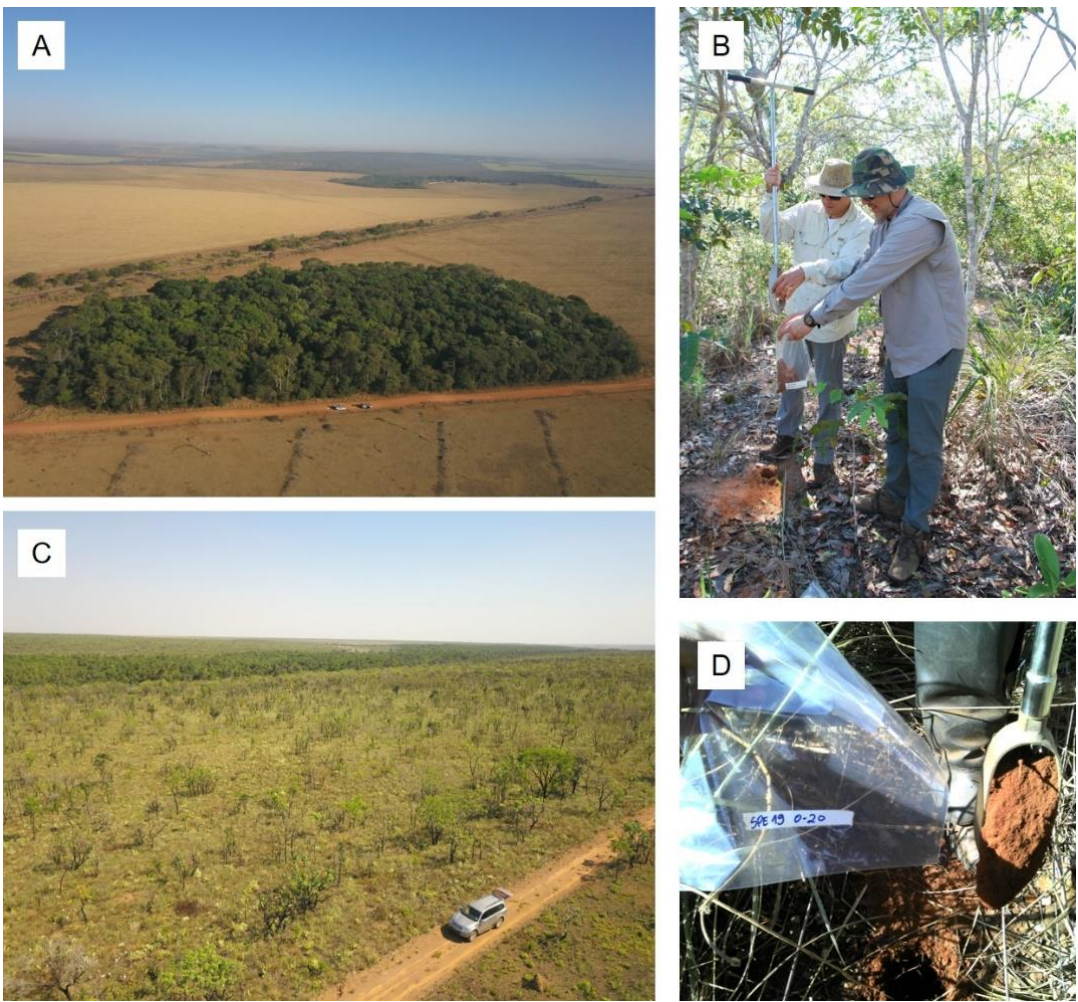


Figura 0.3. Trabalho de coleta de novas amostras de solo para preencher lacunas espaciais na região central do Brasil. A) Visão aérea de um fragmento de vegetação natural no estado de Goiás, onde uma amostra foi coletada; B) Processo de coleta de uma amostra de solo usando um trado holandês; C) Visão aérea de uma área do Parque Nacional das Emas, onde diversas amostras foram coletadas; D) Identificação de uma das amostras de solo coletadas.

Foi utilizado um total de 278 pontos distribuídos em sete países e sete biomas da América do Sul. Como variáveis preditoras, foram usadas variáveis climáticas (média anual de precipitação, temperatura, índice de aridez e potencial de evapotranspiração), pedológicas (densidade aparente, carbono orgânico, capacidade de troca catiônica, pH, teor de argila, silte e areia), biológica (produção primária líquida) e altitude. Além disso, foram inseridos nas análises os limites dos biomas e ecorregiões como variáveis discretas. Os valores de cada covariável foram extraídos para cada ponto para formar a matriz de regressão. Apenas 80% dos pontos foram usado na modelagem. O restante foi usado para a validação do modelo. Foram testados três algoritmos de *machine learning*: floresta

randômica, *gradient boosting machine* e *cubist*. O melhor entre os três modelos testados foi o de floresta randômica, usada na predição final da isoscape de $\delta^{15}\text{N}$ do solo.

O **capítulo 3** é a parte final da tese, onde o modelo isotópico espacial gerado no capítulo 2 foi aplicado para estimar perdas de N dos ecossistemas naturais da América do Sul. O objetivo deste capítulo foi estimar as perdas de N por vias gasosas, base para a modelagem dos fluxos de perda N gasoso e dissolvido. Para isso, a isoscape de $\delta^{15}\text{N}$ do solo criada no capítulo 2 foi aplicada ao modelo isotópico de balanço de massa de Bai et al. (2012). Esperou-se encontrar diferenças significativas entre os resultados do modelo baseado na isoscape de Amundson et al. (2003) e os resultados do modelo gerado pela isoscape desta tese, principalmente nos biomas onde houve ampliação da base de dados de $\delta^{15}\text{N}$.

Para isso, foram usados modelos de fixação biológica de N (FBN) e deposição atmosférica de N para o continente para representar o total de entrada de N nos ecossistemas naturais. Posteriormente, foi calculada a fração de N perdida por vias gasosas (f_{gas}) com base nos modelos de $\delta^{15}\text{N}$ do solo e de entrada e no efeito do fracionamento isotópico da desnitrificação, lixiviação e volatilização da amônia. A partir desta etapa os fluxos de perdas de N por vias gasosas e por lixiviação foram calculados. Na sequência, todo o procedimento metodológico foi repetido, desta vez usando outra isoscape de $\delta^{15}\text{N}$ do solo (Amundson et al. 2003), para posterior comparação entre os resultados das duas abordagens.

Resultados e Discussões Gerais

No **capítulo 1**, os principais conceitos e aplicações de isoscapes foram discutidos, e os principais desafios para a elaboração desses modelos no Brasil foram levantados. As isoscapes são elaboradas nas mais variadas escalas espaciais ao redor do mundo. Nas escalas global e continental, a maior parte dos modelos de isoscapes está relacionada aos isótopos da água (^2H e ^{18}O) (Bowen e Revenaugh 2003; Terzer et al. 2013). Isso ocorre porque a distribuição geográfica do $\delta^2\text{H}$ e do $\delta^{18}\text{O}$ da precipitação é controlada basicamente pela evaporação da água do oceano e circulação atmosférica do vapor d'água, tornando os gradientes isotópicos mais fáceis de serem identificados em comparação com outros isótopos estáveis. Esses modelos são usados principalmente nos estudos sobre os padrões globais e regionais de precipitação. Além disso, os padrões latitudinais bem definidos e o efeito da continentalidade tornam as isoscapes de $\delta^2\text{H}$ e

$\delta^{18}\text{O}$ úteis em estudos forenses, principalmente na detecção de origem geográfica de animais e objetos (Bowen and West 2008).

Em relação ao $\delta^{13}\text{C}$, o principal processo que define seu fracionamento é o caminho fotossintético das plantas. Plantas C₄ discriminam menos o isótopo mais pesado em comparação com as plantas C₃, deixando os valores de $\delta^{13}\text{C}$ do primeiro grupo maiores (~ -12‰) e os do segundo grupo menores (~ -28‰). Esses valores são incorporados em toda a teia trófica e na decomposição da matéria orgânica do solo, facilitando o uso de isoscapes de $\delta^{13}\text{C}$ como marcadores da fonte de alimento dos consumidores e da fonte de matéria orgânica do solo. Além disso, isoscapes de $\delta^{13}\text{C}$ em escala global refletem as alterações nas emissões de CO₂ para a atmosfera.

Ao contrário dos outros isótopos estáveis estudados, não é apenas um mecanismo ou processo responsável pela variação espacial do $\delta^{15}\text{N}$. Os isótopos estáveis de N sofrem fracionamento em quase todos os níveis do complexo ciclo do N (Robinson, 2001). Devido a essa complexidade, isoscapes de $\delta^{15}\text{N}$ são mais difíceis de serem elaboradas. Apenas dois modelos globais de isoscapes foram elaborados (Amundson et al., 2003; Houlton et al., 2015). Apesar de não apresentar um mapa de isoscape, Craine et al. (2015) mostraram como os valores de $\delta^{15}\text{N}$ do solo estão distribuídos nos gradientes climáticos do planeta e os mecanismos que podem estar influenciando esse padrão. Essas informações são base para outras isoscapes de $\delta^{15}\text{N}$. Esses modelos podem ser aplicados em estudos forenses em conjunto com isoscapes de outros elementos (Hobson et al., 2012). Em escalas locais e regionais, isoscapes de $\delta^{15}\text{N}$ são importantes para o estudo dos ciclos biogeoquímicos dos ecossistemas (Weintraub et al., 2016).

Não existem trabalhos que utilizam explicitamente a abordagem de isoscapes no Brasil, embora muitos estudos utilizem os padrões espaciais de isótopos estáveis para resolver problemas científicos. Considerando o contexto apresentado, este capítulo tem potencial para embasar futuras pesquisas que utilizam padrões espaciais de isótopos estáveis nos biomas brasileiros. Além disso, oferece perspectivas de trabalhos futuros utilizando essa metodologia.

No **capítulo 2**, três algoritmos de *machine learning* foram testados para a modelagem de $\delta^{15}\text{N}$. O algoritmo de floresta randômica (RF) teve a melhor performance entre os modelos testados depois da validação cruzada ($R^2 = 0,64$) em comparação com *cubist* ($R^2 = 0,61$) e *gradient boosting machine* ($R^2 = 0,60$). RF também apresentou a melhor na comparação do RMSE e MAE. RF também foi a melhor performance entre modelos testados em outros estudos com abordagem semelhante (Bataille et al., 2018;

Gomes et al., 2019; Hengl et al., 2017). Com relação aos dados de validação (20% do banco de dados que não foram usados no modelo), os valores de $\delta^{15}\text{N}$ preditos pela RF explicaram 62% dos valores observados. Os valores de R^2 semelhantes entre a validação cruzada e os dados de validação indicam que o modelo é confiável. Além disso, não houve autocorrelação espacial nos resíduos entre os dados observados e preditos (Moran's index = -0.02; P -value = 0.77).

O algoritmo de floresta randômica (RF) teve a melhor performance entre os modelos testados depois da validação cruzada ($R^2 = 0,64$) em comparação com *cubist* ($R^2 = 0,61$) e *gradient boosting machine* ($R^2 = 0,60$). RF também foi melhor na comparação do RMSE e MAE. RF também foi a melhor performance entre modelos testados em outros estudos com abordagem semelhante (Bataille et al., 2018; Gomes et al., 2019; Hengl et al., 2017). Com relação aos dados de validação (20% do banco de dados), os valores de $\delta^{15}\text{N}$ preditos pela RF explicaram 62% dos valores observados. Os valores de R^2 semelhantes entre a validação cruzada e os dados de validação indicam que o modelo é confiável.

Entre as variáveis preditoras, os limites dos biomas foi a que mais explicou a variação espacial de $\delta^{15}\text{N}$ do solo na América do Sul, seguida por carbono orgânico do solo e precipitação. A grande influência dos limites dos biomas na variação espacial de $\delta^{15}\text{N}$ do solo ocorreu devido à concentração de valores máximos e mínimos dos dados observados dentro de biomas específicos. O algoritmo de RF permite avaliar a dependência parcial da variável alvo com as variáveis contínuas. Para o carbono orgânico do solo, houve uma correlação negativa, com os maiores valores de $\delta^{15}\text{N}$ do solo correspondendo às menores quantidades de carbono no solo. Observou-se uma queda abrupta nos valores de $\delta^{15}\text{N}$ do solo entre 0 e 25 g kg⁻¹ de carbono orgânico. A tendência negativa foi muito menor entre 25 e 100 g kg⁻¹ de carbono orgânico. A queda volta a ser acentuada com os maiores quantidades de carbono orgânico no solo (100 e 150 g kg⁻¹). A análise de dependência parcial também mostrou que baixos valores de MAP estão relacionados com um maior $\delta^{15}\text{N}$ do solo, seguindo uma tendência de correlação negativa até 1100 mm de precipitação. Entre 1100 mm e 1900 mm, os valores preditos de $\delta^{15}\text{N}$ do solo foram muito menores; há ainda uma tendência parcial de correlação positiva entre $\delta^{15}\text{N}$ do solo e MAP entre 1300 mm e 1900 mm. Depois disso, a tendência volta a ser negativa e os valores preditos voltam a ser elevados.

Os maiores valores de $\delta^{15}\text{N}$ do solo ($11,9\text{‰} \pm 3,6$) foram modelados na região nordeste do Brasil, correspondente ao clima semi-árido da Caatinga. Esses padrões são

consistentes com o padrão de déficit hídrico e elevado pH no solo, que favorece perdas gasosas em detrimento das perdas por lixiviação, deixando o solo enriquecido em $\delta^{15}\text{N}$ (Högberg, 1997). A inclusão dos limites dos biomas foi, portanto, um fator crucial para o aumento da amplitude dos valores de $\delta^{15}\text{N}$ do solo em comparação com modelos globais anteriores (Amundson et al. 2003). Entre os demais biomas, as florestas tropicais úmidas apresentaram a segunda maior média de $\delta^{15}\text{N}$ do solo no modelo ($7,4\text{‰} \pm 2,0$), seguido pelas florestas tropicais secas ($6,8\text{‰} \pm 1,9$). Nas áreas de florestas tropicais úmidas, o modelo identificou um gradiente regional de aumento dos valores de $\delta^{15}\text{N}$ do solo com a diminuição de MAP. Esse padrão já havia sido reportado em observações empíricas (Nardoto et al., 2014, 2008).

As áreas de savanas tropicais e savanas e campos alagados apresentaram valores intermediários de $\delta^{15}\text{N}$, de $5,5\text{‰} \pm 1,6$ e $5,0\text{‰} \pm 1,4$, respectivamente. Esses valores baixos em comparação com outros ecossistemas tropicais ocorrem porque as savanas da América do Sul têm uma baixa disponibilidade de N comparado com as florestas tropicais, com um déficit hídrico menor que os da região de semi-árido. As áreas de Cerrado, por exemplo, têm uma baixa taxa de decomposição, mineralização líquida de N, e alta produção em NH_4^+ , o que deixa o solo com baixos valores de $\delta^{15}\text{N}$ (Bustamante et al., 2004). Os menores valores foram modelados nas regiões de clima temperado: florestas mistas temperadas ($1,1\text{‰} \pm 3,0$); e campos e savanas temperados ($3,4\text{‰} \pm 2,6$). Nos ecossistemas temperados as taxas de decomposição da matéria orgânica presente no solo são baixas, o que inibe as perdas de N por vias gasosas, reduzindo o fracionamento isotópico no solo e deixando os valores de $\delta^{15}\text{N}$ baixos (Martinelli et al., 1999).

No **capítulo 3**, o modelo elaborado com base na isoscape de $\delta^{15}\text{N}$ do solo do capítulo 2 indicou que 32,4% do N que entra nos ecossistemas terrestres não fertilizados da América do Sul voltam para a atmosfera via desnitrificação a cada ano. A fração de perdas por desnitrificação modelada para a América do Sul (32,4%) foi semelhante aos 35% encontrados por Bai et al. (2012) para a escala global. Os resultados também concordam com o padrão encontrado por Houlton e Bai (2009), que apontaram uma perda de aproximadamente 1/3 do N por desnitrificação de volta para a atmosfera. Entretanto, a amplitude de perdas por desnitrificação (f_{gas}) encontrada nesse estudo (0% a 84%) foi maior que a mapeada por Bai et al. (2012) (0% a 69%).

Na região nordeste do continente, de clima semi-árido, 60,5% ($\pm 15,5\%$) do N é perdido por vias gasosas. Por outro lado, nas regiões de florestas mistas temperadas, esse valor é de apenas 11,2% ($\pm 7,1\%$). Nas áreas de clima temperado, o caminho de saída de

N predominante é a lixiviação. Nestas regiões, a baixa temperatura provavelmente é um fator limitante da decomposição da matéria orgânica, o que deixa o solo com baixa quantidade de nitrato, limitando assim a desnitrificação na maior parte do ano (Seitzinger et al., 2006). Por isso, as perdas por desnitrificação ficam restritas, abaixo de 20%. A região de campos e savanas alagadas teve um f_{gas} médio calculado em 28,6% ($\pm 4,6\%$). Esses valores indicam que aproximadamente 71 % do N que entra na região de savanas alagadas via deposição ou fixação biológica de N é perdido como N dissolvido. Esse padrão foi semelhante ao modelado para as áreas de savanas tropicais, onde 27,7% ($\pm 6,4\%$) do N volta para a atmosfera via desnitrificação, e para os campos de clima temperado (28,8% $\pm 7,1\%$).

Nas regiões de floresta tropical úmida, a fração gasosa das perdas de N foi 32,9% ($\pm 9,3\%$) (Figura 3). Esse padrão situa-se entre aqueles encontrados por Houlton et al. (2006) nas florestas tropicais úmidas do Havaí, de 24% a 53%. Weintraub et al. (2016) estimaram uma amplitude de 10% a 60% de perdas gasosas por desnitrificação em uma área de floresta tropical úmida de montanha na Costa Rica. Nas áreas baixas de florestas tropicais úmidas este valor é estimado entre 14% e 32%, dependendo do efeito do fracionamento do modelo (Soper et al., 2018).

A partir do modelo de f_{gas} , foi possível estimar o fluxo de N gasoso, considerando os modelos de FBN e deposição atmosférica (Bai et al. 2012). As estimativas do modelo deste estudo mostraram que $1,3 \pm 1,1 \text{ g N m}^{-2}\text{ano}^{-1}$ é perdido em média para atmosfera pelo processo de desnitrificação nos ecossistemas terrestres não fertilizados da América do Sul. O modelo de fluxo de saída de N por lixiviação mostrou que $2,5 \pm 1,8 \text{ g N m}^{-2}\text{ano}^{-1}$ ¹ sai dos ecossistemas terrestres naturais da área de estudo como compostos de N dissolvido. As estimativas de fluxo de perda de N serviram para mostrar os padrões espaciais do efeito cumulativo da desnitrificação em cada bioma.

A comparação entre o modelo de fluxo de N deste estudo com o de Bai et al. (2012) teve como objetivo apontar a importância e as inconsistências decorrentes da precisão da isoscape de $\delta^{15}\text{N}$ do solo. Entre os principais ecossistemas testados, a área de desertos e arbustos xéricos foi a única na qual o modelo apresentado neste estudo teve valores significativamente maiores que os valores de desnitrificação de Bai et al. (2012) (teste de Wilcoxon; $W = 41958$, $p < 0,01$) (Figura 5). As áreas de florestas tropicais úmidas e florestas tropicais secas tiveram valores modelados menores que a abordagem de Bai et al. (2012) ($W = 3146400$, $p < 0,001$; $W = 104140$, $p < 0,01$, respectivamente). Entretanto, as maiores diferenças entre os dois modelos se encontram nos ecossistemas

de savanas tropicais ($W = 273890$, $p < 0,001$) e nos campos e savanas alagadas ($W = 1576$, $p < 0,001$). Em ambos os ecossistemas os valores médios das perdas de N por atividade microbiológica foram significativamente inferiores ao modelo usado na comparação (Figura 5).

Ao incorporar a nova isoscape de $\delta^{15}\text{N}$ do solo para a América do sul no modelo de Bai et al. (2012), aumentando a base de dados empíricos coletados em áreas com déficit de amostragem na América do Sul e usando relações não lineares de $\delta^{15}\text{N}$ do solo e múltiplas covariáveis climáticas, pedológicas e biofísicas (Sena-Souza et al., 2019 em revisão – ver capítulo 2), reforça a importância da precisão dos modelos de entrada na interpretação dos resultados do modelo final.

Considerações Finais

Conclusões

A abordagem de isoscape foi fundamental para entender os padrões espaciais do ciclo do N na América do Sul. A inclusão de novos dados evidenciou padrões não lineares de distribuição espacial de $\delta^{15}\text{N}$ no solo que ainda não haviam sido apontados em modelos na escala continental. A abordagem de *machine learning* aplicada mostrou ter grande potencial para ser usada na modelagem espacial de $\delta^{15}\text{N}$ em ecossistemas terrestres. Além disso, um dos principais avanços deste estudo foi mostrar a importância dos limites de ecossistemas regionais como biomas no mapeamento de $\delta^{15}\text{N}$ do solo. As relações não-lineares e o uso de variáveis preditoras representando múltiplos fatores de estado dos ecossistemas permitiram o mapeamento do $\delta^{15}\text{N}$ no solo com padrões coerentes com as observações empíricas. Isso levou a um avanço significativo, principalmente nas áreas de savanas tropicais da América do Sul, antes sub-representadas nas modelagens globais de $\delta^{15}\text{N}$ no solo. Além disso, o modelo de $\delta^{15}\text{N}$ no solo foi eficiente para indicar o padrão de variação espacial dos fluxos de perdas de N por vias gasosas e de lixiviação na América do Sul.

Perspectivas Futuras

Considerando os avanços apontados pelo uso de *machine learning* no mapeamento do $\delta^{15}\text{N}$ no solo, essa abordagem deve ser ampliada para a escala global. Essa ampliação já é possível, uma vez que todas as variáveis preditoras usadas neste estudo estão disponíveis para toda a biosfera terrestre. Entretanto, antes desse esforço, é

recomendado que haja uma prospecção de áreas com déficit de amostragem entre os ecossistemas. Com isso, parcerias internacionais podem ser criadas para preencher as lacunas espaciais identificadas. Um mapeamento mais preciso refinado do $\delta^{15}\text{N}$ no solo na escala global deve contribuir de forma mais eficiente com estudos de projeções de mudanças climáticas e mudanças ambientais globais causadas pelas mudanças no ciclo do N. Isso porque essa abordagem permitirá a realização de estimativas de perdas de N por desnitificação e lixiviação total na escala global a partir do modelo isotópico de balanço de massa. Com isso, será possível estimar o papel das áreas naturais no balanço global do N.

A partir das estimativas de f_{gas} geradas com a isoscape do presente estudo, foi possível calcular o fluxo de saída de N por desnitificação e lixiviação para cada pixel do modelo. Entretanto, novos modelos espaciais de FBN e deposição atmosférica de N também devem ser elaborados com dados atualizados e com uma resolução espacial mais detalhada. A disponibilização de novos modelos de entradas de N nos ecossistemas terrestres será essencial na melhoria das estimativas de fluxos de N para a atmosfera e para os corpos d'água. O próximo passo para o modelo de fluxo de N por desnitificação será a aplicação do submodelo que separa o fluxo de gás total em fluxo de NO, N_2O e N_2 . Esse modelo foi proposto por Bai et al. (2012) e depende apenas de informação espacialmente explícita sobre o espaço do solo preenchido por água (WFPS%). Essa abordagem permitirá estimar a forma preferencial na qual o N é perdido em cada ecossistema, possibilitando ainda inserir o aspecto temporal das emissões.

A abordagem metodológica usada demonstrou um potencial em evidenciar padrões regionais na distribuição espacial de $\delta^{15}\text{N}$ no solo. Isso foi visto principalmente no gradiente identificado nas florestas tropicais. Portanto, os resultados apresentados aqui podem ser detalhados para a escala local e regional. Futuros trabalhos podem se aprofundar nas relações não lineares entre o $\delta^{15}\text{N}$ no solo e os fatores de estado de ecossistemas específicos, como o Cerrado e o Pantanal. No capítulo 1, um dos desafios apontados é o desenvolvimento de isoscapes regionais e locais no Brasil. Existe o potencial de ampliar o banco de dados de $\delta^{15}\text{N}$ no solo do Brasil, considerando não apenas áreas naturais, mas também áreas agrícolas e pastagens. Isso permitirá a elaboração de isoscapes mais detalhadas levando a modelos mais robustos do ciclo de N no Brasil. Consequentemente, os modelos auxiliarão na elaboração de políticas públicas para a mitigação e diminuição dos problemas causados pela alteração da cobertura vegetal,

aplicação de fertilizantes nitrogenados e deposição de N. Além disso, estas isoscapes mais detalhadas poderão ser usadas em estudos ecológicos, antropológicos e forenses.

Referências Bibliográficas

- Amundson, R., Austin, A.T., Schuur, E.A.G., Yoo, K., Matzek, V., Kendall, C., Uebersax, A., Brenner, D., Baisden, W.T., 2003. Global patterns of the isotopic composition of soil and plant nitrogen. *Global Biogeochem. Cycles* 17, 31/1-31/10. <https://doi.org/10.1029/2002GB001903>
- Austin, A.T., Bustamante, M.M.C., Nardoto, G.B., Mitre, S.K., Pérez, T., Ometto, J.P.H.B., Ascarrunz, N.L., Forti, M.C., Longo, K., Gavito, M.E., Martinelli, L. a, 2013. Latin America ' s Nitrogen Challenge. *Science* (80-.). 340, 149. <https://doi.org/10.1126/science.1231679>
- Bai, E., Houlton, B.Z., Wang, Y.P., 2012. Isotopic identification of nitrogen hotspots across natural terrestrial ecosystems. *Biogeosciences* 9, 3287–3304. <https://doi.org/10.5194/bg-9-3287-2012>
- Barton, L., McLay, C.D.A., Schipper, L.A., Smith, C.T., 1999. Annual denitrification rates in agricultural and forest soils: a review. *Aust. J. Soils Res.* 37, 1073–1093.
- Bataille, C.P., von Holstein, I.C.C., Laffoon, J.E., Willmes, M., Liu, X.M., Davies, G.R., 2018. A bioavailable strontium isotope for Western Europe: A machine learning approach. *PLoS One* 13, 1–27. <https://doi.org/10.1371/journal.pone.0197386>
- Bowen, G.J., 2010. Isoscapes : Spatial Pattern in Isotopic Biogeochemistry. *Annu. Rev. Earth Planet. Sci.* 161–187. <https://doi.org/10.1146/annurev-earth-040809-152429>
- Bowen, G.J., Revenaugh, J., 2003. Interpolating the isotopic composition of modern meteoric precipitation. *Water Resour. Res.* 39, 1–13. <https://doi.org/10.1029/2003WR002086>
- Bowen, G.J., West, J.B., 2008. Isotope Landscapes for Terrestrial Migration Research. *Terr. Ecol.* 2, 79–105. [https://doi.org/10.1016/S1936-7961\(07\)00004-8](https://doi.org/10.1016/S1936-7961(07)00004-8)
- Boyer, E.W., Alexander, R.B., Parton, W.J., Li, C., Butterbach-Bahl, K., Donner, S.D., Skaggs, W., Gross, S.J. Del, 2006. Modeling denitrification in terrestrial and aquatic ecosystems at regional scales. *Ecol. Appl.* 16, 2123–2142.
- Bustamante, M.M.C., Martinelli, L.A., Silva, D.A., Camargo, P.B., Klink, C.A., Domingues, T.F., Santos, R. V, 2004. 15N natural abundance in woody plants and soils of central brazilian savannas (Cerrado). *Ecol. Appl.* 14, 200–213. <https://doi.org/10.1890/01-6013>
- Butterbach-Bahl, K., Baggs, E.M., Dannenmann, M., Kiese, R., Zechmeister-Boltenstern, S., 2013. Nitrous oxide emissions from soils: How well do we understand the processes and their controls? *Philos. Trans. R. Soc. B Biol. Sci.* 368. <https://doi.org/10.1098/rstb.2013.0122>
- Butterbach-Bahl, K., Willibald, G., Papen, H., 2002. Soil core method for direct simultaneous determination of N₂ and N₂O emissions from forest soils. *Global*

Biogeochem. Cycles 240, 105–116.

- Chen, C., Jia, Y., Chen, Y., Mehmood, I., Fang, Y., Wang, G., 2018. Nitrogen isotopic composition of plants and soil in an arid mountainous terrain: South slope versus north slope. Biogeosciences 15, 369–377. <https://doi.org/10.5194/bg-15-369-2018>
- Cheng, W., Chen, Q., Xu, Y., Han, X., Li, L., 2009. Climate and ecosystem ^{15}N natural abundance along a transect of Inner Mongolian grasslands: Contrasting regional patterns and global patterns. Global Biogeochem. Cycles 23, 1–11. <https://doi.org/10.1029/2008GB003315>
- Conen, F., Zimmermann, M., Leifeld, J., Seth, B., Alewell, C., 2008. Relative stability of soil carbon revealed by shifts in ^{15}N and $\text{C}:\text{N}$ ratio. Biogeosciences 4, 2915–2928.
- Craine, J.M., Elmore, A.J., Wang, L., Augusto, L., Baisden, W.T., Brookshire, E.N.J., Cramer, M.D., Hasselquist, N.J., Hobbie, E. a., Kahmen, A., Koba, K., Kranabetter, J.M., Mack, M.C., Marin-Spiotta, E., Mayor, J.R., McLauchlan, K.K., Michelsen, A., Nardoto, G.B., Oliveira, R.S., Perakis, S.S., Peri, P.L., Quesada, C. a., Richter, A., Schipper, L. a., Stevenson, B. a., Turner, B.L., Viani, R. a. G., Wanek, W., Zeller, B., 2015. Convergence of soil nitrogen isotopes across global climate gradients. Sci. Rep. 5, 8280. <https://doi.org/10.1038/srep08280>
- Dalal, R.C., Allen, D.E., 2008. Greenhouse gas fluxes from natural ecosystems. Aust. J. Bot. 1, 369–407.
- Denk, T.R.A., Mohn, J., Decock, C., Lewicka-szczebak, D., Harris, E., Butterbach-bahl, K., Kiese, R., Wolf, B., 2017. Soil Biology & Biochemistry The nitrogen cycle : A review of isotope effects and isotope modeling approaches. Soil Biol. Biochem. 105, 121–137. <https://doi.org/10.1016/j.soilbio.2016.11.015>
- Firestone, M.K., Davidson, E.A., 1989. Microbiological Basis of NO and N_2O Production and Consumption in Soil. Exch. trace gases between Terr. Ecosyst. Atmos. 7–21. <https://doi.org/citeulike-article-id:6223743>
- Freitas, A.D.S., de Sa Barreto Sampaio, E.V., Menezes, R.S.C., Tiessen, H., 2010. ^{15}N natural abundance of non-fixing woody species in the Brazilian dry forest (caatinga). Isotopes Environ. Health Stud. 46, 210–8. <https://doi.org/10.1080/10256016.2010.488805>
- Galloway, J.N., Dentener, F.J., Capone, D.G., Boyer, E.W., Howarth, R.W., Seitzinger, S.P., Asner, G.P., Cleveland, C.C., Green, P.A., Holland, E.A., Karl, D.M., Michaels, A.F., Porter, J.H., Townsend, A.R., Vörösmarty, C.J., 2004. Nitrogen cycles: Past, present, and future, Biogeochemistry. <https://doi.org/10.1007/s10533-004-0370-0>
- Galloway, J.N., Townsend, A.R., Erisman, J.W., Bekunda, M., Cai, Z., Freney, J.R., Martinelli, L.A., Seitzinger, S.P., Sutton, M.A., 2008. Transformation of the nitrogen cycle: Recent trends, questions, and potential solutions. Science (80-.). 320, 889–892. <https://doi.org/10.1126/science.1136674>
- Garcia-Perez, B., Hobson, K.A., 2014. A multi-isotope (d^2H , d^{13}C , d^{15}N) approach to establishing migratory connectivity of Barn Swallow (*Hirundo rustica*). Ecosphere 5, 1–12.

- Gomes, L.C., Faria, R.M., de Souza, E., Veloso, G.V., Schaefer, C.E.G.R., Filho, E.I.F., 2019. Modelling and mapping soil organic carbon stocks in Brazil. *Geoderma* 1–14. <https://doi.org/10.1016/j.geoderma.2019.01.007>
- Groffman, P.M., Butterbach-Bahl, K., Fulweiler, R.W., Gold, A.J., Morse, J.L., Stander, E.K., Tague, C., Tonitto, C., Vidon, P., 2009. Challenges to incorporating spatially and temporally explicit phenomena (hotspots and hot moments) in denitrification models. *Biogeochemistry* 93, 49–77. <https://doi.org/10.1007/s10533-008-9277-5>
- Handley, L.L., Austin, A.T., Robinson, D., Scrimgeour, C.M., Raven, J.A., Heaton, T.H.E., Schmidt, S., Stewart, G.R., 1999. The $\delta^{15}\text{N}$ natural abundance ($\delta^{15}\text{N}$) of ecosystem samples reflects measures of water availability. *Aust. J. Plant Physiol.* 26, 185–199. <https://doi.org/10.1071/PP98146>
- Hengl, T., Jesus, J.M. De, Heuvelink, G.B.M., Ruiperez, M., Kilibarda, M., Blagoti, A., Shangguan, W., Wright, M.N., Geng, X., Bauer-marschallinger, B., Guevara, M.A., Vargas, R., Macmillan, R.A., Batjes, N.H., Leenaars, J.G.B., Ribeiro, E., Wheeler, I., Mantel, S., Kempen, B., 2017. SoilGrids250m : Global gridded soil information based on machine learning. *PLoS One* 1–40. <https://doi.org/10.1371/journal.pone.0169748>
- Hilton, R.G., Galy, A., West, A.J., Hovius, N., Roberts, G.G., 2013. Geomorphic control on the $\delta^{15}\text{N}$ of mountain forests. *Biogeosciences* 10, 1693–1705. <https://doi.org/10.5194/bg-10-1693-2013>
- Hobson, K. a., Van Wilgenburg, S.L., Wassenaar, L.I., Powell, R.L., Still, C.J., Craine, J.M., 2012. A multi-isotope ($d^{13}\text{C}$, $d^{15}\text{N}$, $d^2\text{H}$) feather isoscape to assign Afrotropical migrant birds to origins. *Ecosphere* 3, art44. <https://doi.org/10.1890/ES12-00018.1>
- Hobson, K.A., van Wilgenburg, S.L., Wassenaar, L.I., Powell, R., Still, C.J., Craine, J.M., 2012. A multi-isotope ($d^{13}\text{C}$, $d^{15}\text{N}$, $d^2\text{H}$) feather isoscape to assign Afrotropical migrant birds to origins. *Ecosphere* 3, 1–20.
- Högberg, P., 1997. $\delta^{15}\text{N}$ natural abundance in soil-plant systems. *New Phytol.* 137, 179–203. <https://doi.org/10.1046/j.1469-8137.1997.00808.x>
- Houlton, B.Z., Bai, E., 2009. Imprint of denitrifying bacteria on the global terrestrial biosphere. *Proc. Natl. Acad. Sci.* 106, 21713–21716. <https://doi.org/10.1073/pnas.0912111106>
- Houlton, B.Z., Marklein, A.R., Bai, E., 2015. Representation of nitrogen in climate change forecasts. *Nat. Publ. Gr.* 5, 398–401. <https://doi.org/10.1038/nclimate2538>
- Houlton, B.Z., Sigman, D.M., Hedin, L.O., 2006. Isotopic evidence for large gaseous nitrogen losses from tropical rainforests. *Proc. Natl. Acad. Sci.* 103, 8745–8750. <https://doi.org/10.1073/pnas.0510185103>
- Howarth, R.W., Billen, G., Swaney, D., Townsend, A., Jaworski, N., Lajtha, K., Downing, J.A., Elmgren, R., Caraco, N., Jordan, T., Berendse, F., Freney, J., Kudeyarov, V., Murdoch, P., Zhu, Z.L., 1996. Regional nitrogen budgets and riverine N & P fluxes for the drainages to the North Atlantic Ocean: Natural and human influences. *Biogeochemistry* 35, 75–139. <https://doi.org/10.1007/BF02179825>

- Jones, L., Provins, A., Holland, M., Mills, G., Hayes, F., Emmett, B., Hall, J., Sheppard, L., Smith, R., Sutton, M., Hicks, K., Ashmore, M., Haines-Young, R., Harper-Simmonds, L., 2014. A review and application of the evidence for nitrogen impacts on ecosystem services. *Ecosyst. Serv.* <https://doi.org/10.1016/j.ecoser.2013.09.001>
- LeBauer, D.S., Treseder, K.K., 2008. Nitrogen limitation of net primary productivity in terrestrial ecosystems is globally distributed. *Ecology* 89, 371–379. <https://doi.org/10.1890/06-2057.1>
- Li, C., Frolking, S., Frolking, T.A., 1992. A model of nitrous oxide evolution from soil driven by rainfall events: 2. Model applications. *J. Geophys. Res. Atmos.* 97, 9777–9783. <https://doi.org/10.1029/92jd00510>
- Liao, J.D., Boutton, T.W., Jastrow, J.D., 2006. Organic matter turnover in soil physical fractions following woody plant invasion of grassland: Evidence from natural ^{13}C and ^{15}N . *Soil Biol. Biochem.* 38, 3197–3210. <https://doi.org/10.1016/j.soilbio.2006.04.004>
- Mallette, J.R., Casale, J.F., Jordan, J., Morello, D.R., Beyer, P.M., 2016. Geographically Sourcing Cocaine's Origin – Delineation of the Nineteen Major Coca Growing Regions in South America. *Sci. Rep.* 6, 23520. <https://doi.org/10.1038/srep23520>
- Martinelli, L. a., Piccolo, M.C., Townsend, a. R., Vitousek, P.M., Cuevas, E., McDowell, W., Robertson, G.P., Santos, O.C., Treseder, K., 1999. Nitrogen stable isotopic composition of leaves and soil: Tropical versus temperate forests. *Biogeochemistry* 46, 45–65. <https://doi.org/10.1007/BF01007573>
- McClain, M.E., Boyer, E.W., Dent, C.L., Gergel, S.E., Grimm, N.B., Groffman, P.M., Hart, S.C., Harvey, J.W., Johnston, C.A., Mayorga, E., McDowell, W.H., Pinay, G., 2003. Biogeochemical Hot Spots and Hot Moments at the Interface of Terrestrial and Aquatic Ecosystems. *Ecosystems* 6, 301–312. <https://doi.org/10.1007/s10021-003-0161-9>
- Nardoto, G.B., Ometto, J.P.H.B., Ehleringer, J.R., Higuchi, N., Bustamante, M.M.D.C., Martinelli, L.A., 2008. Understanding the Influences of Spatial Patterns on N Availability Within the Brazilian Amazon Forest. *Ecosystems*. <https://doi.org/10.1007/s10021-008-9189-1>
- Nardoto, G.B., Quesada, C.A., Patiño, S., Saiz, G., Baker, T.R., Schwarz, M., Schrodt, F., Feldpausch, T.R., Domingues, T.F., Marimon, B.S., Marimon Junior, B.-H., Vieira, I.C.G., Silveira, M., Bird, M.I., Phillips, O.L., Lloyd, J., Martinelli, L.A., 2014. Basin-wide variations in Amazon forest nitrogen-cycling characteristics as inferred from plant and soil ^{15}N : ^{14}N measurements. *Plant Ecol. Divers.* 7, 173–187. <https://doi.org/10.1080/17550874.2013.807524>
- Pardo, L.H., Nadelhoffer, K.J., 2010. Using Nitrogen Isotope Ratios to Assess Terrestrial Ecosystems at Regional and Global Scales, in: *Isoscapes: Understanding Movement, Pattern, and Process on Earth Through Isotope Mapping*. pp. 221–249.
- Parton, W.J., Hartman, M., Ojima, D., Schimel, D., 1998. DAYCENT and its land surface submodel: description and testing. *Glob. Planet. Change* 19, 35–48. [https://doi.org/10.1016/S0921-8181\(98\)00040-X](https://doi.org/10.1016/S0921-8181(98)00040-X)

- Phoenix, G.K., Hicks, W.K., Cinderby, S., Kuylenstierna, J.C.I., Stock, W.D., Dentener, F.J., Giller, K.E., Austin, A.T., Lefroy, R.D.B., Gimeno, B.S., Ashmore, M.R., Ineson, P., 2006. Atmospheric nitrogen deposition in world biodiversity hotspots: The need for a greater global perspective in assessing N deposition impacts. *Glob. Chang. Biol.* 12, 470–476. <https://doi.org/10.1111/j.1365-2486.2006.01104.x>
- Potter, S., Matson, A., Vitousek, M., 1996. Process modeling of controls on nitrogen trace gas emissions from soil worldwide. *J. Geophys. Res.* 101, 1361–1377.
- Robinson, D., 2001. δ 15 N as an integrator of the nitrogen. *Trends Ecol. Evol.* 16, 153–162. [https://doi.org/10.1016/s0169-5347\(00\)02098-x](https://doi.org/10.1016/s0169-5347(00)02098-x)
- Scott Bechtold, J., Naiman, R.J., 2006. Soil texture and nitrogen mineralization potential across a riparian toposequence in a semi-arid savanna. *Soil Biol. Biochem.* 38, 1325–1333. <https://doi.org/10.1016/j.soilbio.2005.09.028>
- Seitzinger, S., Harrison, J.A., Böhlke, J.K., Bouwman, A.F., Lowrance, R., Peterson, B., Tobias, C., Drecht, G. V., 2006. Denitrification across Landscapes and Waterscapes: A synthesis. *Ecol. Appl.* 16, 2064–2090. [https://doi.org/10.1890/1051-0761\(2006\)016\[2064:DALAWA\]2.0.CO;2](https://doi.org/10.1890/1051-0761(2006)016[2064:DALAWA]2.0.CO;2)
- Soper, F.M., Taylor, P.G., Wieder, W.R., Weintraub, S.R., Cleveland, C.C., Porder, S., Townsend, A.R., 2018. Modest Gaseous Nitrogen Losses Point to Conservative Nitrogen Cycling in a Lowland Tropical Forest Watershed. *Ecosystems* 21, 901–912. <https://doi.org/10.1007/s10021-017-0193-1>
- Terzer, S., Wassenaar, L.I., Araguás-Araguás, L.J., Aggarwal, P.K., 2013. Global isoscapes for δ 18O and δ 2H in precipitation: Improved prediction using regionalized climatic regression models. *Hydrol. Earth Syst. Sci.* 17, 4713–4728. <https://doi.org/10.5194/hess-17-4713-2013>
- van Egmond, K., Bresser, T., Bouwman, L., 2002. The European nitrogen case. *Ambio* 31, 72–8.
- Vitousek, P.M., Cassman, K., Cleveland, C., Crews, T., Field, C.B., Grimm, N.B., Howarth, R.W., Marino, R., Martinelli, L., Rastetter, E.B., Sprent, J.I., 2002. Towards an Ecological Understanding of Biological Nitrogen Fixation. *Biogeochemistry* 57/58, 1.
- Vitousek, P.M., Menge, D.N.L., Reed, S.C., Cleveland, C.C., 2013. Biological nitrogen fixation: Rates, patterns and ecological controls in terrestrial ecosystems. *Philos. Trans. R. Soc. B Biol. Sci.* 368. <https://doi.org/10.1098/rstb.2013.0119>
- Wang, L., Okin, G.S., D'Odorico, P., Caylor, K.K., Macko, S.A., 2013. Ecosystem-scale spatial heterogeneity of stable isotopes of soil nitrogen in African savannas. *Landsc. Ecol.* 28, 685–698. <https://doi.org/10.1007/s10980-012-9776-6>
- Wang, Y.P., Law, R.M., Pak, B., 2010. A global model of carbon, nitrogen and phosphorus cycles for the terrestrial biosphere. *Biogeosciences* 7, 2261–2282. <https://doi.org/10.5194/bg-7-2261-2010>
- Weintraub, S.R., Cole, R.J., Schmitt, C.G., All, J.D., 2016. Climatic controls on the isotopic composition and availability of soil nitrogen across mountainous tropical forest. *Ecosphere* 7, 1–13. <https://doi.org/10.1002/ecs2.1412>
- Xing, G.X., Zhu, Z.L., 2002. Regional nitrogen budgets for China and its major

watersheds. *Biogeochemistry* 57–58, 405–427.
<https://doi.org/10.1023/A:1016508323200>

Zheng, X., Fu, C., Xu, X., Yan, X., Huang, Y., Han, S., Hu, F., Chen, G., 2002. The Asian Nitrogen Cycle Case Study. *Ambio* 31, 79–87.

CAPÍTULO 1 - BACKGROUND AND THE USE OF ISOSCAPES IN THE BRAZILIAN CONTEXT: ESSENTIAL TOOL FOR ISOTOPE DATA INTERPRETATION AND NATURAL RESOURCES MANAGING*

*Artigo de revisão publicado na revista Ambiente & Água – An Interdisciplinary Journal of Applied Science:

SENA-SOUZA, João Paulo; COSTA, Fábio José Viana; NARDOTO, Gabriela Bielefeld. 2019. Background and the use of isoscapes in the Brazilian context: essential tool for isotope data interpretation and natural resources managing. Ambi. Água 14(2), e2282. <https://doi.org/10.4136/ambi-agua.2282>

Abstract

Spatial patterns of stable isotope ratios can be represented in spatial models called isoscapes and have been widely used to track biogeochemical processes in natural and anthropic systems. Isoscapes have the potential to improve isotope dissemination and interpretation of spatial patterns, increase scientific results appropriation by non-specialists and improve natural resources management. However, the use of isoscapes has not commonly been used in studies performed in the Brazilian context. Isoscapes with oxygen, hydrogen, nitrogen and carbon stable isotopes contribute in areas such as animal migration, forensics, hydrological, and studies on population, community and ecosystem level, among others. Here, we show the well-known global use and applications of isoscapes in different studies worldwide as a background to point out the potential for more Brazilian researchers to employ this approach in their studies, taking advantage of existing methods and filling spatial and methodological gaps. The incorporation of isoscapes may broaden the understanding of mechanisms and processes of major biogeochemical cycles in Brazil, assist in solving crimes, illicit drug origins, and wild animal trafficking, and increase Brazilian knowledge about the hydrological cycle and animal migration patterns in the Neotropics.

Keywords: isotopic landscape, spatial patterns, stable isotope

Introduction

Stable isotopes ratios distribution is related to the geographic space. This is a fundamental feature that has led to the emergence of many studies in this growing field of knowledge with a series of new applications in recent years. This spatial variation is related to how spatially explicit variables influence the isotopic fractionation and discrimination. For example, altitude and latitude highly influence the $\delta^2\text{H}$ and $\delta^{18}\text{O}$, differences in regional nitrogen cycles influence the $\delta^{15}\text{N}$, and differences in the plant photosynthetic pathways (C_3 or C_4) influence the $\delta^{13}\text{C}$.

Spatial patterns of stable isotope ratios have been represented in spatial models, called isoscapes (Isoscapes = isotopic + landscapes), which allow the visualization and help both the data interpretation and decision making when managing natural resources (Bowen 2010a). Isoscapes enable statistically filling of spatial gaps where isotope ratios information has not been represented (Bowen 2010a). Isoscapes can be based on any of both abiotic elements, such as water (Terzer et al., 2013) and soil (Weintraub et al., 2016), as well as biotic elements, as plant (Powell et al., 2012), animal (Vander Zanden et al., 2018) and human tissues (Valenzuela et al., 2011). For this reason, isoscapes have been used in a wide range of scientific areas, such as ecology, climate change, biogeochemistry, hydrology, forensic sciences, anthropology, commercial regulation, among others have been using isoscapes (Bowen et al., 2009).

The effort to map isotope ratios in the landscape precedes the term "isoscope", which was idealized in the year of 2006 (West et al., 2006). Before that, mathematical models were developed to map global $\delta^{15}\text{N}$ patterns in soil (Amundson et al., 2003), global $\delta^{13}\text{C}$ patterns in biosphere focusing on carbon isotope discrimination during photosynthesis (Lloyd and Farquhar, 1994), and of $\delta^{18}\text{O}$ in atmospheric CO_2 (Farquhar et al., 1993). The $\delta^{18}\text{O}$ and $\delta^2\text{H}$ global maps were also developed, mainly based on a database with precipitation isotopic ratios provided by the Global Network for Isotopes in Precipitation (GNIP) (Bowen and Revenaugh, 2003). With improvements in mapping technologies, interpolation techniques, and transfer functions, the isoscope approach has become a fertile scientific application field (West et al., 2010).

Reviews on isoscapes (Bowen et al., 2009; Bowen, 2010a) and a book focused on isoscapes concepts and techniques (West et al., 2010) have already been published.

However, the present compilation is the first that presents an extensive update on isoscape application followed by indications of perspectives and future applicability in Brazil, a region recognized worldwide by its high biological diversity and landscapes heterogeneity. For being a country of continental size, Brazilian scientific works that use stable isotopes can adapt global isoscapes from literature to solve national scientific problems. In addition, creating new isoscapes in different spatial and temporal scales to Brazil may fill existent scientific gaps on stable isotopes distribution, improving the knowledge on spatial patterns of carbon and nitrogen biogeochemical cycles, hydrological cycles, trophic niches and animal movements, and food authentication and forensics.

In this context, we explore here the key concepts and methods used in the design of isoscapes presenting a brief explanation about stable isotope spatial distribution mechanisms, the major problems related to scale definition, and the already used methodologies to generate isoscapes. With that in mind associated to a summary of the main applications of isoscapes in the areas of water cycle, ecosystem ecology, animal movement and forensic studies, we present how the use of isoscapes could be an essential tool for isotope data interpretation and natural resources managing in Brazil.

Methodology

We searched for publications in the Web of Science databases using the word "isoscape" OR "isoscapes" as a topic (present in the abstract, keyword, or title). In order to expand the search, we explored the reference lists of the retrieved articles. We classified the articles according to the topics defined in this work: water cycle studies, ecosystem approach studies, animal movement, and forensic applications. Although there are isoscapes of several elements, we restricted the search to $\delta^2\text{H}$, $\delta^{18}\text{O}$, $\delta^{13}\text{C}$ and $\delta^{15}\text{N}$ isoscapes. To present papers in which isoscapes could be used in order to show the potential use of this approach in Brazil context, we searched for articles using the word "stable isotopes". This search was performed on Web of Science and Scielo databases.

To illustrate some existent isoscapes that can be used in the Brazilian context, we used isoscapes available in literature. World precipitation $\delta^2\text{H}$ and $\delta^{18}\text{O}$ isoscapes are accessible to download on <http://www.waterisotopes.org> in raster format, with 10 km x 10 km spatial resolution. We used climatic data from <http://www.worldclim.org> to elaborate soil $\delta^{15}\text{N}$ isoscape to Brazil based in Amundson et al. (2003) equation for 0 –

10 cm depth ($\delta^{15}\text{N}_{\text{soil}(0-10)} = 0.134 * \text{MAT} - 0.0005 * \text{MAP} + 3.1985$). For $\delta^{13}\text{C}$ isoscape, we used the model elaborated by Powell et al. (2012) to South America under their previous authorization.

Key concepts and methods used in the design of isoscapes

Describing stable isotopes and their natural variations

Isotopes are atopic species of the same element. Therefore, it contains the same number of protons in the atomic nucleus, but different numbers of neutrons. The stable isotopes are those that do not emit any kind of radiation. Carbon stable isotopes, for example, are ^{12}C , ^{13}C . The first one contains 6 protons and 6 neutrons in the nucleus, rather than second with the same number of protons, but 7 neutrons. The elements of major biogeochemical cycles that have more than one isotope (hydrogen, oxygen, carbon and nitrogen) are so called the light stable isotopes.

The natural abundance of heavier isotope atoms is significantly smaller compared to the lighter atoms. Therefore, the isotope ratio (R) of the sample is compared to the R of a preset international standard to define the value of delta: $\delta = (R_{\text{sample}}/R_{\text{standard}} - 1) * 1000$, where R_{sample} is the ratio between heavier and lighter atoms of the sample, and R_{standard} is the ratio between heavier and lighter atoms of a standard. The R value is dimensionless and via criteria of provenance is less than zero. Thus, its value is multiplied by a thousand, creating a notation called δ per mil (‰).

Biogeochemical and physical processes lead to differences in reaction between light-heavy isotopes generating different proportion of them on materials or environment. The main process that lead the carbon isotope discrimination ($\Delta^{13}\text{C}$) is photosynthesis. Two are the main metabolic pathways of CO₂ absorption by plants: C₃ (Calvin Cycle) and C₄ (Hatch-Slack Cycle). C₃ plants discriminate more ^{13}C from CO₂, thus have lower $\delta^{13}\text{C}$, varying between -35 ‰ and -20 ‰. In contrast, C₄ plants have higher $\delta^{13}\text{C}$ values, with variation pattern between -15 ‰ and -11 ‰ (Powell et al., 2012). In general, C₃ plants are tree and shrub species, while C₄ ones are represented by tropical grasses (e.g. corn and sugar cane). The $\delta^{13}\text{C}$ isoscapes are generally elaborated through methods that differentiate plants with C₃ or C₄ metabolisms (Powell et al., 2012).

However, differences in carbon isotope ratio can be found into the same photosynthetic group (C₃ or C₄) or even in multiple individuals in the same species. Those differences occur due to environmental control or genotype-specific physiological

influences in carbon isotopic discrimination among plants (Cernusak et al., 2013). In C₃ plants, leaf $\delta^{13}\text{C}$ might decrease with increasing the ratio of intercellular to ambient CO₂ concentrations (ci/ca), which is in function of CO₂ supply from the atmosphere to the intercellular air spaces through stomata (Orchard et al., 2010). In addition to allowing the diffusion of CO₂ in the leaf, the stoma prevents water loss. Therefore, soil water availability and atmospheric pressure also influence $\Delta^{13}\text{C}$. Plant $\delta^{13}\text{C}$ has a negative relationship with the transpiration efficiency and has been used to access water-use efficiency, which can change following environmental gradients. Generally, $\Delta^{13}\text{C}$ decreases with the decrease of MAP (Cernusak et al. 2013).

There is a general pattern of increasing $\delta^{13}\text{C}$ value with the increase of elevation among C₃ plants. In higher altitudes, the ci/ca ratio decreases with the decrease of atmospheric pressure. The lower temperature in high altitudes can increase the $\Delta^{13}\text{C}$ as well. The availability of nutrients in the soil is another factor that influences the isotopic discrimination of carbon by the C₃ plant due to the direct influence on photosynthetic capacity. Discrimination of the carbon isotope decreases with increasing N concentration in the leaf (Cernusak et al., 2013). Light availability is the main environmental condition that causes $\Delta^{13}\text{C}$ variation among C₄ plants. Generally, $\Delta^{13}\text{C}$ increases with irradiance in C₄ plants. Water use efficiency also influences C₄ plants $\Delta^{13}\text{C}$, however with an opposite trend comparing to C₃ plants. Besides, there may be a trend for increased isotope carbon discrimination with increased drought stress in C₄ plants (Murphy and Bowman, 2009).

Global atmospheric circulation of water is the most important process that influences global distribution of $\delta^{18}\text{O}$ and $\delta^2\text{H}$. Oxygen and hydrogen isotope ratios of water change primarily from the isotopic discrimination by sea water evaporation and precipitation. The standard mean ocean water (SMOW) is the international standard for $\delta^{18}\text{O}$ and $\delta^2\text{H}$, which is 0‰, by convention. Furthermore, $\delta^{18}\text{O}$ and $\delta^2\text{H}$ ratios become negative due to differential evaporation between heavier and lighter molecules, where lighter molecules evaporate more easily. In the process of rain formation and precipitation, clouds turn more negative as they advance toward the continent. In this way, $\delta^{18}\text{O}$ and $\delta^2\text{H}$ ratios present latitudinal, longitudinal and/or altitude variation, undergoing continental effects.

At smaller scales, water isotopes differ according to the scale and processes that drive the hydrological cycle. In a watershed, regardless of its extent, the water isotopic variation goes beyond the influence of precipitation. The O and H isotope ratios of the surface water depend mainly on the water source (Bowen and Good, 2015; Liu et al. 2010;

Birkel et al., 2018) and downstream transport-related processes during the terrestrial water fluxes in a watershed (Jasechko et al., 2013). Differences in soil texture or hillslope angle can drive differential variation in the evaporation leading to variation in water isotope values at local scales (Mueller et al., 2014). Differences in environmental conditions (temperature and air humidity) influence leaf water evaporation leading to possible variation of tissue O and H isotope ratios and it can vary according to the plant species (West et al., 2008).

The spatial variation of $\delta^{15}\text{N}$ depends on a complex set of processes. Each process of oxidation and reduction of nitrogen causes isotope fractionation. Nitrogen makes up about 78% of the atmosphere in the form of N_2 , a little reactive gas. This gas is the international standard for $\delta^{15}\text{N}$ which is 0‰, by convention. Processes such as dry and / or wet deposition of N, and decomposition of organic matter transform N into more reactive forms. When nitrogen is transformed from N_2 to NH_3 and NH_4^+ , assimilated by the organisms and transformed into organic molecules, $\delta^{15}\text{N}$ values of the substrate increases. Therefore, soil $\delta^{15}\text{N}$ is generally high, especially in tropical ecosystems (Amundson et al., 2003).

Climatic influences on soil $\delta^{15}\text{N}$ values occur mainly due to the higher gaseous N losses in hot/dry places than in wet/cold places (Craine et al, 2015a). High values of $\delta^{15}\text{N}$ in the soil can indicate high relative losses of N for the atmosphere while N losses due to leaching and erosion do not cause significant fractionation. Soil $\delta^{15}\text{N}$ varies as a function of clay content and soil organic carbon concentration at global scale (Craine et al, 2015a) while at local and regional scales, soil $\delta^{15}\text{N}$ values are a function of organic matter decomposition (Craine et al., 2015b). Generally, the higher the level of organic matter decomposition, the greater the soil $\delta^{15}\text{N}$ (Craine et al., 2015b). Moreover, topographic position influences soil particle size by erosion and deposition processes and can be an important predictive variable to nitrogen cycle, which consequently influence soil $\delta^{15}\text{N}$ spatial variation (Berhe et al., 2018).

Scaling isoscapes

Scale is a fundamental aspect of studying all phenomena and processes that vary in space and/or time (Goodchild, 2011). In general, a scale reflects the limit of a given phenomenon representation. Several studies use categoric terminology from geographical scale approach in the application or elaboration of isoscapes or in works on processes that lead to a spatial variation of isotopic fractionation and discrimination, which can be used

as predictive variables for isoscape elaboration (eg.: landscape-scale - Bai et al., 2009; continental-scale - Powell et al., 2012; ecosystem-scale Wang et al., 2013; community-scale - Rascher et al., 2012).

Isoscapes of large scales often need to be simplified and generalized due to the necessary match with secondary data sources available at these scales (Bowen, 2010a). In this sense, global or continental-scale isoscapes may not be suitable for landscape-scale applications without going through a downscaling process considering more variables. Likewise, isoscapes elaborated on very detailed scales may not address issues at larger scales (Bowen, 2010a).

The isotope ratio of a given substrate varies with time, location, and spatially and therefore, depending on the chosen scale, the predictive variables of a given isotopic ratio may change. The spatial variation of water stable isotopes of precipitation ($\delta^{18}\text{O}$ and $\delta^2\text{H}$), for example, is clearly influenced mainly by climatic patterns, with the main variables predicting the annual mean precipitation and temperature (Terzer et al., 2013). However, in smaller scales, the influence of other variables such as topography may be more evident (Baisden et al., 2016).

Mapping isoscapes

One of the main principles of isoscapes is to determine isotopic composition in places where there is no sampling, extrapolating a limited number of sampled sites. Therefore, we mainly use methods and algorithms from the geostatistics. The choice of the appropriate method for the mapping depends on the purpose of the work, the number of spatially explicit dependent variables and predictors available, and the scale. At the local and regional scale, it is feasible the collection of samples in the field to feed isoscapes models. Usually, these studies have used ordinary kriging after semivariogram fit to construct the isoscapes (Oliver and Webster, 2014).

Isoscapes with larger scales are usually built by the compilation of data from literature. Another way is the creation of global networks of isotopic monitoring. As an example, $\delta^{18}\text{O}$ and $\delta^2\text{H}$ isoscapes in water based the GNIP database that has been applied in hydrological and ecological approaches in many spatial scales (IAEA/WMO, 2015).

Spatial autocorrelation is considered as a fundamental condition for the application of geostatistical methods. That is, values from nearby places tend to be more similar than values from more spaced places in space. In this sense, the independent or predictive variable must influence the values of the target variable, which are the stable isotope

values. Geostatistical models usually bring an error that must be measured and considered in the studies. The model settings seek to reduce the error, increasing accuracy.

When the spatial process influencing the variable is well known, the search for a methodological standardization is more feasible. It is the case of the influence of atmospheric water circulation on precipitation $\delta^{18}\text{O}$ and $\delta^2\text{H}$, for example, which allows the application of special regression in most mappings (Bowen, 2010b).

Most of the well-known global isoscapes are for $\delta^{18}\text{O}$ and $\delta^2\text{H}$ and they are basically based on equations of spatial regressions, with variations and adaptations between studies. Since there are global isoscapes of environmental elements such as precipitation water, they can be adjusted for global isoscapes of biological tissues, as was done for leaf water (West et al., 2014) and bird feathers (Bowen et al., 2005; Hobson et al., 2012a). It is important to highlight here the work from Terzer et al. (2013) that proposed a new approach to raise accuracy of $\delta^{18}\text{O}_p$ and $\delta^2\text{H}_p$ isotope global models, called Regionalized Cluster-based Water Isotope Precipitation (RCWIP). The method differs from the previous ones because the authors made a more accurate model from a set of regionalized multivariate regression equations. The predictive variables were gridded climatic and geographic variables (elevation, latitude / longitude). Terzer et al. (2013) compared the results with the model of Bowen and Wilkinson (2002) showing that the uncertainty decreased in general. These results are available for download on the internet in raster format with $10' \times 10'$ spatial resolution on <http://www.iaea.org/water>.

The only one for nitrogen was proposed by Amundson et al. (2003), based on a regression using global patterns of precipitation and temperature as predictive variables. They used values of foliar $\delta^{15}\text{N}$, soil $\delta^{15}\text{N}$, and enrichment factor available in the literature at that time, showing that, on a global scale, soil and plant $\delta^{15}\text{N}$ have a negative relation with MAP and positive relation with MAT. It served as a first proxy of $\delta^{15}\text{N}$ global distribution. However, it presented considerable limitations due to the complexity of factors that affect $\delta^{15}\text{N}$ fractionation, many gaps in spatial distribution data, which results in augmented error in the final model (Pardo and Nadelhoffer, 2010).

For carbon isoscapes, Still and Powell (2010) developed a methodology to estimate the percentage of C₃ and C₄ plants by area unit, allowing $\delta^{13}\text{C}$ plant spatial distribution patterns estimation in a large mapping scale. Powell et al. (2012) used similar methodology to map $\delta^{13}\text{C}$ in South America in the year of 2000, using empirical measurements of plants and soils. They estimated $\delta^{13}\text{C}$ values for plants and soil organic matter from the vegetation type mapping (grasses, shrubs and trees) by classifying each

pixel of an image as potentially favorable for C₃ plant or C₄ plant. The authors used temperature and precipitation dataset incorporated to previous classifications of agricultural cover and type of crop. First, they considered vegetation pattern and visual interpretation of satellite image and incorporated information of managed agro-ecosystems. Second, they partitioned the area considered herbaceous in the previous step in natural grasses % and crops % based on global data of agricultural areas distribution, separating in C₃ and C₄ plant culture from a global database of types of agriculture. This approach may be applied at regional-scale by incorporating new dataset that represent regional relationships between ¹³C discrimination and abiotic factors.

Main applications of the isoscapes

Water isoscapes

Global and regional $\delta^{18}\text{O}$ and $\delta^2\text{H}$ isoscapes provide information that integrate a number of water cycle mechanisms and have strong spatial correlation (Bowen and Good, 2015). This approach serves as base to models that assign samples to their regions of origin, such as animal migration and forensic models. Due to the importance and utility of maps for water $\delta^{18}\text{O}$ and $\delta^2\text{H}$ many works adapted methodologies by downscaling precipitation, surface water and groundwater isoscapes for different locations. Water isoscapes have been used to measure contributions of surface water and groundwater to rivers, water loss to atmosphere through evaporation or transpiration, and rain types contribution to total precipitation (Aggarwal et al., 2016). Precipitation $\delta^{18}\text{O}$ isoscapes also contribute for the understanding about climatic variations and anomalies (Kern et al., 2014) and determination of seasonal variation in water sources (Brooks et al., 2012). In the latter, during the dry season, the major contribution was found to be from snow accumulated on higher altitudes (60-80%), helping to conclude about the vulnerability of Willamette river hydrographical system in the climate change scenario (Brooks et al., 2012).

Isoscapes on ecosystem ecology approach

Isoscapes have been used in the ecosystem approach mainly to provide a basis for studies of carbon and nitrogen biogeochemical cycles from local to global scales.

At global scale, atmospheric and plant $\delta^{13}\text{C}$ isoscapes provide fundamental information to the comprehension of CO₂ exchanges between biosphere and atmosphere

by calculating net assimilation of carbon by plants based on carbon discrimination models (Lloyd and Farquhar, 1994; Suit et al., 2005); global plant $\delta^{13}\text{C}$ isoscape models have great potential to improve estimates of the carbon sinks and sources spatial distribution, knowledge about plant physiology, and their interaction with climatic and edaphic factors (Powell et al., 2012); global isoscapes of soil $\delta^{15}\text{N}$ integrate important information about N global input and output tendencies of ecosystems (Amundson et al., 2003; Houlton et al., 2015).

At smaller scales, isoscapes have been used for both aquatic and terrestrial environments with an ecosystem approach to understand regional and local patterns of carbon and nitrogen cycles as well as human activities and local environmental changes are affecting the dynamics of these elements. In aquatic ecosystems, $\delta^{13}\text{C}$ and $\delta^{15}\text{N}$ isoscapes have been coupled with various elemental ratios to analyze nutrient dynamics (N and P) (Fourqurean et al., 2015). In terrestrial ecosystems, soil $\delta^{15}\text{N}$ spatial variation may be shaped considering elevation, which has direct relation with climatic patterns (e.g.: MAT and MAP) (Arnold et al., 2009; Weintraub et al., 2016), but may also help to compose future predictive models about nutrient cycling and CO₂ emission in a climate change scenario (Houlton et al., 2015). $\delta^{13}\text{C}$ and $\delta^{15}\text{N}$ isoscapes have also been applied to measure spatial correlation of soil $\delta^{13}\text{C}$ in natural environments and pastures (Powers, 2006), to evaluate invasive plant effects in local ecosystem processes (Bai et al., 2009; 2012a; 2013; Rascher et al., 2012; Hellmann et al., 2016a; 2016b; 2017; Nielsen et al., 2016) and to assess the effects of land use change to nutrient cycle in rural areas (Nitzsche et al., 2016) as well as in urban areas (Boeckx et al., 2006). Local $\delta^{13}\text{C}$ and $\delta^{15}\text{N}$ isoscapes have been also used to track soil organic matter dynamics. For instance, variations on tropical forests soil $\delta^{15}\text{N}$ may also be explained by topographic variations, mainly by slope (Hilton et al., 2013; Weintraub et al., 2015) and elevation (Arnold et al., 2009; Weintraub et al., 2016).

Isoscapes on animal movement and biological conservation studies

There are two major approaches to use isoscapes in animal migration studies: nominal assignment and continuous surface assignment (Wunder, 2012). Nominal assignment approach divides the continuous surface with isotopic ratios (predictive variables) in smaller named blocks, easier to manipulate (categoric variables). The most used methods in nominal assignment approach are decision trees or discriminatory functions that create attributions and clusters (Hobson et al., 2012b; Vander Zanden et

al., 2015). Continuous surface assignment approach is based on continuous surface models with isotopic ratios attributed to each pixel on a model. In these cases, continuous surface approach requires a small set of sample data adjusted to inorganic variable models (as precipitation, for instance) (Wunder, 2012).

Assignments have usually been made by applying Bayesian analysis in order to estimate the likelihood that each isoscape pixel represents the origin of a given sample. The same approach is used in forensic studies (see section below). Some prior information may lead to greater likelihood that an unknown sample may have originated from an area. In the absence of isotope data, given the greater natural abundance of individuals from a same species in a region versus in another region, it is reasonable to think that the target individual would have a greater chance to have come from the former region. This way of thinking may be traduced to mathematical terms using Bayesian rules: $P(B/A) = P(A/B) * P(B)/P(A)$, where, $P(B/A)$ is the posterior probability of an event B given event A , $P(A/B)$ is the probability of the observed data given the model parameters (for example, the normal probability function cited below), $P(B)$ is the prior probability for B and $P(A)$ is a marginal probability that serves as a normalizing constant.

There are several algorithms and computational platforms that supports the Bayesian analysis specific for sample assignment to isoscapes. One of the most used platforms is the IsoMAP, cyber-GIS system the supports basic isoscape modeling and sample assignment based on Bayesian analysis (<http://isomap.org>; Bowen et al., 2014). Recently, many packages have emerged on the R statistical computing environment (R Core Team, 2018) that permits geostatistical analyses, isoscape modelling, and sample assignment. Some of them combined different GIS packages in one specific for isoscape assignment, such as IsoriX package, for example (Courtiol et al., 2019).

Assignment models use tissue isoscape as a probability surface, where an unknown origin sample value may be assigned to a region as a function of a normal distribution, given its isotopic value and the expected standard deviation (Wunder, 2010; Reed et al., 2018; Hobson et al., 2018). For that reason, the creation of tissue isoscapes is a priority for studies on animal migration. Researches with this objective should consider the characteristics of each species and generate isoscape models with appropriate spatial resolution. Besides that, the majority of existing models are static, not taking into account temporal variation that may be incorporated to animal tissue. Isoscapes based on global databases, for example, should be associated to field validated samplings and other, more refined, local climatic models (Hobson et al., 2010). The mechanisms of tissue renewal

and how they affect isotopic fractionation in the animal must be considered in the analysis (Wunder and Norris 2008). Studies about migratory species using isoscapes in countries with few available data should elaborate ground validated models for the species in question (Gutiérrez-Expósito et al., 2015). The tissue calibrated isoscape can be made by using the residual from a regression analysis between the environment isoscape and the target tissue isotopic value (Hobson et al., 2018). The individuals to calibrate the isoscapes must have known origins.

Scientists must be aware about the challenges of using organic tissue for stable isotope analysis, mainly for $\delta^2\text{H}$ values (Hobson et al., 2012a; Soto et al., 2017). Samples for this type of analysis are very sensitive to contamination by any water from the natural ambient humidity. The analysis of the same sample at different sites may also affect the final result, which can be solved by more intensive drying of the sample (Soto et al., 2017). Even more complex is the exchangeable nature of some hydrogen molecules, which may affect the final bulk tissue $\delta^2\text{H}$ value. That is due to the characteristics of some chemical structures of the materials, such as amino (NH_2), carboxyl (COOH), hydroxyl (OH), or thiol (SH), which can exchange hydrogen atoms with ambient water (Meier-Augenstein et al., 2013). Therefore, exchangeable hydrogen must be considered in the analysis to maintain the accuracy of assignment models with precipitation isoscapes (Meier-Augenstein et al., 2013; Soto et al., 2017).

Building an organic tissue $\delta^2\text{H}$ dataset must follow controlled methods to determine non-exchangeable ^2H abundance in animal tissue, so the analysis can be validated and applied in spatial models (Meier-Augenstein et al., 2013). Some methods have recently been accessed in an attempt to standardize $\delta^2\text{H}$ analyzes on tissues in different laboratories and should be considered in future analyzes (Soto et al., 2017). These challenges must be considered on any analysis that uses organic tissue $\delta^2\text{H}$ to track animal movement, as well as any forensic application involving tracking humans, food provenance, and illegal trade of wildlife, timber and drugs.

Most papers on the use of isoscapes in animal migration studies are focused on birds, due to the large number of migratory species (eg Vander Zanden et al., 2015; Reed et al., 2018). However, the isoscape approach has been used in studies on the movement of any species or group of animals that exhibit some geographic variation during the life cycle. In terms of wild fauna conservation studies, regional isoscapes have been used with great potential to assist decision makers (Hénaux et al., 2011). As example, Hénaux et al. (2011) observed the dispersion routes of pumas (*Puma concolor*) using $\delta^2\text{H}$ and $\delta^{13}\text{C}$

isoscapes in preys with sedentary behavior, being an important work in identifying critical conservation areas for big carnivores, and Rodríguez-Pérez et al. (2018) identified critical habitats of vaquitas (*Phocoena sinus*) using sediment and zooplankton $\delta^{13}\text{C}$ and $\delta^{15}\text{N}$ isoscapes in marine ecosystems.

Isoscapes on forensic applications

The success of prior uses of animal tissue isoscapes has led to increased use of isoscape approach in human forensic studies. Stable isotopes serve as geographical indications of illegal material seized, such as drugs or trafficked wild animals and have the potential to link these materials to geographic positions (Bowen et al., 2007; Ehleringer et al., 2008; Warner et al., 2018; Chesson et al., 2018).

The success of using isoscapes for helping solving forensic questions depends on a series of factors. Firstly, is important to know how mechanisms and chemical material used on fixation and storage affect the material, component or organism isotope ratio. Secondly, is necessary to know the predictive power of the model, which may be recognized from a regression, to describe relations between a specimen isotopic ratio with environmental variables (Ehleringer et al., 2010).

Ehleringer et al. (2008) mapped $\delta^2\text{H}$ and $\delta^{18}\text{O}$ human hair for United States continuous while Valenzuela et al. (2011) elaborated human hair isoscapes for the United States, but using $\delta^{15}\text{N}$, $\delta^{13}\text{C}$, and $\delta^{34}\text{S}$. Both papers discussed about possible applications of this model to identify the region of unidentified human origin, movement reconstruction, and studies on individuals and human diet. Isoscape from tap water is also a solid base to forensic studies (Bowen et al., 2007) and has been useful in identifying human geographical origin (Warner et al., 2018). Hydrogen and oxygen isoscapes have been also employed on the identification of food geographic region of production, such as wine, olive oil, coffee, meat (Ehleringer et al., 2000; Carter et al., 2015; Chiocchiani et al., 2016), beer, bottled water, soda, and milk (Chesson et al., 2010a; 2010b).

Although the use of isoscapes are efficient in numerous forensic studies, generally the models are not capable of predicting the exact specimen origin place due to climatic conditions that shape stable isotopes spatial patterns in similar ways in different regions (Ehleringer et al., 2010). If there is some previous knowledge of the specimen probable origin areas or assistance from other complementary tools, it is possible to increase the predictive capacity of coupled models. As an example, Mallette et al. (2016) used O and H isoscapes coupled to alkaloid studies to detect the possible origin of seized cocaine in

the United States among 19 crop areas in South America, but also, they could compare between cocaine isotopic ratios to a geographically validated database and that allowed the authors to discover new cocaine cultivation areas formerly unknown.

Potential use of isoscapes in Brazil

In Brazil, the number of studies using light stable isotope ratios to track local and regional carbon and nitrogen dynamics in the soil-plant-atmosphere system from different Brazilian regions has raised considerably in the last decades: in the North region - Amazonia (Ometto et al., 2002; 2005; 2006; Pérez et al., 2006; Nardoto et al., 2008; 2014); northeastern region - Caatinga (Teixeira et al., 2006; Freitas et al., 2010), Central region - Cerrado (Bustamante et al., 2004; Coletta et al., 2009; Viani et al., 2011), southeastern region – Atlantic forest (Lins et al., 2016; Vitoria et al., 2018).

The combination of $\delta^{15}\text{N}$ and $\delta^{13}\text{C}$ has been the basis for studies about diet of different animals such as aquatic macrofaunal (Hardt et al., 2013; Castro et al., 2016), fishes and dolphins (Di Beneditto et al., 2013), arthropods (Salgado et al., 2014) and small mammals (Galetti et al., 2016), and human diet in different regions of Brazil (Nardoto et al., 2006, 2011; Gragnani et al., 2014; Rodrigues et al., 2016).

The $\delta^2\text{H}$ and $\delta^{18}\text{O}$ have been applied to hydrological cycle studies in Brazil. These isotopes have been applied in the understanding of local and regional hydrological cycles (Martinelli et al., 2004; Soler i Gil and Bonotto 2014). Mixture models of $\delta^2\text{H}$ and $\delta^{18}\text{O}$ indicated the role of plant transpiration and soil evaporation on local hydrological cycle in Amazonia (Moreira et al., 1997), Cerrado (Jackson et al., 1999), and Atlantic forest ecosystems (Cassana et al., 2015). An isotope map has been made to verify chemical and isotopic characteristics at the west portion of Guarani Aquifer System (among the states of Mato Grosso do Sul, Mato Grosso and Goiás) for a paleoclimate study (Gastmans et al., 2010) while Martinelli et al. (2004) showed the potential of using $\delta^2\text{H}$ and $\delta^{18}\text{O}$ isotopes from precipitation and river water in the Piracicaba's river basin hydrological monitoring station, in São Paulo State.

The applications of stable isotopes to detect food authentication and adulteration have also been used in Brazil to evaluate the quality and origin of Brazilian wines (Martinelli et al., 2003) and beers (Mardegan et al., 2012), soy sauce (Morais et al., 2018), but also to determine differences in diet of barn versus free-range chickens for studying animal nutrition with food authentication implications (Coletta et al., 2012).

Stable isotopes forensic studies have sporadically been used in Brazil. $\delta^{15}\text{N}$ and $\delta^{13}\text{C}$ helped to identify the origin of Brazilian marijuana seized (Shibuya et al., 2007), to trace origin and effect of illegal discharge of residues in streams and sediment (Barbieri et al., 2014; Roth et al., 2015), but also an isotopic assessment on helping to understanding the effects of the 2012 Brazilian Forest Act on tropical riparian zones (Salemi et al., 2016).

A very few studies using $\delta^{13}\text{C}$ spatial patterns have been employed to measure land use effects in aquatic (Sanaiotti et al., 2002; Augusto et al., 2015) and terrestrial ecosystems (Assad et al., 2013; Salemi et al., 2016; Figueira et al., 2016), which, therefore, might be the close-fitting what has been applied in Brazil in terms of the isoscape approach in any published study leaded by Brazilian research groups.

Perspectives of using isoscapes in Brazil

Published global and continental isoscape models can be downloaded for Brazilian context. These isoscapes may serve as a first approximation to perform larger scales mapping in Brazilian biomes. $\delta^{13}\text{C}$ isoscape elaborated by Powell et al. (2012) to South America shows C stable isotope spatial distribution patterns along Brazilian biomes (Figure 1.1 A). The equations from Amundson et al. (2003) for soil and vegetation $\delta^{15}\text{N}$ may be applied to Brazil from records of spatial climatic variables (Figura 1.1 B).

Global precipitation $\delta^2\text{H}$ and $\delta^{18}\text{O}$ isoscapes can also be downloaded and easily applied in Brazilian scale (Figure 1.2). However, elaboration of local and regional isoscapes in the Brazilian context is essential in order to reduce associated model errors. Developing precipitation isoscape models specific for Brazil is imperative, since current global models mask part of the natural variations of isotopic ratios. For instance, average rates presented in Figure 1.2, shows a significantly lower spatial variation in comparison to temporal and spatial fluctuation found by Soler i Gil and Bonotto (2014) only in the area of São Paulo State.

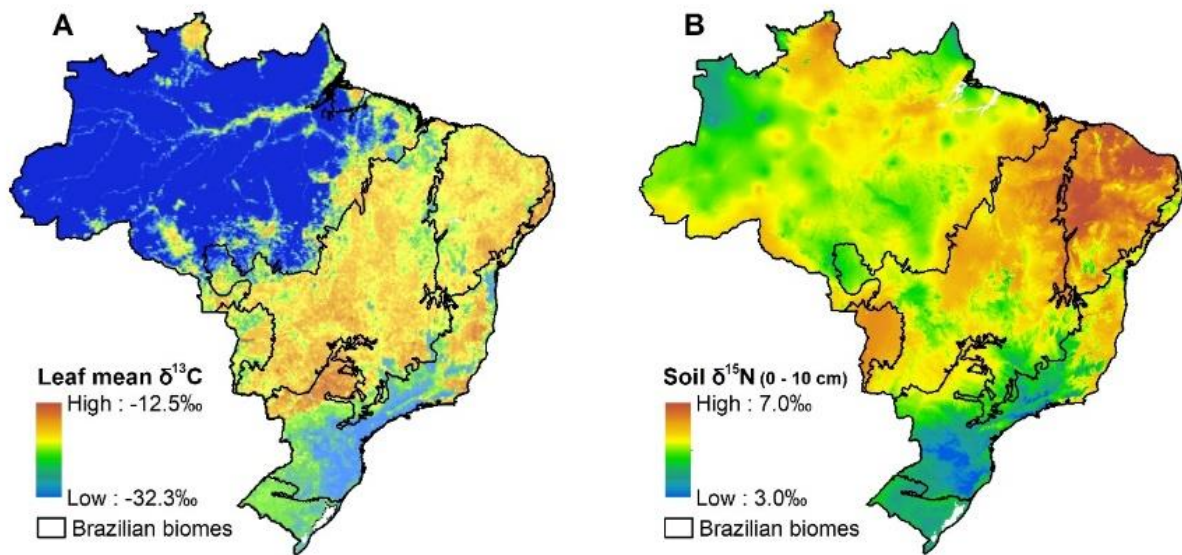


Figure 1.1. Plant $\delta^{13}\text{C}$ isoscape from Powell et al. (2012) with author's authorization (A); and soil $\delta^{15}\text{N}$ isoscape based in Amundson et al. (2003) equation for 0 – 10 cm depth ($\delta^{15}\text{N}_{\text{soil}(0-10)} = 0.134 * \text{MAT} - 0.0005 * \text{MAP} + 3.1985$) applied using climatic data from <http://www.worldclim.org> to elaborated (B).

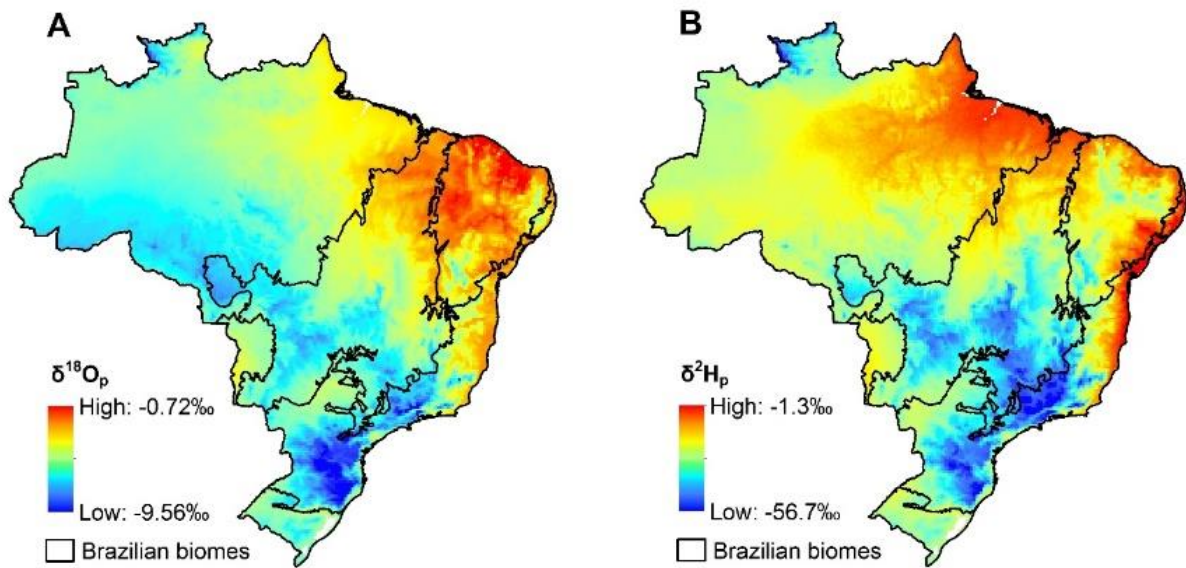


Figure 1.2. Mean annual precipitation $\delta^{18}\text{O}$ (A) and $\delta^2\text{H}$ (B) isoscapes. Data were downloaded from <http://www.waterisotopes.org>.

Taking into account the number of studies that have been using the stable isotope approach in Brazil together with the facility to use the equations and methods already tested and applied worldwide, the potential to develop C, N, O and H and isoscapes with

improved scale will definitely support both basic and applied studies in different areas of knowledge as pointed out in the section 4 above.

In terms of developing $\delta^{2}\text{H}$ and $\delta^{18}\text{O}$ local to region isoscapes to study hydrological cycles in different regions of Brazil could be easily applied to groundwater management in Brazil and should be complemented by spatial modelling for isoscapes creation that would facilitate data interpretation. There are 26 geographic locations with precipitation stable isotope historic data from GNIP stations in Brazil, which are available for download in shapefile format (<http://wateriso.utah.edu/>). Currently, 10 GNIP monitoring stations are operating in Brazil (Peeva, 2018). This amount of GNIP stations cannot represent the climatic and hydrographic diversity for the Brazilian territory. Some alternatives are suggested in the literature as the Ehleringer et al. (2008) work collecting tap water and human hair or using specific resident species (Hobson et al., 2009) to construct indirectly water based isoscapes in a continental level. These approaches can be used to fill up gaps on water based isoscapes for the continental territory of Brazil.

Future $\delta^{13}\text{C}$ isoscapes for Brazil should be made using samples with large spatial representation, such as the one performed by Assad et al. (2013) to study changes in C stock caused by land use changes. It may help to decrease model errors. For the Cerrado region, for example, Powell et al (2012) indicated considerable uncertainty due to a huge land cover heterogeneity in Cerrado biome. Brazilian researchers can integrate soil and vegetation samples from collections of previous field work and publications to increase the number of sampling sites for biogeochemical studies, both for C and N stable isotopes.

Local and regional biogeochemical changes results in problems related to N_r in Latin America (Austin et al., 2013), especially in Brazil. $\delta^{15}\text{N}$ isoscapes for vegetation and, mainly, for soil are important tools to study N input and output mechanisms from ecosystems (Bai et al., 2012b, Houlton et al., 2015). Nitzsche et al. (2016) discussed the importance of $\delta^{15}\text{N}$ mapping in complex agricultural areas to disclose results to farmers and decision makers. It may be applied in Brazil, considering the large extension of agricultural areas. Another possibility would be to map $\delta^{15}\text{N}$ in agricultural areas considering landforms, potential ways in which the land can influence soil characteristics and agricultural productivity (Siqueira et al., 2010). In this case, a regional and local soil $\delta^{15}\text{N}$ isoscape could point to the topographic position where N losses to the atmosphere or leaching area are happening, aiding agricultural management.

Some plants used in agriculture and livestock were introduced in natural ecosystems in Brazil. There are at least 54 potentially invasive plants in Brazil and their effects on

local biogeochemical cycles are little known (Zenni and Ziller 2011; Dias et al., 2013). Similar approaches as above described (Bai et al., 2013) should be used to help in the understanding of invasion vectors and the biogeochemical cycles changing (Rascher et al., 2012, Bai et al., 2012a, Hellmann et al., 2016a, 2017).

Considering the extensive biodiversity and animal migration in Brazil, existing global isoscape models may base animal wintering and reproduction localities origins first approximations. Geographic assignment models of migratory birds to geographic origins have already been made for South America (García-Pérez and Hobson 2014; Hobson and Kardynal 2016). Despite the use of water isoscapes applicability to infer origin or wintering places of animals at regional and continental scales, the highest potential of this approach lies at medium to high latitude regions due to the strong spatial gradient of isotopic ratios in precipitation. However, this limitation does not narrow the application of isoscapes in issues of this nature in regions of low latitude such as South America and Africa. In these cases, a multi-isotope approach coupling $\delta^2\text{H}$ isoscapes with $\delta^{13}\text{C}$ and $\delta^{15}\text{N}$ isoscapes may raise the inference efficiency (García-Pérez and Hobson 2014; Hobson and Kardynal 2016). Another way to raise the isoscape efficiency is to perform an integrated use with other tracing methods such as satellite tracking or combined with genetic markers (Rundel et al., 2013).

Isoscape approach used in animal migration studies could be adapted to determine the origin of seized animals and trafficking routes. There is still a huge number of live animals and animal products being seized every year in illegal activities (Alves et al., 2012; Regueira and Bernard, 2012). Illegal animal trade, most of times, results in animal withdrawal from those natural origins and move them to other regions where illegal markets, intermediate sellers or final consumers are present (Alves et al., 2012; Destro et al., 2012). Transportation caused by illegal wildlife traffic may be compared to natural bird migration, as both imply on the animal displacement at a continental scale (Destro et al., 2012).

In the forensic context, many applications should be accomplished in numerous investigation cases since it is usually necessary to link crime traces to their geographical origin (Cerling et al., 2016). In addition to wildlife illegal trade, other common crimes, such as illicit drug trafficking, wood trafficking, food frauds cases, and individual human crime investigations would benefit from isoscape approaches in the Brazilian context. All material or component seized that goes through isotopic analysis should have their isotopic ratios compared to spatial databases which may indicate the origin or traveled

path (see Cerling et al, 2016). For example, U.S. Drug Enforcement Agency (DEA) has a drug signature program, with the aim to construct specific drugs isoscapes (Chesson et al., 2018). This initiative should be replicated here, for marijuana and cocaine drugs. Shibuya et al. (2007) studied different marijuana producing regions in Brazil and could assign seized samples. This knowledge can be updated and used for drug enforcement.

Illegal logging in Brazil, especially in the Amazon region, is still a big issue, with selected species being collected using frauds in mechanisms of control (Brancalion et al., 2018). Considering the Brazilian potential for wood commercialization, certification of commercialized wood would benefit from isoscape approach considering the well-known relation between local water and wood isotopic ratios (Gori et al., 2018).

Provenance of food production for human consumption is also a forensic issue. Regional certified products have specific organoleptic and culinary qualities, such as wine, cheese, and coffee, which sometimes are subject to mislabeling or another fraud (Camim et al., 2017). Camim et al. (2017) reviewed methods and necessary legal aspects to state geographic origins of food products. Besides basic element isoscape knowledge, they state the importance of complementing isotopic information with standard values of authentic products in available databases.

Synthesis and future

The isoscape approach has been applied in different scales and its use as a basis for many scientific subjects has increased in the last decade. Its main advantage is deriving isotopic ratios with a statistical consistency in real samples points gap. Since spatial and temporal isotopic continuous maps integrate chemical processes occurring in ecosystems, the use of grid-based isoscape models has facilitated and simplified the isotope interpretation in different contexts, from terrestrial to aquatic ecosystems, either in natural or anthropic conditions.

Both global and regional $\delta^2\text{H}$ and $\delta^{18}\text{O}$ isoscapes indicate elements of water cycle, such as inputs and outputs in water pools, and have helped in water management. However, these isoscapes are also used as tracers to identify origin of animals, products and chemical elements and may amplify its utility when coupled with $\delta^{15}\text{N}$ and/or $\delta^{13}\text{C}$ isoscapes.

Existential global and continental isoscapes can already be framed into the Brazilian boundaries and applied in many studies, although they are general models with relatively

low spatial resolution, not being able to represent regional or local variations of stable isotope values. However, by improving technologies and possibilities of isoscape applications, studies tend to seek more refined isoscapes, with better spatial and temporal resolution. There is a tendency pointed out by Bowen (2010a), a transition from descriptive models to comprehensive models, where isoscapes come to help explain ecosystem mechanisms and processes, and it must be incorporated in future studies in Brazil. The Brazilian challenge will be to develop regional and local isoscapes, upscaling existing isoscapes and/or elaborating new ones from new systematic sampling.

There is a global trend for the development of an integrated and centralized isotopic database. An example is an initiative from scientists, museum curators, data analysts, and educators to build the IsoBank, which they say would be a dynamic and sustainable repository that would accelerate the resolution of urgent issues in all disciplines involving stable isotopes (Pauli et al., 2017).

Another example is the GNIP for precipitation data, which has currently 10 stations in operation in Brazil. The integration of laboratories and the establishment of a national network could increase the number of monitoring stations. However, to build a national network to collect water samples regularly and to have them analyzed to $\delta^2\text{H}$ and $\delta^{18}\text{O}$ is far from being an easy task considering the Brazilian immense territory and especially the logistics and infrastructure involved. It should take into account the need to measure the years, on a regular basis (rainfall event or least monthly). The most important is to be aware of the global networks and to be integrated with them.

Brazil has a basic structure of laboratories that carry out isotopic analyzes in the northeastern, central-western and southeastern regions, however the challenge is to increase the number of specific funding involving stable isotope research. The establishment of museum networks and integrated access to animals and plants collections has great potential to increase the spatial distribution of samples with isotopic values in Brazil. The same is for an integrated network for accessing soil samples from collections in Brazilian laboratories. Both networks would improve the access to data and the construction of isoscapes to answer current issues in biogeochemistry, ecology, conservation and forensics.

References

- Aggarwal, P.K., Romatschke, U., Araguas-Araguas, L., Belachew, D., Longstaffe, F. J., Berg, P., Schumacher, C., Funk, A., 2016. Proportions of convective and stratiform precipitation revealed in water isotope ratios. *Nat. Geosci.* 9, 624-629. <http://dx.doi.org/10.1038/ngeo2739>
- Alves, R.R.N., Pereira Filho, G.A., Vieira, K.S., Souto, W.M.S., Mendonça, L.E.T., Montenegro, P.F.G.P., Almeida, W.O., Vieira, W.L.S., 2012. A zoological catalogue of hunted reptiles in the semiarid region of Brasil. *J. Ethnobiol. Ethnomed.* 8, 1-29. <http://dx.doi.org/10.1186/1746-4269-8-27>
- Amundson, R., Austin, A.T., Schuur, E.A.G., Yoo, K., Matzek, V., Kendall, C., Uebersax, A., Brenner, D., Baisden, W. T., 2003. Global patterns of the isotopic composition of soil and plant nitrogen. *Global Biogeochem. Cycles* 17, 1031-1041. <http://dx.doi.org/10.1029/2002GB001903>
- Arnold, J., Corre, M.D., Veldkamp, E., 2009. Soil N cycling in old-growth forests across an Andosol toposequence in Ecuador. *For. Ecol. Manag.* 257, 2079-2087.
- Assad, E.D., Pinto, H.S., Martins, S.C., Groppo, J.D., Salgado, P.R., Evangelista, B., Vasconcellos, E., Sano, E.E., Pavão, E., Luna, R., Camargo, P.B., Martinelli, L.A., 2013. Changes in soil carbon stocks in Brazil due to land use: Paired site comparisons and a regional pasture soil survey. *Biogeosciences* 10, 6141-6160, <http://dx.doi.org/10.5194/bg-10-6141-2013>
- Augusto, F.G., Tassoni Filho, M., Ferrera, A., Pereira, A.L., Camargo, P.B., Martinelli, L.A., 2015. Land use change in the Atlantic Forest affects carbon and nitrogen sources of streams as revealed by the isotopic composition of terrestrial invertebrates. *Biota Neotrop.* 15. <http://dx.doi.org/10.1590/1676-06032015018814>
- Austin, A.T., Bustamante, M.M.C., Nardoto, G.B., Mitre, S.K., Pérez, T., Ometto, J.P. H.B., Ascarrunz, N.L., Forti, M.C., Longo, K., Gavito, M.E., Martinelli, L.A., 2013. Latin America's nitrogen challenge. *Science* 340, 149. <http://dx.doi.org/10.1126/science.1231679>
- Bai, E., Boutton, T.W., Ben Wu, X., Liu, F., Archer, S.R., 2009. Landscape-Scale vegetation dynamics inferred from spatial patterns of soil $\delta^{13}\text{C}$ in a subtropical savanna parkland. *J. Geophys. Res. Biogeosciences.* 114, 1-10. <http://dx.doi.org/10.1029/2008JG000839>
- Bai, E., Boutton, T.W., Liu, F., Ben Wu, X., Hallmark, C.T., Archer, S.R., 2012a. Spatial variation of soil $\delta^{13}\text{C}$ and its relation to carbon input and soil texture in a subtropical lowland woodland. *Soil Biol. Biochem.* 44, 102-112. <http://dx.doi.org/10.1016/j.soilbio.2011.09.013>
- Bai, E., Boutton, T., Liu, F., Wu, X., Archer, S., 2013. ^{15}N isoscapes in a subtropical savanna parkland: spatial-temporal perspectives. *Ecosphere* 4, n1-17. <http://dx.doi.org/10.1890/ES12-00187.1>
- Bai, E., Houlton, B.Z., Wang, Y.P., 2012b. Isotopic identification of nitrogen hotspots across natural terrestrial ecosystems. *Biogeosciences* 9, 3287-3304. <http://dx.doi.org/10.5194/bg-9-3287-2012>
- Baisden, W.T., Keller, E.D., Van Hale, R., Frew, R.D., Wassenaar, L.I., 2016. Precipitation isoscapes for New Zealand: enhanced temporal detail using

- precipitation-weighted daily climatology. *Isotopes. Environ. Health. Stud.* 52, 343-352. <http://dx.doi.org/10.1080/10256016.2016.1153472>
- Barbieri, C.B., Sarkis, J.E.S., Martinelli, L.A., Bordon, I.C.A.C., Mitteregger, H., Hortellani, M.A., 2014. Forensic evaluation of metals (Cr, Cu, Pb, Zn), isotopes ($\delta^{13}\text{C}$ and $\delta^{15}\text{N}$), and C:N ratios in freshwater sediment. *Environ. Forensics* 15, 134-146. <http://dx.doi.org/10.1080/15275922.2014.890144>
- Berhe, A.A., Bernes, R.T., Six, J., Marín-Spiotta, E., 2018. Role of soil erosion in biogeochemical cycling of essential elements: Carbon, Nitrogen, and Phosphorous. *Annu. Rev. Earth Planet. Sci.* 46, 521-548. <https://doi.org/10.1146/annurev-earth-082517-010018>
- Birkel, C., Helliwell, R., Thornton, B., Gibbs, S., Cooper, P., Soulsby, C., Tetzlaff, L., Spezia, L., Esquivel-Hernández, G., Sánchez-Murillo, R., Midwood, A.J., 2010. Characterization of surface water isotope spatial patterns of Scotland. *J. Geochem. Explor.* 194, 71-80. <http://dx.doi.org/10.1016/j.gexplo.2018.07.011>
- Boeckx, P., Van Meirvenne, M., Raulo, F., Van Cleemput, O., 2006. Spatial patterns of $\delta^{13}\text{C}$ and $\delta^{15}\text{N}$ in the urban topsoil of Gent, Belgium. *Org. Geochem.* 37, 1383-1393. <http://dx.doi.org/10.1016/j.orggeochem.2006.04.015>
- Bowen, G.J., 2010a. Isoscapes: Spatial Pattern in Isotopic Biogeochemistry. *Annu. Rev. Earth Planet. Sci.* 38, 161-187. <http://dx.doi.org/10.1146/annurev-earth-040809-152429>
- Bowen, G.J., 2010b. Statistical end geostatistical mapping of precipitation water isotope ratios. In: Isoscapes: Understanding movement, pattern, and process on earth through isotope mapping. Netherlands: Springer p.p. 139-150. http://dx.doi.org/10.1007/978-90-481-3354-3_7
- Bowen, G.J., Ehleringer, J.R., Chesson, L.A., Stange, E., Cerling, T.E., 2007. Stable isotope ratios of tap water in the contiguous United States. *Water Resour. Res.* 43, 1-12. <http://dx.doi.org/10.1029/2006WR005186>
- Bowen, G.J., Good, S.P., 2015. Incorporating water isoscapes in hydrological and water resource investigations. *WIREs Water* 2, 107-119. <http://dx.doi.org/10.1002/wat2.1069>
- Bowen, G.J., Liu, Z., Vander Zanden, H. B., Zhao, L., Takahashi, G., 2014. Geographic assignment with stable isotopes in IsoMAP. *Methods Ecol. Evol.* 5, 201-206. <https://doi.org/10.1111/2041-210X.12147>
- Bowen, G.J., Revenaugh, J., 2003. Interpolating the isotopic composition of modern meteoric precipitation. *Water Resour. Res.* 39, 1-13. <http://dx.doi.org/10.1029/2003WR002086>
- Bowen, G.J., Wassenaar, L.I., Hobson, K.A., 2005. Global application of stable hydrogen and oxygen isotopes to wildlife forensics. *Oecologia* 143, 337-348. <http://dx.doi.org/10.1007/s00442-004-1813-y>
- Bowen, G.J., West, J.B., Hoogewerff, J., 2009. Isoscapes: Isotope mapping and its applications. *J. Geochemical Explor.* 102, v-vii. <http://dx.doi.org/10.1016/j.gexplo.2009.05.001>
- Bowen, G.J., Wilkinson, B., 2002. Spatial distribution of $\delta^{18}\text{O}$ in meteoric precipitation. *Geology* 30, 315-318. [http://dx.doi.org/10.1130/0091-7613\(2002\)030<0315](http://dx.doi.org/10.1130/0091-7613(2002)030<0315)

- Brancalion, P.H.S., Almeida, D.R.A., Vidal, E., Molin, P.G., Sontag, V.E., Souza, S.E. X.F., Schulze, M.D., 2018. Fake legal logging in the Brazilian Amazon. *Sci. Adv.* 4, 1-7. <http://dx.doi.org/10.1126/sciadv.aat1192>
- Brooks, J.R., Wigington, P.J., Phillips, D.L., Comeleo, R., Coulombe, R., 2012. Willamette River Basin surface water isoscape ($\delta^{18}\text{O}$ and $\delta^2\text{H}$): temporal changes of source water within the river. *Ecosphere* 3, 1-21. <http://dx.doi.org/10.1890/ES11-00338.1>
- Bustamante, M.M.C., Martinelli, L.A., Silva, D.A., Camargo, P.B., Klink, C.A., Domingues, T.F., Santos, R.V., 2004. ^{15}N natural abundance in woody plants and soils of central Brazilian savannas (Cerrado). *Ecol. Appl.* 14, 200-213. <http://dx.doi.org/10.1890/01-6013>
- Camin, F., Boner, M., Bontempo, L., Fauhl-Hassek, C., Kelly, S.D., Riedl, J., Rossmann, A., 2017. Stable isotope techniques for verifying the declared geographical origin of food in legal cases. *Trends Food Sci. Technol.* 61, 176-187. <http://dx.doi.org/10.1016/j.tifs.2016.12.007>
- Carter, J.F., Yates, H.S.A., Tinggi, U., 2015. The isotopic and elemental composition of roasted coffee as a guide to authenticity and origin. *J. Agric. Food Chem.* 63, 5771-5779. <http://dx.doi.org/10.1021/acs.jafc.5b01526>
- Cassana, F.F., Eller, C.B., Oliveira, R.S., Dillenburg, L.R., 2015. Effects of soil water availability on foliar water uptake of *Araucaria angustifolia*. *Plant Soil* 399. <http://dx.doi.org/10.1007/s11104-015-2685-0>
- Castro, D.M.P., Carvalho, D.R., Pompeu, P.D.S., Moreira, M.Z., Nardoto, G.B., Callisto, M., 2016. Land use influences niche size and the assimilation of resources by benthic macroinvertebrates in tropical headwater streams. *PLoS One* 11, 1-19. <http://dx.doi.org/10.1371/journal.pone.0150527>
- Cerling, T.E., Barnette, J.E., Bowen, G.J., Chesson, L.A., Ehleringer, J.R., Remien, C.H., Shea, P., Tipple, B.J., West, J.B., 2016. Forensic stable isotope biogeochemistry. *Annu. Rev. Earth Planet. Sci.* 44, 175-206. <http://dx.doi.org/10.1146/annurev-earth-060115-012303>
- Cernusak, L.A., Ubierna, N., Winter, K., Holtum, J.A.M., Marshall, J.D., Farquhar, G.D., 2013. Environmental and physiological determinants of carbon isotope discrimination in terrestrial plants. *New Phytol.* 200, 950-965. <http://dx.doi.org/10.1111/nph.12423>
- Chesson, L.A., Barnette, J.E., Bowen, G.J., Brooks, J.R., Casale, J.F., Cerling, T.E., Cook, C.S., Douthitt, C.B., Howa, J.D., Hurley, J.M., Kreuzer, H.W., Lott, M.J., Martinelli, L.A., O'grady, S.P., Podlesak, D.W., Tipple, B.J., Valenzuela, L.O., West, J.B., 2018. Applying the principles of isotope analysis in plant and animal ecology to forensic science in the Americas. *Oecologia* 187, 1007-1094. <http://dx.doi.org/10.1007/s00442-018-4188-1>
- Chesson, L.A., Valenzuela, L.O., O'grady, S.P., Cerling, T.E., Ehleringer, J.R., 2010a. Hydrogen and oxygen stable isotope ratios of milk in the United States. *J. Agric. Food Chem.* 58, 2358-2363. <http://dx.doi.org/10.1021/jf904151c>
- Chesson, L.A., Valenzuela, L.O., O'grady, S.P., Cerling, T.E., Ehleringer, J.R., 2010b. Links between purchase location and stable isotope ratios of bottled water, soda,

- and beer in the united states. *J. Agric. Food Chem.* 58, 7311-7316.
<http://dx.doi.org/10.1021/jf1003539>
- Chiocchini, F., Portarena, S., Ciolfi, M., Brugnoli, E., Lauteri, M., 2016. Isoscapes of carbon and oxygen stable isotope compositions in tracing authenticity and geographical origin of Italian extra-virgin olive oils. *Food Chem.* 202, 291-301.
<http://dx.doi.org/10.1016/j.foodchem.2016.01.146>
- Coletta, L.D., Nardoto, G.B., Latansio-Aidar, S.R., Rocha, H.R., 2009. Isotopic view of vegetation and carbon and nitrogen cycles in a Cerrado ecosystem, southeastern Brazil. *Scientia Agricola* 66, 467-475. <http://dx.doi.org/10.1590/S0103-90162009000400006>
- Coletta, L.D., Pereira, A.L., Coelho, A.A.D., Savino, V.J.M., Menten, J.F.M., Correr, E., França, L.C., Martinelli, L.A., 2012. Barn vs. Free-range chickens: Differences in their diets determined by stable isotopes. *Food Chem.* 131, 155-160.
<http://dx.doi.org/10.1016/j.foodchem.2011.08.051>
- Courtiol, A., Rousset, F., Rohwäder, M., Soto, D.X., Lehnert, L., Voigt, C.C., Hobson, K.A., Wassenaar, I.I., Kramer-Schadt, S., 2019. Isoscape computation and inference of spatial origins with mixed models using the R package IsoriX. In: *Tracking Animal Migration with Stable Isotopes*, second. London: Elsevier
- Craine, J.M., Brookshire, E.N.J., Cramer, M.D., Hasselquist, N.J., Koba, K., Marin-Spiotta, E., Wang, L., 2015b. Ecological interpretations of nitrogen isotope ratios of terrestrial plants and soils. *Plant Soil* 396, 1-26. <http://dx.doi.org/10.1007/s11104-015-2542-1>
- Craine, J.M., Elmore, A.J., Wang, L., Augusto, L., Baisden, W.T., Brookshire, E.N.J., Cramer, M.D., Hasselquist, N.J., Hobbie, E.A., Kahmen, A., Koba, K., Kranabetter, J.M., Mack, M.C., Marin-Spiotta, E., Mayor, J.R., McLauchlan, K.K., Michelsen, A., Nardoto, G.B., Oliveira, R.S., Perakis, S.S., Peri, P.L., Quesada, C.A., Richter, A., Schipper, L.A., Stevenson, B.A., Turner, B.L., Viani, R.A.G., Wanek, W., Zeller, B., 2015a. Convergence of soil nitrogen isotopes across global climate gradients. *Sci. Rep.* 5. <http://dx.doi.org/10.1038/srep08280>
- Destro, G.F.G., Pimentel, T.L., Sabaini, R.M., Borges, R.C., Barreto, R., 2012. Efforts to combat wild animals trafficking in Brazil. In: *Biodiversity enrichment in a diverse world*. Intech, p.p. 421-436. <http://dx.doi.org/10.5772/48351>
- Di Benedetto, A.P.M., Rezende, C.E., Camargo, P.B., Kehrig, H.A., 2013. Trophic niche comparison between two predators in northern Rio de Janeiro State, Brazil: a stable isotopes approach. *Biota Neotrop.* 13, 29-33.
<http://dx.doi.org/10.1590/S1676-06032013000300002>
- Dias, J., Fonte, M.A.M.A., Baptista, R., Mantoani, M.C., Holdefer, D.R., Torezan, J.M. D., 2013. Invasive alien plants in Brazil: A nonrestrictive revision of academic works. *Nat. Conserv.* 11, 31-35. <http://dx.doi.org/10.4322/natcon.2013.004>
- Ehleringer, J.R., Bowen, G.J., Chesson, L.A., West, A.G., Podlesak, D.W., Cerling, T.E., 2008. Hydrogen and oxygen isotope ratios in human hair are related to geography. *Proc. Natl. Acad. Sci. U. S. A.* 105, 2788-2793.
<http://dx.doi.org/10.1073/pnas.0712228105>

- Ehleringer, J.R., Casale, J.F., Lott, M.J., Ford, V.L., 2010. Tracing the geographical origin of cocaine: Cocaine carries a chemical fingerprint from the region where the coca was grown. *Nature* 408, 311-312. <http://dx.doi.org/10.1038/35042680>
- Ehleringer, J.R., Thompson, A.H., Podlesak, D., Bowen, G.J., Chessonlesley, L.A., Cerling, T. E., Park, T., Dostie, P., Schwarcz, H., 2010. A framework for the incorporation of isotopes and isoscapes in geospatial forensic investigations. In: *Isoscapes: Understanding movement, pattern, and process on earth through isotope mapping*. Netherlands: Springer, p.p. 357-388. http://dx.doi.org/10.1007/978-90-481-3354-3_17
- Farquhar, G.D., Lloyd, J., Taylor, J.A., Lawrence, F.B., Syvertsen, J.P., Hubick, K.T., Wong, C.S., Ehleringer, J.R., 1993. Vegetation effects on the isotope composition of oxygen in atmospheric CO₂. *Nature* 363, 439-443. <http://dx.doi.org/10.1038/363439a0>
- Figueira, A.M.S., Davidson, E.A., Nagy, R.C., Riskin, S.H., Martinelli, L.A., 2016. Isotopically constrained soil carbon and nitrogen budgets in a soybean field chronosequence in the Brazilian Amazon region. *J. Geophys. Res. Biogeosciences*. 121, 2520-2529. <http://dx.doi.org/10.1002/2016JG003470>
- Fourqurean, J.W., Manuel, S.A., Coates, K.A., Kenworthy, W.J., Boyer, J.N., 2015. Water quality, isoscapes and stoichioscapes of seagrasses indicate general P limitation and unique N cycling in shallow water benthos of Bermuda. *Biogeosciences* 12, 6235-6249. <http://dx.doi.org/10.5194/bg-12-6235-2015>
- Freitas, A.D.S., Sampaio, E.V.S.B., Menezes, R.S.C., Tiessen, H., 2010. ¹⁵N natural abundance of non-fixing woody species in the Brazilian dry forest (caatinga). *Isotopes. Environ. Health. Stud.* 46, 210-218. <http://dx.doi.org/10.1080/10256016.2010.488805>
- Galetti, M., Rodarte, R.R., Neves, C.L., Moreira, M., Costa-Pereira, R., 2016. Trophic niche differentiation in rodents and marsupials revealed by stable isotopes. *PLoS One* 11. <http://dx.doi.org/10.1371/journal.pone.0152494>
- García-Pérez, B., Hobson, K.A., 2014. A multi-isotope ($\delta^2\text{H}$, $\delta^{13}\text{C}$, $\delta^{15}\text{N}$) approach to establishing migratory connectivity of Barn Swallow (*Hirundo rustica*). *Ecosphere* 5, 1-12. <http://dx.doi.org/10.3161/000164514X682896>
- Gastmans, D., Chang, H.K., Hutcheon, I., 2010. Stable isotopes (²H, ¹⁸O and ¹³C) in groundwaters from the northwestern portion of the Guarani Aquifer System (Brazil). *Hydrogeol. J.* 18, 1497-1513. <http://dx.doi.org/10.1007/s10040-010-0612-2>
- Goodchild, M.F., 2011. Scale in GIS: An overview. *Geomorphology* 130, 5-9.
- Gori, Y., Stradiotti, A., Camin, F., 2018. Timber isoscapes. A case study in a mountain area in the Italian Alps. *Plos One* 13, 1-22.
- Gragnani, J.G., Garavello, M.E.P.E., Silva, R.J., Nardoto, G.B., Martinelli, L.A., 2014. Can stable isotope analysis reveal dietary differences among groups with distinct income levels in the city of Piracicaba (southeast region, Brazil)? *J. Acad. Nutr. Diet.* 27, 270-279. <http://dx.doi.org/10.1111/jhn.12148>
- Gutiérrez-Expósito, C., Ramírez, F., Afán, I., Forero, M.G., Hobson, K.A., 2015. Toward a deuterium feather isoscape for sub-Saharan Africa: Progress, challenges

and the path ahead. PLoS One 10, 1-12.
<http://dx.doi.org/10.1371/journal.pone.0135938>

Hardt, F.A.S., Cremer, M.J., Tonello Junior, A.J., Bellante, A., Buffa, G., Buscaino, G., Mazzola, S., Barreto, A.S., Martinelli, L.A., ZUPPI, G.M., 2013. Use of carbon and nitrogen stable isotopes to study the feeding ecology of small coastal cetacean populations in southern Brazil. Biota Neotrop. 13, 90-98.
<http://dx.doi.org/10.1590/S1676-06032013000400009>

Hellmann, C., Grobe-Stoltenberg, A., Thiele, J., Oldeland, J., Werner, C., 2017. Heterogeneous environments shape invader impacts: integrating environmental, structural and functional effects by isoscapes and remote sensing. Sci. Rep. 7, 1-11.

Hellmann, C., Rascher, K.G., Oldeland, J., Werner, C., 2016b. Isoscapes resolve species-specific spatial patterns in plant-plant interactions in an invaded Mediterranean dune ecosystem. Tree Physiol. 36, 1460-1470.
<http://dx.doi.org/10.1093/treephys/tpw075>

Hellmann, C., Werner, C., Oldeland, J., 2016a. A spatially explicit dual-isotope approach to map regions of plant-plant interaction after exotic plant invasion. PLoS One 11, 1-16<http://dx.doi.org/10.1111/j.1461-0248.2012.01761.x>

Hénaux, V., Powell, L.A., Hobson, K.A., Nielsen, C.K., Larue, M.A., 2011. Tracking large carnivore dispersal using isotopic clues in claws: an application to cougars across the Great Plains. Method. Ecol. Evol. 2, 489-499.
<http://dx.doi.org/10.1111/j.2041-210X.2011.00107.x>

Hilton, R.G., Galy, A., West, A.J., Hovius, N., Roberts, G.G., 2013. Geomorphic control on the $\delta^{15}\text{N}$ of mountain forests. Biogeosciences 10, 1693-1705.
<http://dx.doi.org/10.5194/bg-10-1693-2013>

Hobson, K.A., Barnet-Johnson, R., Cerling, T., 2010. Using isoscapes to track animal migration. In: Isoscapes: Understanding movement, pattern, and process on earth through isotope mapping. Netherlands: Springer, p.p. 273-298.
http://dx.doi.org/10.1007/978-90-481-3354-3_13

Hobson, K.A., Doward, K., Kardynal, K.J., Mcneil, J.N., 2018. Inferring origins of migrating insects using isoscapes: a case study using the true armyworm, *Mythimna unipuncta*, in North America. Ecol. Entomol. 43, 332-341.
<http://dx.doi.org/10.1111/een.12505>

Hobson, K.A., Kardynal, K.J., 2016. An isotope ($\delta^{34}\text{S}$) filter and geolocator results constrain a dual feather isoscape ($\delta^2\text{H}$, $\delta^{13}\text{C}$) to identify the wintering grounds of North American Barn Swallows. The Auk: Ornithological Advances 133, 86-98.
<http://dx.doi.org/10.1642/AUK-15-149.1>

Hobson, K.A., Van Wilgenburg, S.L., Larson, K., Wassenaar, L.I., 2009. A feather hydrogen isoscape for Mexico. J. Geochem. Explor. 102, 167-174.
<http://dx.doi.org/10.1016/j.gexplo.2009.02.002>

Hobson, K.A., Van Wilgenburg, S.L., Wassenaar, L.I., Powell, R.L., Still, C.J., Craine, J.M., 2012b. A multi-isotope ($\delta^{13}\text{C}$, $\delta^{15}\text{N}$, $\delta^2\text{H}$) feather isoscape to assign Afrotropical migrant birds to origins. Ecosphere 3, 1-20.
<http://dx.doi.org/10.1890/ES12-00018.1>

Hobson, K.A., Van Wilgenbug, S.L., Wassenaar, L.I., Larson, K., 2012a. Linking hydrogen (d2H) isoscapes in feathers and precipitation: sources of variance and

- consequences for assignment to isoscapes. PLoS One 7, e35137.
<http://dx.doi.org/10.1371/journal.pone.0035137>
- Houlton, B.Z., Marklein, A.R., Bai, E., 2015. Representation of nitrogen in climate change forecasts. Nat. Publ. Gr. 5, 398-401. <http://dx.doi.org/10.1038/nclimate2538>
- IAEA/WMO. Global Network of Isotopes in Precipitation. The GNIP Database. International Atomic Energy Agency, Vienna, Austria. 2015.
- Jackson, P.C., Meinzer, F.C., Bustamante, M., Goldstein, G., Franco, A., Rundel, P. W., Caldas, L., Igler, E., Causin, F., 1999. Partitioning of soil water among tree species in a Brazilian Cerrado ecosystem. Tree Physiol. 19, 717-724.
<http://dx.doi.org/10.1093/treephys/19.11.717>
- Jasechko, S., Sharp, Z.D., Gibson, J. J., Birks, S. J., Yi, Y., Fawcett, P. J., 2010. Terrestrial water fluxes dominated by transpiration. Nature 496, 347-350.
- Kern, Z., Kohán, B., Leuenberger, M., 2014. Precipitation isoscape of high reliefs: Interpolation scheme designed and tested for monthly resolved precipitation oxygen isotope records of an Alpine domain. Atmospheric Chem. Phys. 14, 1897-1907.
<http://dx.doi.org/10.5194/acp-14-1897-2014>
- Lins, S.R.M., Coletta, L.D., Ravagnani, E.C., Gragnani, J.G., Mazzi, E.A., Martinelli, L.A., 2016. Stable carbon composition of vegetation and soils across an altitudinal range in the coastal Atlantic Forest of Brazil. Trees 30, 1315-1329.
<http://dx.doi.org/10.1007/s00468-016-1368-7>
- Liu, Z., Bowen, G.J., Welker, J.M., 2010. Atmospheric circulation in reflected in precipitation isotope gradients over the conterminous United States. J. Geochem. Explor. 115, d22120. <http://dx.doi.org/10.1029/2010JD014175>
- Lloyd, J., Farquhar, G.D., 1994. ^{13}C discrimination during CO_2 assimilation by the terrestrial biosphere. Oecologia 99, 201-215.
<http://dx.doi.org/10.1007/BF00627732>
- Mallette, J.R., Casale, J.F., Jordan, J., Morello, D.R., Beyer, P.M., 2016. Geographically sourcing cocaine's origin - Delineation of the nineteen major cocoa growing regions in South America. Sci. Rep. 6, 1-10. <http://dx.doi.org/10.1038/srep23520>
- Mardegan, S.F., Andrade, T.M.B., Sousa Neto, E.R., Vasconcellos, E.B.C., Martins, L.F.B., Mendonça, T.G., Martinelli, L.A., 2013. Stable carbon isotope composition of Brazilian beers - A comparison between large- and small-scale breweries. J. Food Compos. Anal. 29, 52-57. <http://dx.doi.org/10.1016/j.jfca.2012.10.004>
- Martinelli, L.A., Gat, J.R., Camargo, P.B., Lara, L.L., Ometto, J.P.H.B., 2004. The Piracicaba River basin: isotope hydrology of a tropical river basin under anthropogenic stress. Isotopes. Environ. Health. Stud. 40, 45-56.
<http://dx.doi.org/10.1080/10256010310001652016>
- Martinelli, L.A., Moreira, M.Z., Ometto, J.P.H.B., Alcarde, A.R., Rizzon, L.A., Stange, E., Ehleringer, J.R., 2003. Stable carbon isotopic composition of the wine and CO_2 bubbles of sparkling wines: detecting C_4 sugar additions. J. Agric. Food Chem. 51, 2625-2631. <http://dx.doi.org/10.1021/jf026088c>
- Meier-Augenstein, W., Hobson, K.A., Wassenaar, L.I., 2013. Critique: measuring hydrogen stable isotope abundance of proteins to infer origins of wildlife, food and people. Bioanalysis 5, 751-767. <http://dx.doi.org/10.4155/bio.13.36>

- Morais, M.C., Pellegrinetti, T.A., Sturion, L.C., Sattolo, T.M.S., Martinelli, L.A., 2018. Stable carbon isotopic composition indicates large presence of maize in Brazilian soy sauces (*shoyu*). *J. Food Compos. Anal.* 70, 18-21. <https://doi.org/10.1016/j.jfca.2018.04.001>
- Moreira, M.Z., Sternberg, L.S.L., Martinelli, L.A., Victoria, R.L., Barbosa, E.M., Bonates, L.C.M., Nepstad, D.C., 1997. Contribution of transpiration to forest ambient vapour based on isotopic measurements. *Glob. Chang. Biol.* 3, 439-450. <http://dx.doi.org/10.1046/j.1365-2486.1997.00082.x>
- Mueller, M.H., Alaoui, A., Kuells, C., Leistert, H., Meusburger, K., Stumpp, C., Weiler, M., Alewell, C., 2014. Tracking water pathways in steep hillslopes by $\delta^{18}\text{O}$ depth profiles of soil water. *J. Hydrol.* 519, 340-352. <http://dx.doi.org/10.1016/j.jhydrol.2014.07.031>
- Murphy, B.P., Bowman, D., 2009. The carbon and nitrogen isotope composition of Australian grasses in relation to climate. *Landsc. Ecol.* 23, 1040-1049. <http://dx.doi.org/10.1111/j.1365-2435.2009.01576.x>
- Nardoto, G.B., Murrieta, R.S.S., Prates, L.E.G., Adams, C., Garavello, M.E.P.E., Schor, T., Moraes, A., Rinaldi, F.D., Gragnani, J.G., Moura, E.A.F., Duarte-Neto, P.J., Martinelli, L.A., 2011. Frozen chicken for wild fish: Nutritional transition in the Brazilian Amazon region determined by carbon and nitrogen stable isotope ratios in fingernails. *Am. J. Hum. Biol.* 23, 642-650. <http://dx.doi.org/10.1002/ajhb.21192>
- Nardoto, G.B., Ometto, J.P.H.B., Ehleringer, J.R., Higuchi, N., Bustamante, M.M.C., Martinelli, L.A., 2008. Understanding the influences of spatial patterns on N availability within the Brazilian Amazon Forest. *Ecosystems* 11, 1234-1246. <http://dx.doi.org/10.1007/s10021-008-9189-1>
- Nardoto, G.B., Quesada, C.A., Patiño, S., Saiz, G., Baker, T.R., Schwarz, M., Schrodt, F., Feldpausch, T.R., Domingues, T.F., Marimon, B.S., Marimon, Junior, B.H., Vieira, I.C.G., Silveira, M., Bird, M.I., Phillips, O.L., Lloyd, J., Martinelli, L.A., 2014. Basin-wide variations in Amazon forest nitrogen-cycling characteristics as inferred from plant and soil ^{15}N : ^{14}N measurements. *Plant Ecol. Divers.* 7, 173-187. <http://dx.doi.org/10.1080/17550874.2013.807524>
- Nardoto, G.B., Silva, S., Kendall, C., Ehleringer, J.R., Chesson, L.A., Ferraz, E.S.B., Moreira, M.Z., Ometto, J.P.H.B., Martinelli, L.A., 2006. Geographical patterns of human diet derived from stable-isotope analysis of fingernails. *Am. J. Phys. Anthropol.* 131, 137-146. <http://dx.doi.org/10.1002/ajpa.20409>
- Nielsen, J.A., Frew, R.D., Whigham, P.A., Callaway, R.M., Dickinson, K.J.M., 2016. Thyme travels: ^{15}N isoscapes of *Thymus vulgaris L.* invasion in lightly grazed pastoral communities. *Austral Ecol.* 41, 28-39. <http://dx.doi.org/10.1111/aec.12284>
- Nitzsche, K.N., Verch, G., Premke, K., Gessler, A., Kayler, Z.E., 2016. Visualizing land-use and management complexity within biogeochemical cycles of an agricultural landscape. *Ecosphere* 7, 1-16. <http://dx.doi.org/10.1002/ecs2.1282>
- Oliver, M.A., Webster, R., 2014. A tutorial guide to geostatistics: Computing and modelling variograms and kriging. *Catena* 113, 56-69. <http://dx.doi.org/10.1016/j.catena.2013.09.006>
- Ometto, J.P.H.B., Ehleringer, J.R., Domingues, T.F., Berry, J.A., Ishida, F.Y., Mazzi, E., Higuchi, N., Flanagan, L.B., Nardoto, G.B., Martinelli, L.A., 2006. The stable

carbon and nitrogen isotopic composition of vegetation in tropical forests of the Amazon Basin, Brazil. *Biogeochemistry* 79, 251-274.
<http://dx.doi.org/10.1007/s10533-006-9008-8>

Ometto, J.P.H.B., Flanagan, L.B., Martinelli, L.A., Ehleringer, J.R., 2005. Oxygen isotope ratios of waters and respired CO₂ in Amazonian forest and pasture ecosystem. *Ecol. Appl.* 15, 58-70. <http://dx.doi.org/10.1890/03-5047>

Ometto, J.P.H.B., Flanagan, L.B., Martinelli, L.A., Moreira, M.Z., Higuchi, N., Ehleringer, J.R., 2002. Carbon isotope discrimination in forest and pasture ecosystems of the Amazon Basin, Brazil. *Global Biogeoch. Cycles* 16, 1-10. <http://dx.doi.org/10.1029/2001GB001462>

Orchard, K.A., Cernusak, L.A., Hutley, L.B., 2010. Photosynthesis and water-use efficiency of seedlings from northern Australian monsoon forest, savanna, and swamp habitats grown in a common garden. *Funct. Plant Biol.* 37, 1050-1060. <http://dx.doi.org/10.1071/FP09306>

Pauli, J.N., Newsome, S.D., Cook, J.A., Harrod, C., Shawn, S.A., Baker, C.J.O., Ben-David, M., Bloom, D., Bowen, G.J., Cerling, T.E., Cicero, C., Cook, C., Dohm, M., Dahrampal, P.S., Graves, G., Groppi, R., Hobson, K.A., Jordan, C., Macfadden, B., Birch, S.P., Poelen, J., Ratnasingham, S., Rossel, L., Stricker, C.A., Uhen, M.D., Yarnes, C.T., Hayden, B., 2017. Why we need a centralized repository for isotopic data. *PNAS* 114, 2997-3001. <http://dx.doi.org/10.1073/pnas.1701742114>

Pardo, L.H., Nadelhoffer, K.J., 2010. Using nitrogen isotope ratios to assess terrestrial ecosystems at regional and global scales. In: *Isoscapes: Understanding movement, pattern, and process on earth through isotope mapping*. Netherlands: Springer, p.p. 212-250.

Peeva, A. IAEA Helps Brazil Strengthen Isotope Monitoring of Precipitation. Available in: <<https://www.iaea.org/newscenter/news/iaea-helps-brazil-strengthen-isotope-monitoring-of-precipitation>>. Access in December 2018.

Pérez, T., Garcia-Montiel, D., Trumbore, S., Tyler, S., Camargo, P.B., Moreira, M., Piccolo, M., Cerri, C., 2006. Nitrous oxide nitrification and denitrification ¹⁵N enrichment factors from amazon forest soils. *Ecol. Appl.* 16, 2153-2167. [http://dx.doi.org/10.1890/10510761\(2006\)016\[2153:NONADN\]2.0.CO](http://dx.doi.org/10.1890/10510761(2006)016[2153:NONADN]2.0.CO).

Powell, R.L., Yoo, E.H., Still, C.J., 2012. Vegetation and soil carbon-13 isoscapes for South America: integrating remote sensing and ecosystem isotope measurements. *Ecosphere* 3, 1-25. <http://dx.doi.org/10.1890/ES12-00162.1>

Powers, J.S., 2006. Spatial variation of soil organic carbon concentrations and stable isotopic composition in 1-ha plots of forest and pasture in Costa Rica: Implications for the natural abundance technique. *Biol. Fert. Soils* 42, 580-584. <http://dx.doi.org/10.1007/s00374-005-0054-5>

Rascher, K.G., Hellmann, C., Mágua, C., Werner, C., 2012. Community scale ¹⁵N isoscapes: Tracing the spatial impact of an exotic N₂-fixing invader. *Ecol. Lett.* 15, 484-491. <http://dx.doi.org/10.1111/j.1461-0248.2012.01761.x>

Reed, E.T., Kardynal, K.J., Horrocks, J.A., Hobson, K. A., 2018. Shorebird hunting in Barbados: Using stable isotopes to link the harvest at a migratory stopover site with sources of production. *The Condor* 120, 357-370. <http://dx.doi.org/10.1650/CONDOR-17-127.1>

- Regueira, R.F.S., Bernard, E., 2012. Wildlife sinks: Quantifying the impact of illegal bird trade in street markets in Brazil. *Biol. Conserv.* 149, 16-22.
<http://dx.doi.org/10.1016/j.biocon.2012.02.009>
- Rodrigues, L.P.F., Carvalho, R.C., Maciel, A., Otanasio, P.N., Garavelho, M.E.P. E., Nardoto, G.B., 2016. Food insecurity in urban and rural areas in Central Brazil: Transition from locally produced foods to processed items. *Ecol. Food Nutr.* 55, 365-377. <http://dx.doi.org/10.1080/03670244.2016.1188090>
- Rodríguez-Pérez, M.Y., Auriolles-Gamboa, D., Sánchez-Velasco, L., Lavín, M.F., Newsome, S.D., 2018. Identifying critical habitat of the endangered vaquita (*Phocoena sinus*) with regional $\delta^{13}\text{C}$ and $\delta^{15}\text{N}$ isoscapes of the upper gulf of California, Mexico. *Mar. Mam. Sci.* 34, 790-805.
<http://dx.doi.org/10.1111/mms.12483>
- Roth, F., Lessa, G.C., Wild, C., Kikuchi, R.K.P., Naumann, M.S., 2016. Impact of a high-discharge submarine sewage outfall on water quality in the coastal zone of Salvador (Bahia, Brazil). *Mar. Pollut. Bull.* 106, 43-48.
<http://dx.doi.org/10.1016/j.marpolbul.2016.03.048>
- Rundel, C.W., Wunder, M.B., Alvarado, A.H., Ruegg, K.C., Harrigan, R., Schuh, A., Kelly, J.F., Siegel, R.B., Desante, D.F., Smith, T.B., Novembre, J., 2013. Novel statistical methods for integrating genetic and stable isotope data to infer individual-level migratory connectivity. *Molecular Ecol.* 22, 4163-4176.
<http://dx.doi.org/10.1111/mec.12393>
- Salemi, L.F., Lins, S.R.M., Ravagnani, E.D.C., Frosini, S., Ferraz, D.B., Martinelli, L.A., 2016. Past and present land use influences on tropical riparian zones: an isotopic assessment with implications for riparian forest width determination. *Biota Neotrop.* 16. <http://dx.doi.org/10.1590/1676-0611-BN-2015-0133>
- Salgado, S.S., Motta, P.C., Aguiar, L.M.S., Nardoto, G.B., 2014. Tracking dietary habits of cave arthropods associated with deposits of hematophagous bat guano: A study from a neotropical savanna. *Austral Ecol.* 39, 560-566.
<http://dx.doi.org/10.1111/aec.12116>
- Sanaiotti, T.M., Martinelli, L.A., Victoria, R.L., Trumbore, S.E., Camargo, P.B., 2002. Past vegetation changes in Amazon savannas determined using carbon isotopes of soil organic matter. *Biotropica* 34, 2-16. <http://dx.doi.org/10.1111/j.1744-7429.2002.tb00237.x>
- Shibuya, E.K., Sarkis, J.E.S., Nigrino-Neto, O., Ometto, J.P.H.B., 2007. Multivariate classification based on chemical and stable isotopic profiles in sourcing the origin of marijuana samples seized in Brazil. *J. Braz. Chem. Soc.* 18, 205-214.
<http://dx.doi.org/10.1590/S0103-50532007000100024>
- Siqueira, D.S., Marques, J., Pereira, G.T., 2010. The use of landforms to predict the variability of soil and orange attributes. *Geoderma* 155, 55-66.
<http://dx.doi.org/10.1016/j.geoderma.2009.11.024>
- Soler I Gil, A., Bonotto, D.M., 2014. Hydrochemical and stable isotopes (H, O, S) signatures in deep groundwaters of Paraná basin, Brazil. *Environ. Earth Sci.* 73, 95-113. <http://dx.doi.org/10.1007/s12665-014-3397-0>
- Soto, D.X., Koehler, G., Wassenaar, L.I., Hobson, K.A., 2017. Re-evaluation of the hydrogen stable isotopic composition of keratin calibration standards for wildlife

- and forensic science applications. *Rapid. Commun. Mass. Spectrom.* 31, 1193-1203. <http://dx.doi.org/10.1002/rcm.7893>
- Still, C.J., Powell, R.L., 2010. Continental-scale distributions of vegetation stable carbon isotope ratios. In: Isoscapes: Understanding movement, pattern, and process on earth through isotope mapping. Netherlands: Springer, pp. 179-194. http://dx.doi.org/10.1007/978-90-481-3354-3_9
- Suits N.S., Denning A.S., Berry J.A., Still C.J., Kaduk J., Miller J.B., Baker I.T., 2005. Simulation of carbon isotope discrimination of the terrestrial biosphere. *Global Biogeoch. Cycles* 19, 1-15. <http://dx.doi.org/10.1029/2003GB002141>
- Teixeira, F.C.P., Reinert, F., Rumjanek, N.G., Boddey, R.M., 2006. Quantification of the contribution of biological nitrogen fixation to *Cratylia mollis* using the ^{15}N natural abundance technique in the semi-arid Caatinga region of Brazil. *Soil Biol. Biochom.* 38, 1989-1993. <http://dx.doi.org/10.1016/j.soilbio.2005.11.013>
- Terzer, S., Wassenaar, L.I., Araguás-Araguás, L.J., Aggarwal, P.K., 2013. Global isoscapes for $\delta^{18}\text{O}$ and $\delta^2\text{H}$ in precipitation: Improved prediction using regionalized climatic regression models. *Hydrol. Earth Syst. Sci.* 17, 4713-4728. <http://dx.doi.org/10.5194/hess-17-4713-2013>
- Valenzuela, L.O., Chesson, L.A., O'grady, S.P., Cerling, T.E., Ehleringer, J.R., 2011. Spatial distributions of carbon, nitrogen and sulfur isotope ratios in human hair across the central United States. *Rapid. Commun. Mass. Spectrom.* 25, 861-868. <http://dx.doi.org/10.1002/rcm.4934>
- Vander Zanden, H.B., Nelson, D., Wunder, M.B., Conkling, T.J., Katzner, T., 2018. Application of isoscapes to determine geographic origin of terrestrial wildlife for conservation and management. *Biol. Conserv.* 228, 268-280. <https://doi.org/10.1016/j.biocon.2018.10.019>
- Vander Zanden, H.B., Wunder, M.B., Hobson, K.A., Van Wilgenburg, S.L., Wassenaar, L.I., Welker, J.M., Bowen, G.J., 2015. Space-time tradeoffs in the development of precipitation-based isoscape models for determining migratory origin. *J. Avian Biol.* 46, 658-667. <http://dx.doi.org/10.1111/jav.00656>
- Viani, R.A.G., Rodrigues, R.R., Dawson, T.E., Oliveira, R.S., 2011. Functional differences between woodland savannas and seasonally dry forests from south-eastern Brazil: Evidence from ^{15}N natural abundance studies. *Austral Ecol.* 36, 974-982. <http://dx.doi.org/10.1111/j.1442-9993.2010.02233.x>
- Vitória, A.P., Ávila-Lovera, E., Vieira, T.O., Couto-Santos, A.P.L., Pereira, T.J., Funch, L.S., Freitas, L., Miranda, L.D.P., Rodrigues, P.J.F.P., Rezende, C.E., Santiago, L.S., 2018. Isotopic composition of leaf carbon ($\delta^{13}\text{C}$) and nitrogen ($\delta^{15}\text{N}$) of deciduous and evergreen understorey trees in two tropical Brazilian Atlantic forests. *J. Trop. Ecol.* 34, 145-156. <http://dx.doi.org/10.1017/S0266467418000093>
- Wang, L., Okin, G.S., D'odorico, P., Caylor, K.K., Macko, S.A., 2013. Ecosystem-scale spatial heterogeneity of stable isotopes of soil nitrogen in African savannas. *Landsc. Ecol.* 28, 685-698.
- Warner, M.M., Plemons, A.M., Heemann, N.P., Regan, L.A., 2018. Refining stable oxygen and hydrogen isoscapes for the identification of human remains in Mississippi. *J. Forensic Sci.* 63, 395-402.

- Weintraub, S.R., Cole, R.J., Schmitt, Cg., All, J.D., 2016. Climatic controls on the isotopic composition and availability of soil nitrogen across mountainous tropical forest. *Ecosphere* 7, 1-13. [http://dx.doi.org/10.1002/ecs2.1412/supinfo](http://dx.doi.org/10.1002/ecs2.1412)
- Weintraub, S.R., Taylor, P.G., Porder, S., Cleveland, C.C., Asner, G.P., Townsend, A.R., 2015. Topographic controls on soil nitrogen availability in a lowland tropical forest. *Ecology* 96, 1561-1574. <http://dx.doi.org/10.1890/14-0834.1>
- West, J.B., Bowen, G.J., Cerling, T.E., Ehleringer, J.R., 2006. Stable isotope as one of nature's ecological recorders. *Trends Ecol. Evol.* 21, 408-414. <http://dx.doi.org/10.1016/j.tree.2006.04.002>
- West, J.B., Bowen, G.J., Dawson, T.E., Tu, K.P., 2010. Isoscapes: Understanding movement, pattern, and process on earth through isotope mapping. Netherlands: Springer.
- West, J.B., Sobek, A., Ehleringer, J.R., 2008. A simplified GIS approach to modeling global leaf water isoscapes. *PLoS One* 3, 1-8. <http://dx.doi.org/10.1371/journal.pone.0002447>
- Wunder, M.B., 2012. Determining geographic patterns of migration and dispersal using stable isotopes in keratins. *J. Mammal.* 93, 360-367. <http://dx.doi.org/10.1644/11-MAMM-S-182.1>
- Wunder, M.B., Norris, D.R., 2008. Improved estimates of certainty in stable-isotope-based methods for tracking migratory animals. *Ecol. Appl.* 18, 549-559.
- Zenni, R.D., Ziller, S.R., 2011. An overview of invasive plants in Brazil. *Rev. Bras. Bot.* 34, 431-446.

CAPÍTULO 2 - RECONSTRUCTING CONTINENTAL-SCALE VARIATION IN SOIL $\delta^{15}\text{N}$: A MACHINE LEARNING APPROACH IN SOUTH AMERICA*

*Artigo em revisão na revista *Ecosphere*:

SENA-SOUZA, João Paulo; HOULTON, Benjamin Z; MARTINELLI, Luiz Antônio; NARDOTO, Gabriela Bielefeld. 2019. Reconstructing continental-scale variation in soil $\delta^{15}\text{N}$: A machine learning approach in South America. *Ecosphere*. under review.

Abstract

Soil nitrogen isotope composition ($\delta^{15}\text{N}$) is an essential tool for investigating ecosystem nitrogen balances, plant-microbe interactions, ecological niches, animal migration, food origins, and forensics. Advancement of these and other applications are limited by a lack of robust geo-spatial models that are capable of capturing variation in soil $\delta^{15}\text{N}$ (i.e., isotopic landscapes or isoscapes). Due to the complexity of the nitrogen cycle and general scarcity of isotopic information, previous approaches have reconstructed regional to global soil $\delta^{15}\text{N}$ patterns via highly uncertain linear regression models. Here, we develop a new machine learning approach to ascertain a finer-scale understanding of geographic differences in soil $\delta^{15}\text{N}$, using the S. American continent as a test case. We use a training set spanning 278 geographic locations across the continent, spanning all major biomes. We tested three different machine-learning methods: Cubist, Random Forest (RF), and Stochastic Gradient Boosting (GBM). 10-fold cross-validation revealed that the RF method outperformed both the Cubist and GBM approaches. Variable importance analysis of the RF framework pointed to biome-type as the most crucial auxiliary variable, followed by soil organic carbon content, in determining the model performance. We thereby created a biogeographic boundary map, which predicted an expected multi-scale spatial pattern of soil $\delta^{15}\text{N}$ with a high degree of confidence ($R^2 = 0.62$, $p < 0.001$) performing substantially better than all previous approaches for the continent of South America. Therefore, the new RF machine learning framework showed to be a great opportunity to explore upon a broad array ecological, biogeochemical, and forensic issues through the lens of soil $\delta^{15}\text{N}$.

Keywords: isoscape, machine learning, nitrogen cycle, stable nitrogen isotopes, soil nitrogen, random forest.

Introduction

Coherent patterns of soil nitrogen (N) isotope composition ($\delta^{15}\text{N}$) have been used to constrain an array of N cycling processes, including N fixation, mineralization, nitrification, denitrification, and leaching, leading to improved understanding of global biogeochemical fluxes and forecasts (e.g., Robinson, 2001, Houlton and Bai, 2009, Vitousek et al., 2013, Houlton et al., 2015, Zhu and Riley, 2015, Denk et al., 2017). Moreover, $\delta^{15}\text{N}$ isotopic landscapes, or isoscapes, can provide critical spatial baseline information for examining animal migration (Hobson et al., 2012, Garcia-Perez and Hobson, 2014), forensic drug trafficking, and tracing food origins (Chesson et al., 2018). However, uncertainty over spatial patterns of soil $\delta^{15}\text{N}$ is a significant obstacle to further advancing various N isotopic modeling approaches, with widespread implications for diverse fields of inquiry (Amundson et al., 2003, Bai and Houlton, 2009, Bai et al. 2012).

The first spatially explicit soil $\delta^{15}\text{N}$ map was created by using as simple regressions between $\delta^{15}\text{N}$ and climate, based on a select number of the data extrapolated to continents and the globe (Amundson et al., 2003). More recently, studies have included clay and organic carbon content in such global soil $\delta^{15}\text{N}$ analysis (Craine et al., 2015b). While these past approaches have proven insightful, they are yet to provide a robust, spatial representation of N isotope composition across diverse ecosystems and landscapes, where soil $\delta^{15}\text{N}$ can vary from -4 ‰ in temperate ecosystems to 20 ‰ in tropical ecosystems (Martinelli et al., 1999). Furthermore, previous global models tend to mask critical regional variations of soil $\delta^{15}\text{N}$ within biomes (Freitas et al., 2010). Within savanna ecosystems, for example, the spatial pattern of soil $\delta^{15}\text{N}$ at regional scale does not adhere to predictions of global models (Cheng et al., 2009, Chen et al., 2018, Freitas et al., 2010). Therefore, methods that integrate discrete and categorical variables can be essential tools for advancing our ability to reconstruct soil $\delta^{15}\text{N}$ variation, both within and among ecosystems.

Here, we explore the use of machine learning approaches in the assessment of spatial patterns of soil $\delta^{15}\text{N}$ in S. America. Ensemble learning algorithms are a class of machine learning techniques that combine several models to build a robust final prediction. Unlike other approaches, ensemble learning algorithms have the distinct advantage of integrating digital mapping of soil attributes as both discrete and continuous variables (Hengl et al., 2017, Gomes et al., 2019). Recent papers have shown that ensemble machine learning methods can produce more accurate results in mapping soil

attributes when compared to neural networks and linear models (Bataille et al., 2018, Gomes et al. 2019, Hengl et al., 2018). Among the most widely used ensemble learning algorithms are the cubist (Adhikari et al., 2014, Gray et al., 2015, Viscarra Rossel et al., 2016), stochastic gradient boosting (Yang et al., 2016), and random forest (Bataille et al., 2018, Gomes et al. 2019, Hengl et al., 2018, Hounkpatin et al., 2018, Yang et al., 2016) varieties. These methods are also emerging as a robust alternative for mapping isotopic variations in the environment (Bataille et al., 2018).

Despite the full range of applications in mapping soil attributes, machine learning approaches are yet to be systematically applied to the problem of soil $\delta^{15}\text{N}$, at regional to continental scales. Our objective was to generate soil $\delta^{15}\text{N}$ isoscape for S. America by testing a variety of machine learning approaches. This information is useful for constraining fluxes of nitrogen in this globally important set of ecosystems.

Methods

Study area and soil $\delta^{15}\text{N}$ dataset

We added 422 new samples to our compilation of 1169 published soil $\delta^{15}\text{N}$ analyses in unmanaged vegetation to create the training data set and validation of our machine learning model. We used the Web Plot Digitizer to extract values from plots when data were not available in tables (Rohatgi, 2018). We used a total of 278 georeferenced locations distributed across Brazil, Argentina, Chile, Peru, Venezuela, Ecuador, and Colombia (Appendix S1, Table S1 – ANEXO A) in our study. We converted the geographic coordinate system to decimal latitude and longitude WGS-84. We considered only soil sampled above 20 cm of depth. For locations with multiple depth values between 0 and 20 cm, we standardized $\delta^{15}\text{N}$ by calculating weighted means of N percent. We did not select deeper soil, because there is a strong correlation between surface and deep soil $\delta^{15}\text{N}$ (Amundson et al. 2003). The geographic distribution of data encompassed seven of the nine biomes in South America, according to World Wild Foundation biomes boundaries (Olson et al., 2001) (Figure 2.1).

We aggregated geographical locations ≤ 1 km distance (~ 0.01 degree) and calculated mean soil $\delta^{15}\text{N}$ among aggregated points by using the *aggregate* function in R package *sp*, thus reducing over-representation of specific sites and any spatial biases.

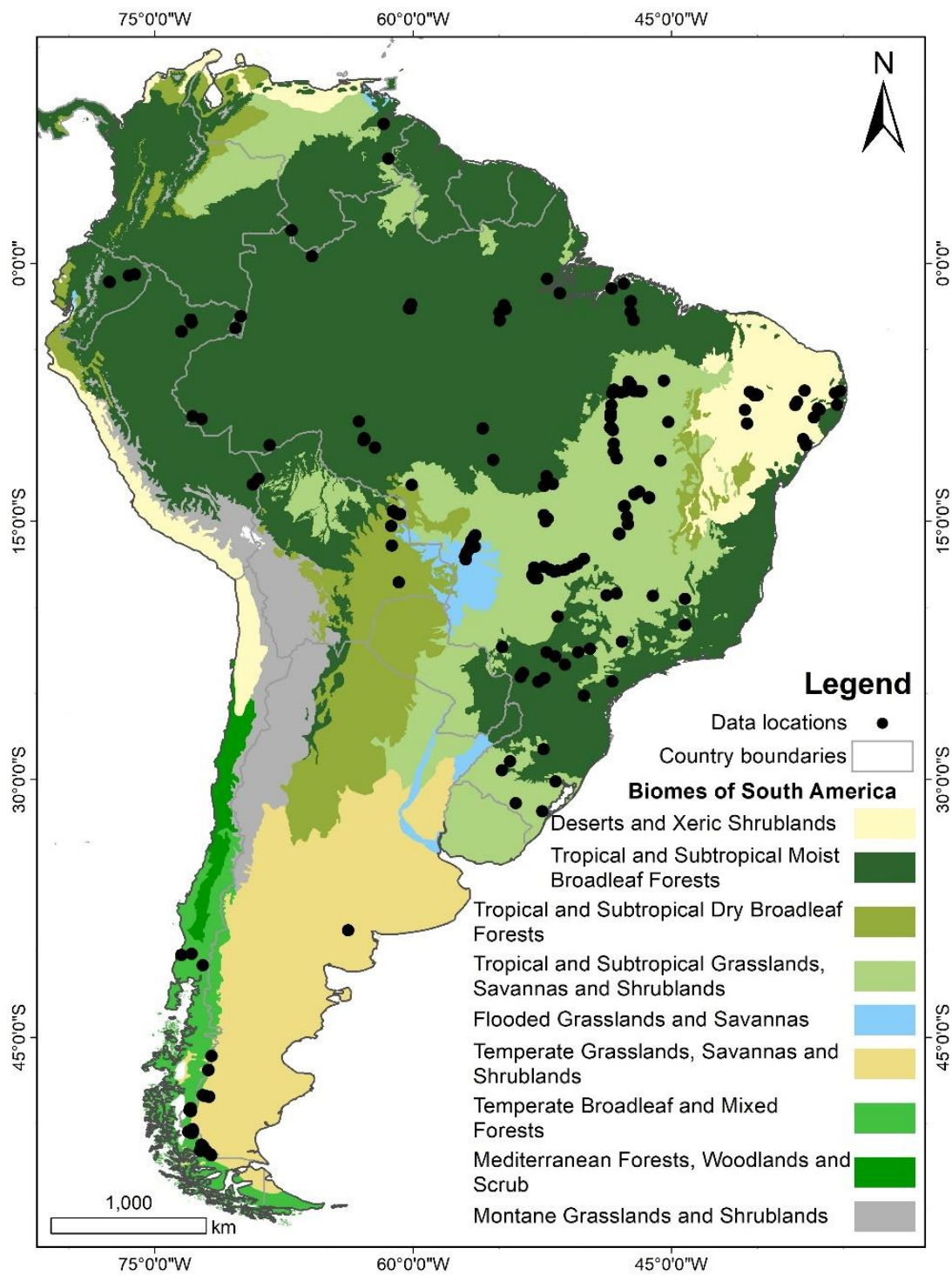


Figure 2.1. South America continent showing its biomes (see legend) and geographical locations of the compiled dataset (black circles).

Soil sampling and isotopic analysis

We collected some set of samples for this study in fragments of original vegetation. We sampled at 0-20 cm depth interval by using a Dutch soil sampler. Soil samples were air dried and sieved using 2 mm mesh to a level of Air-Dried Fine Earth (ADFE). A subsample of 30 to 35 mg of soil was placed into tin capsules for N and

isotopic analysis using an elemental analyzer (Carlo Erba, model 1110, Milan, Italy). Combustion products were purified in a gas chromatography column and introduced directly into a mass spectrometer for isotopic analysis (ThermoQuest-Finnigan Delta Plus, Finnigan-MAT, California, USA). Natural abundance of $^{15}\text{N}/^{14}\text{N}$ is expressed as deviations per mil (‰), an internationally recognized standard, through the equation $\delta = (\text{R}_{\text{sample}}/\text{R}_{\text{standard}} - 1) * 1000$, where R is the $^{15}\text{N}/^{14}\text{N}$ ratio of the sample and standard. The standard for N is the air with an N isotopic composition of 0 ‰. The analytical error was plus or minus 0.30 ‰. Isotopic analyses were performed at the Isotope Ecology laboratory at the Center for Nuclear Energy in Agriculture (CENA), University of São Paulo, Piracicaba, Brazil.

Auxiliary variables

We used predictive variables from global geospatial datasets in our model (Table 1). Climatic variables were taken from the WorldClim database (Hijmans et al., 2005). We used means of annual temperature (MAT) and mean annual precipitation (MAP) in our model. As a complement to MAT and MAP, we used aridity index (ai) and potential evapotranspiration (pet) in the analysis.

At the global scale, soil $\delta^{15}\text{N}$ has been shown to correlate with both climatic variables and pedological variables, such as soil organic carbon content and clay content (Craine et al., 2015). For soil covariates, we used the Soilgrid database for South America with a spatial resolution of 250 meters (Hengl et al., 2017). In addition to soil organic carbon and clay content, we used bulk density, cation exchange capacity, pH (H₂O and KCl extractable), silt and sand content in our analysis (Table 2.1). A Digital Elevation Model (DEM) from the Shuttle Radar Topography Mission (SRTM) was used for elevation (Jarvis et al. 2008).

Net Primary Production (NPP) was taken from MODIS/Terra data (MOD17A3) (Zhao et al., 2005). We specifically aggregated annual NPP grids over the period between 2000 and 2015 to estimate annual averages for NPP. We obtained all NPP grids from the Numerical Terradynamic Simulation Group at the University of Montana. The biome and ecoregion maps used in our analysis were obtained from the World Wild Foundation (Olson et al., 2001). The biome and ecoregion maps are available in shapefile format and were transformed to raster using ESRI ArcGIS (ESRI, 2016).

Table 2.1. List of, climatic, pedological, biogeographical and topographic variables. D = Discrete, C = Continuous.

Covariates				
(tif name)	Meaning	Resolution	Type	Reference
tmp	Mean Annual Temperature WorlsClim (°C)	1 km	C	Hijmans et al., 2005
pre	Annual Precipitation WorldClim (mm)	1 km	C	Hijmans et al., 2005
ai	Aridity Index	1 km	C	Zomer et al., 2008
pet	Potencial Evapotranspiration (annual mean)	1 km	C	Zomer et al., 2008
density	Bulk density (fine earth) in kg / cubic-meter - 5 cm	250 m	C	Hengl et al., 2017
cec	Cation exchange capacity of soil in cmolc/kg - 5 cm	250 m	C	Hengl et al., 2017
clay	Clay content (0-2 micro meter) mass fraction in % - 5 cm	250 m	C	Hengl et al., 2017
orc	Soil organic carbon content (fine earth fraction) in g per kg - 5 cm	250 m	C	Hengl et al., 2017
phh2o	Soil pH x 10 in H ₂ O - 5 cm	250 m	C	Hengl et al., 2017
phkcl	Soil pH x 10 in KCl - 5 cm	250 m	C	Hengl et al., 2017
silt	Silt content (2-50 micro meter) mass fraction in % - 5 cm	250 m	C	Hengl et al., 2017
sand	Sand content (50-2000 micro meter) mass fraction in % at depth 0.05 m	250 m	C	Hengl et al., 2017
npp	MODIS17 A3 Net Primary Production mean 2000-20 ¹⁵ (g C.m ² .yr ⁻¹)	30-arc sec	C	Zhao et al., 2005
alt	Elevation (m)	1 km	C	Jarvis et al., 2008
biome	Major biome boundaries for S. America		D	Olson et al., 2001
ecoreg	Ecoregions		D	Olson et al., 2001

Modelling

We based the spatial analysis of soil $\delta^{15}\text{N}$ on the *caret* package on R (Kuhn, 2008). The script used here is attached (*ANEXO B*). First, we projected all auxiliary data into the pattern projection WGS-84. Then, we resampled all auxiliary data at 1 km grid-cells, by using the bilinear interpolation method for continuous variables and nearest neighbor interpolation for categorical variables. After standardizing the spatial resolution of auxiliary data, we extracted the values for each geographical location to build the regression matrix, which was used to train the spatial prediction models in the *caret* package (Kuhn, 2008). We stacked the covariates to assess the accuracy and uncertainty of model outcomes. We compared three regression methods available in the *caret* package (Kuhn, 2008): Cubist, Random Forest (RF), and Stochastic Gradient Boosting (GBM) (Figure 2.2).

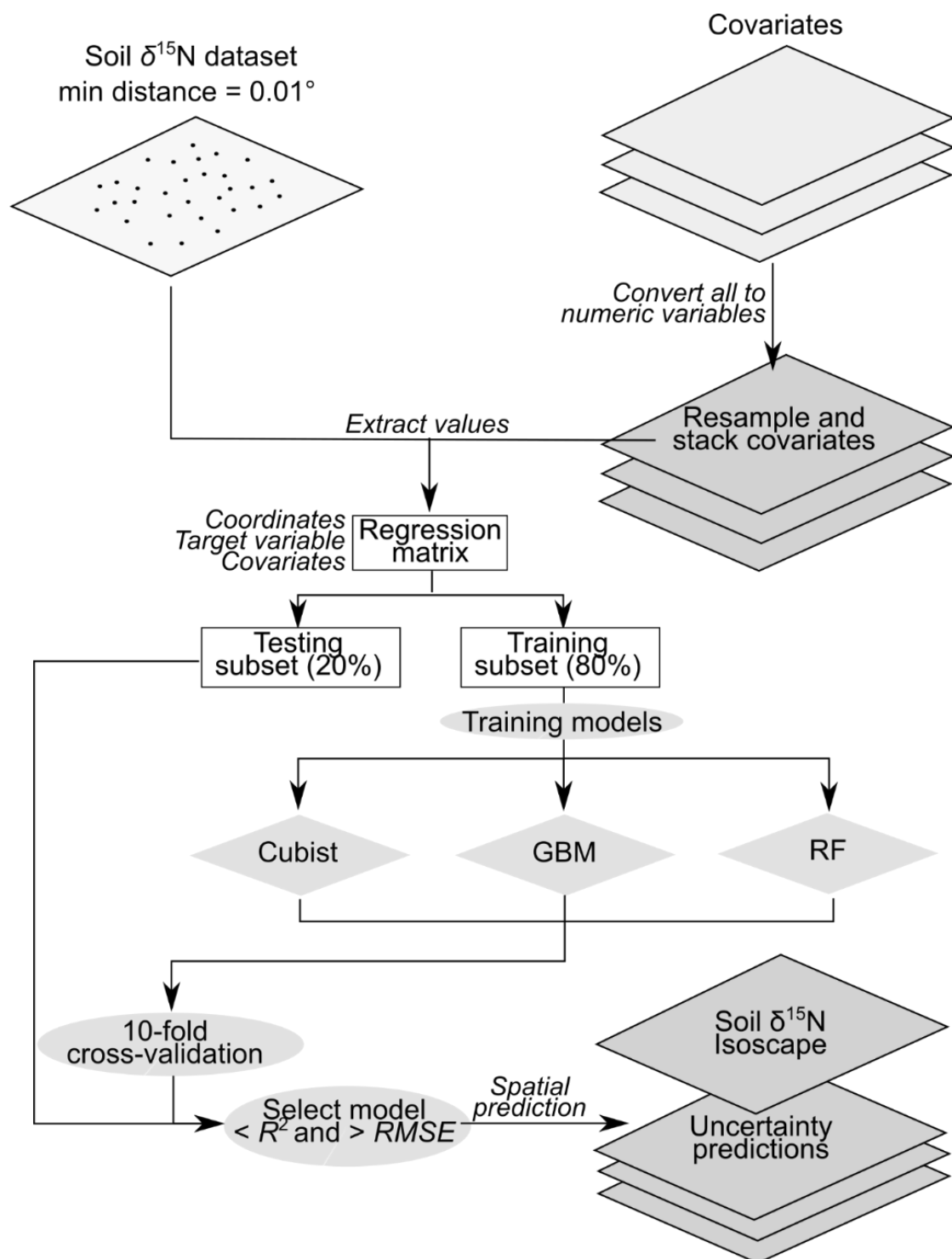


Figure 2.2. Workflow used for the modeling of soil $\delta^{15}\text{N}$ in South America. The covariates are listed in Table 1.

RF and GBM methods are similar to classification and regression trees (CART), which analyze variables that best appropriate values into two distinct groupings. This process is repeated for subsets until a regression tree is constructed. The RF model is

formed by a large number of random trees during the model-training process. All random trees are merged into a single prediction to reduce the noise and increase accuracy of results. The random trees are averaged, resulting in low prediction variance. This approach is known as ensemble learning (bagging) (Kuhn, 2008). Model error is estimated by using the out-of-bag data (OOB). The main parameter of the RF method is the number of features tested in each node (*m.try* argument), which is used for model optimization (Liaw and Wiernier, 2002, Hengl et al., 2018).

In addition to RF, GBM is also an ensemble learning approach. The main difference is that trees in the GBM method are built following a sequence as opposed to the random pattern approach of RF. After each regression tree is created, a new subsample is selected at random from the training dataset, which is used in the following interactions (Friedman, 2002). The errors created by the previous trees are corrected in the subsequent tree created in the GBM. Common parameters used for tuning GBMs are the number of trees or the number of boosting interactions (*n.trees* argument), the depth of trees (*interaction.depth* argument), and the learning rate (*shrinkage* argument) (Greenwell et al., 2019).

Cubist is a rule-based model where, for each node of the model tree, a linear regression is generated, which is smoothed by the linear regression of the previous node. Initially, the model tree is defined by a set of rules, which in turn can be combined or eliminated for model simplification. The committee is the main tuning parameter of the Cubist method, and works as a boosting scheme with the creation of interactive trees in sequence, in addition to establishing the number of trees (Kuhn and Quinlan, 2018). Subsequent model trees are created by adjusting the error of the previous model trees. The final prediction is established by the outcome linear regression model, with influence from previous models along the same path through the model tree.

We predicted soil $\delta^{15}\text{N}$ by applying each of the three tested models using all covariates to select the most accurate one. We separated the dataset randomly into a training subset (80% of the total dataset) and a testing holdout subset for validation (20% of the total dataset) (Figure 2). We used 10-fold cross-validation with five repetitions with the training data to access the variability of the predictions. Hence, each model was repeated five times using 90% of the training data, while the remaining 10% (OOB) was used for validation. That procedure gave the average value of root mean squared error (RMSE), mean absolute error (MAE), and R-square (R^2), as statistical metrics for model performance. To evaluate the final model's performance, we applied the fitted model to

the testing holdout data (20%) and used the statistical metrics RMSE, MAE, and R^2 to validate overall model efficacy

We visualized the importance of each covariate to the final model by calculating the percentage increase in the mean standard error (%IncMSE) of each covariate. Besides, we assessed how the most essential covariates influenced the target variable by using partial dependence plots, where the y-axes indicate the mean marginal effect of each value of a given covariate to the final prediction (Friedman, 2001). This approach has the advantage of graphically displaying the correlation between a given feature and the target variable.

Spatial prediction of soil $\delta^{15}\text{N}$ isoscape

We applied the whole dataset ($n = 278$ geographical locations) on the best performing model to create the final soil $\delta^{15}\text{N}$ isoscape map for S. America. We performed the spatial predictions by using the *prediction* function in *raster* package on R, and applying the chosen model to the stacked covariate raster. There is no function to predict the spatial uncertainty from the random forest model. An alternative way is to make several model predictions in order to calculate the coefficient of variation ($CV\% = (\text{standard deviation}/\text{mean}) * 100$) (Gomes et al., 2019). For this research, we applied 20 spatial predictions to RF models.

Results

Model performances and comparisons

Cross-validation values of RMSE, R^2 , and MAE from the RF, Cubist and GBM algorithms showed that RF was lightly best able to capture geospatial variation in soil $\delta^{15}\text{N}$ in South America (Figure 2.3). Although the models were not statistical different (Kruskal-Wallis test, P -value > 0.05), the average R^2 was slightly higher in RF ($R^2 = 0.64$) vs. Cubist ($R^2 = 0.61$) and GBM ($R^2 = 0.60$) (Figure 2.3A) models. For RMSE, the average was lower in RF algorithm (1.85 %) than in Cubist (1.92 %) and GBM (1.97 %) (Figure 2.3B). The same pattern was observed for MAE, where RF had the lowest average value (1.37 %), followed by Cubist (1.40 %) and GBM (1.52 %) (Figure 2.3C).

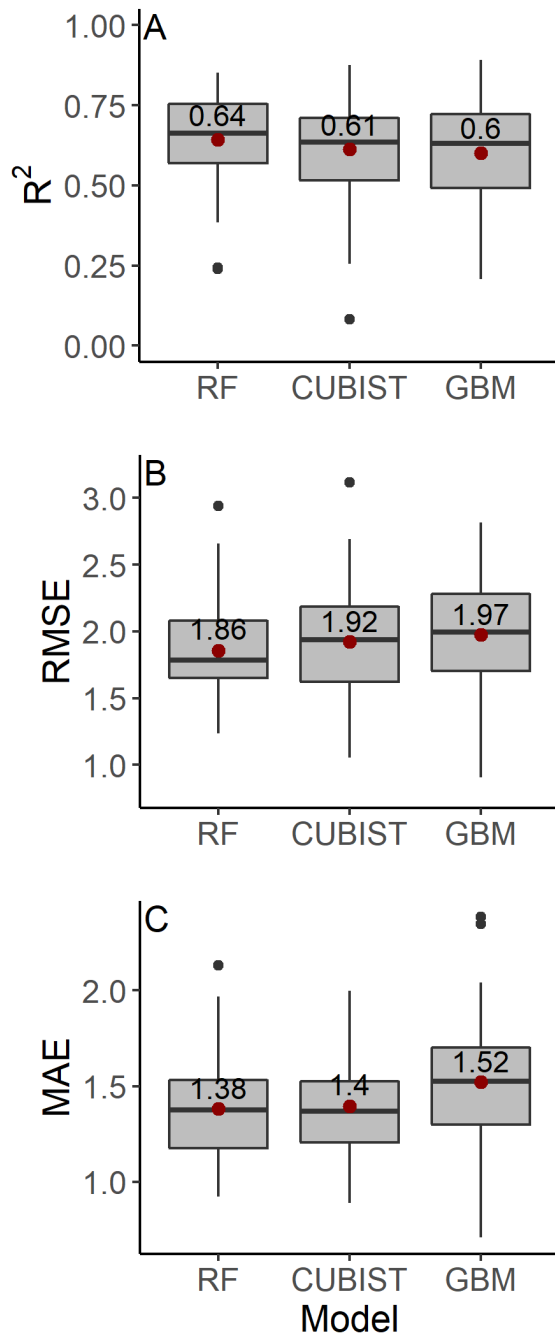


Figure 2.3. Summary of tested machine learning algorithms after 10-fold cross-validation with five repetitions: A. Boxplot of the correlation coefficient – R^2 , B. Boxplot of the root mean square error – RMSE, C. Boxplot of the mean absolute error – MAE. Model abbreviations: RF – Random forest regression, CUBIST – Cubist, GBM – Stochastic gradient boosting. The dark red circles represent the mean value showed above the dots. The horizontal lines in the boxplot represent the median values, the boxes the 1st (above) and the 3rd (below) quartiles, and the bars 1.75 x the interquartile difference. Black dots indicate outliers.

Soil $\delta^{15}\text{N}$ predicted by the RF algorithm explained 94% of the observations in the training data, with an RMSE of 0.63 ‰ ($P\text{-value} < 0.01$) (Figure 2.4A). After 10-fold cross-validation, the predicted $\delta^{15}\text{N}$ values explained 64% of the values observed in the

training data, with an RMSE of 1.85 ‰ (P -value < 0.01) (Figure 2.4B). However, the most robust performance evaluation approach involves a comparison between model-predicted $\delta^{15}\text{N}$ and the holdout testing data that we did not used in the model ($n = 50$). In this case, the predicted values explained 62% of the variation in the holdout testing data, with an RMSE of 1.72 ‰ (P -value < 0.01) (Figure 2.4C).

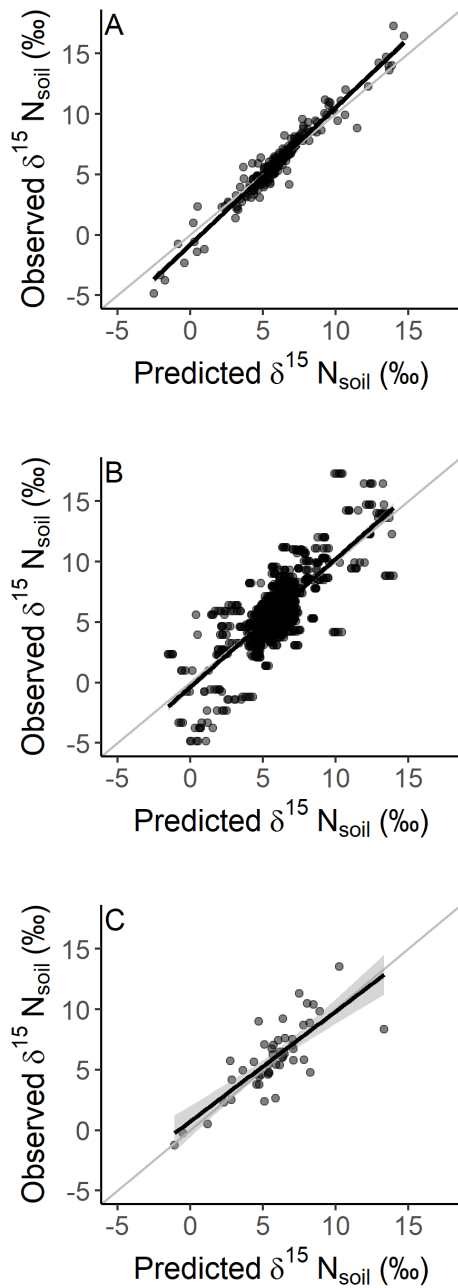


Figure 2.4. Scatter plots of observed vs predicted soil $\delta^{15}\text{N}$. A. Training dataset, B. Prediction after 10-fold cross-validation, C. Holdout testing dataset. The light grey line represents the 1:1 line. The bold black line is the regression line.

Importance of covariates

Biome type was the most important predictor variable for geospatial soil $\delta^{15}\text{N}$ in S. America. Covariate analysis showed that biome contributed 17.5 % to the decrease in mean accuracy (Figure 2.5). Soil organic carbon was the second most important variable, with a 16.4 % contribution, followed by climatic variables related to precipitation (pre, ai), bulk density and NPP (Figure 2.5).

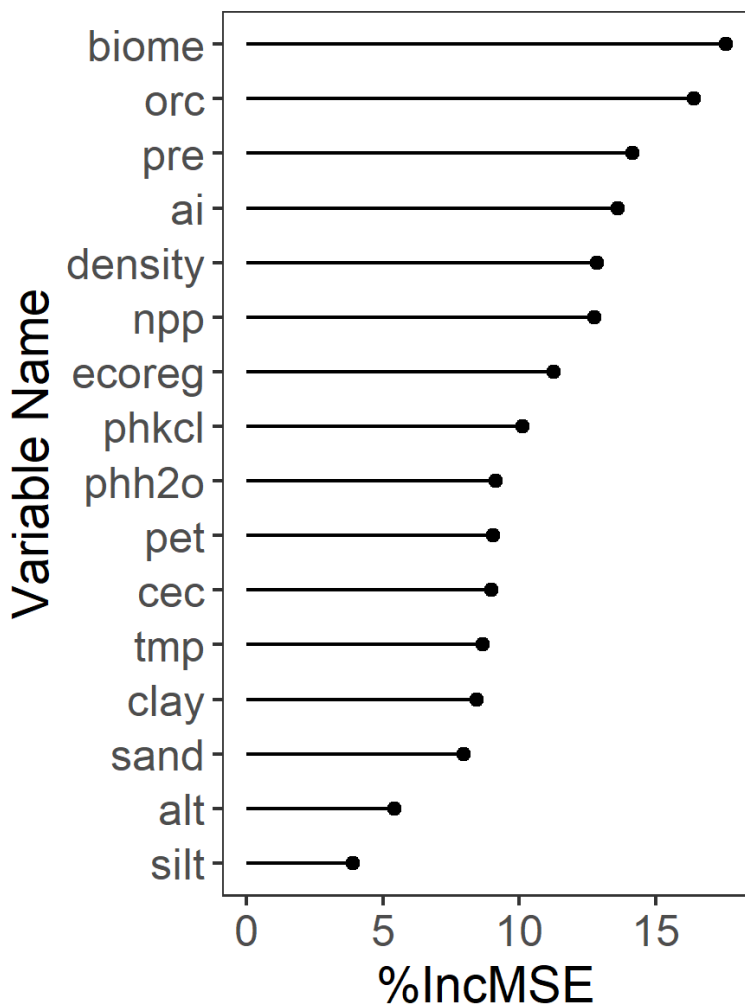


Figure 2.5. The relative importance of each covariate for soil $\delta^{15}\text{N}$ prediction in South America using random forest algorithm. %IncMSE refers to the decrease in mean accuracy. For covariates abbreviation, check Table 1.

The influence of the six most crucial covariates for predicting soil $\delta^{15}\text{N}$ is shown in Figure 2.6. Each biome has a distinct signature range in soil $\delta^{15}\text{N}$. Deserts and xeric shrublands have the highest values of soil $\delta^{15}\text{N}$ between the observed data ($11.9\text{‰} \pm 3.6$). Tropical moist forests have the second highest soil $\delta^{15}\text{N}$ value ($7.4\text{‰} \pm 2.0$). Conversely, temperate biomes showed the lowest values of soil $\delta^{15}\text{N}$: Temperate mixed forests show

the lowest mean value of soil $\delta^{15}\text{N}$ between all represented biomes ($1.1\text{‰} \pm 3.0$), followed by temperate grasslands, savannas and shrublands ($3.4\text{‰} \pm 2.6$). Tropical dry forests, Tropical savannas, and shrublands, and Flooded grasslands were intermediate, with soil $\delta^{15}\text{N}$ ranging from $6.8\text{‰} \pm 1.9$, $5.5\text{‰} \pm 1.6$, and $5.0 \pm 1.4\text{‰}$, respectively (Figure 2.6A).

For soil organic carbon content, there is a negative correlation at the highest predicted soil $\delta^{15}\text{N}$, corresponding to the lowest organic carbon values. We found an abrupt drop in soil $\delta^{15}\text{N}$ between 0 and 25 g kg^{-1} of organic carbon. The negative trend is much less between 25 and 100 g kg^{-1} of organic carbon, and again has a sharp drop between 100 and 150 g kg^{-1} of organic carbon (Figure 2.6B). Low MAP is related to higher soil $\delta^{15}\text{N}$, following a negative correlation trend up to 1100 mm of precipitation. Between 1100 mm and 1900 mm MAP, the predicted marginal values are much smaller than the values for other MAP ranges, and it is also possible to observe an increase in the partial value of predicted $\delta^{15}\text{N}$ as precipitation increases, followed by a sharp increase at 2000 mm. After this value, the inverse correlation returns, with higher values of $\delta^{15}\text{N}$ (Figure 2.6C). The same is seen for the aridity index since it is a covariate correlated with MAP (Figure 2.6D).

Bulk density exhibits a general pattern of positive correlation with $\delta^{15}\text{N}$, with a sharp increase in $\delta^{15}\text{N}$ values between 900 and 1000 kg m^{-3} . Partial dependence continues to rise as bulk density values range from 1000 kg m^{-3} to 1400 kg m^{-3} , but less strongly (Figure 2.6E). The influence of NPP on predicted soil $\delta^{15}\text{N}$ exhibits greater complexity, with a negative correlation between 200 and $600\text{ g C m}^2\text{ yr}^{-1}$ of NPP, a positive correlation between 600 g and $700\text{ g C.m}^2\text{ yr}^{-1}$, and a negative between 700 and $900\text{ g C m}^2\text{yr}^{-1}$. The correlation is again positive between 1000 and $1200\text{ g C.m}^2\text{ yr}^{-1}$ before stabilizing (Figure 2.6F).

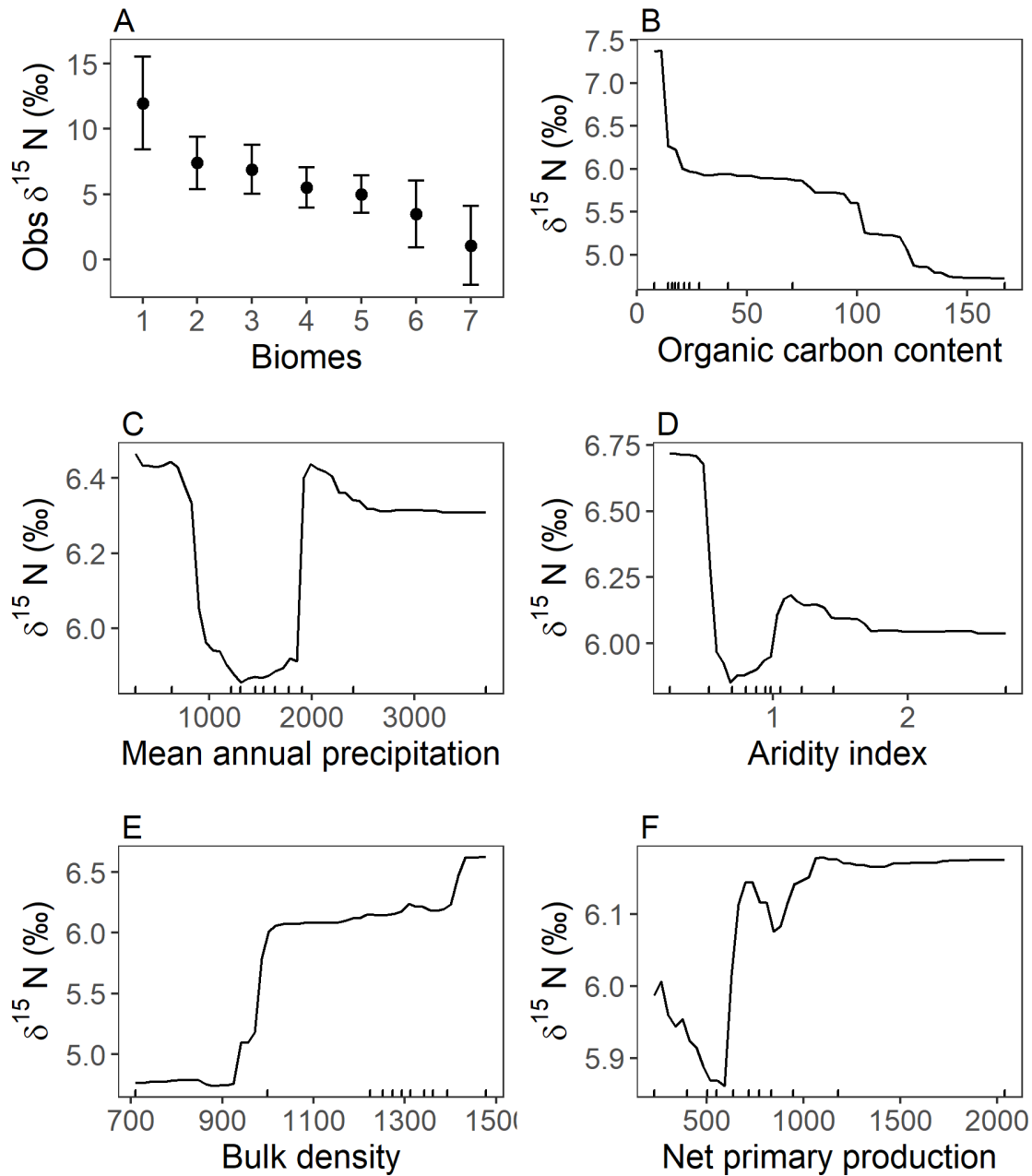


Figure 2.6. Plots showing the influence of the six most important variables to soil $\delta^{15}\text{N}$ prediction using random forest algorithm. A. Plot showing observed mean \pm SD values of observed soil $\delta^{15}\text{N}$ by biome as categorical variable, reordered from the higher to the lower mean value: 1 – Deserts and Xeric Shrublands, 2 – Tropical and Subtropical Moist Broadleaf Forest, 3 – Tropical and Subtropical Dry Broadleaf Forest, 4 – Tropical and Subtropical Grasslands, Savannas and Shrublands, 5 – Flooded Grasslands, Savannas and Shrublands, 6 – Temperate Grasslands, Savannas and Shrublands, 7 – Temperate Broadleaf and Mixed Forest. B, C, D, E, F are partial dependence plots for some important variables: B. Soil organic carbon, C. Mean annual precipitation, D. Aridity index, E. Bulk density, F. Net primary production. For detailed information about covariates, check Table 1. Marks on the x-axis indicate the data distribution.

Uncertainty of the model

Regression residuals between observed and predicted soil $\delta^{15}\text{N}$ did not exhibit spatial autocorrelation (Moran's index = -0.02, P -value = 0.77). The extreme values of residuals, both positive and negative, were concentrated in the areas with maximum and minimum observed soil $\delta^{15}\text{N}$, specifically in the northeastern region of Brazil and in Patagonia in Argentina (Figure 2.7A). The coefficient of variation map calculated from the predictions showed larger inconsistencies in the southern area of the continent (Figure 2.7B). CV higher than 40% was observed for mountainous area along the Andes. On the other hand, lowest CV was concentrated in the northern region corresponding to tropical forests, in the semi-arid tropical region, and in the tropical savannas (Figure 2.7B). The spatial pattern of the CV followed the spatial distribution of available data, with higher values in places with little or no sampling.

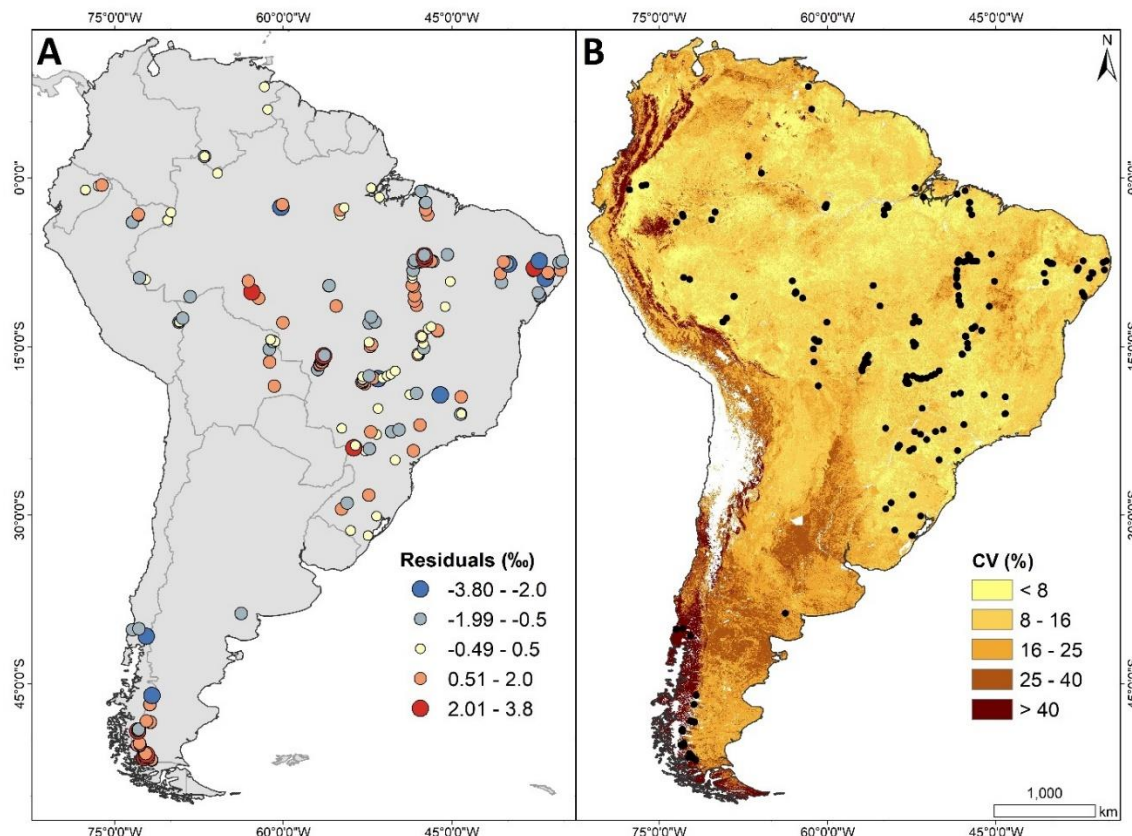


Figure 2.7. Spatial patterns of model uncertainty: A. Residuals from observed vs predicted regression of the whole dataset, B. Coefficient of variation (CV).

Prediction of soil $\delta^{15}\text{N}$ for South America

The highest soil $\delta^{15}\text{N}$ was modeled for the northeastern region of Brazil, where modeled values of soil $\delta^{15}\text{N}$ (0-20 cm) reaching approximately 15 ‰ (Figure 2.8). High soil $\delta^{15}\text{N}$ values were also mapped in the northern region of Brazil (between 8 and 11 ‰,

approximately), in the Amazon Forest region, and in the southern areas of Bolivia and northwestern Argentina. The lowest values appeared in the extreme southwest and south of South America, with negative isotopic ratios reaching approximately -3 ‰. Negative or near zero soil $\delta^{15}\text{N}$ also appeared in the northwest region of South America, following the mountainous Andes between Peru and Colombia. Intermediate values, between 3 and 7 ‰, were mainly in the central region of Brazil, where the tropical savannas occur, and to the south in a continuous range that follows from the central region of Paraguay to the south of Argentina, where the temperate savannas predominate (Figure 2.8).

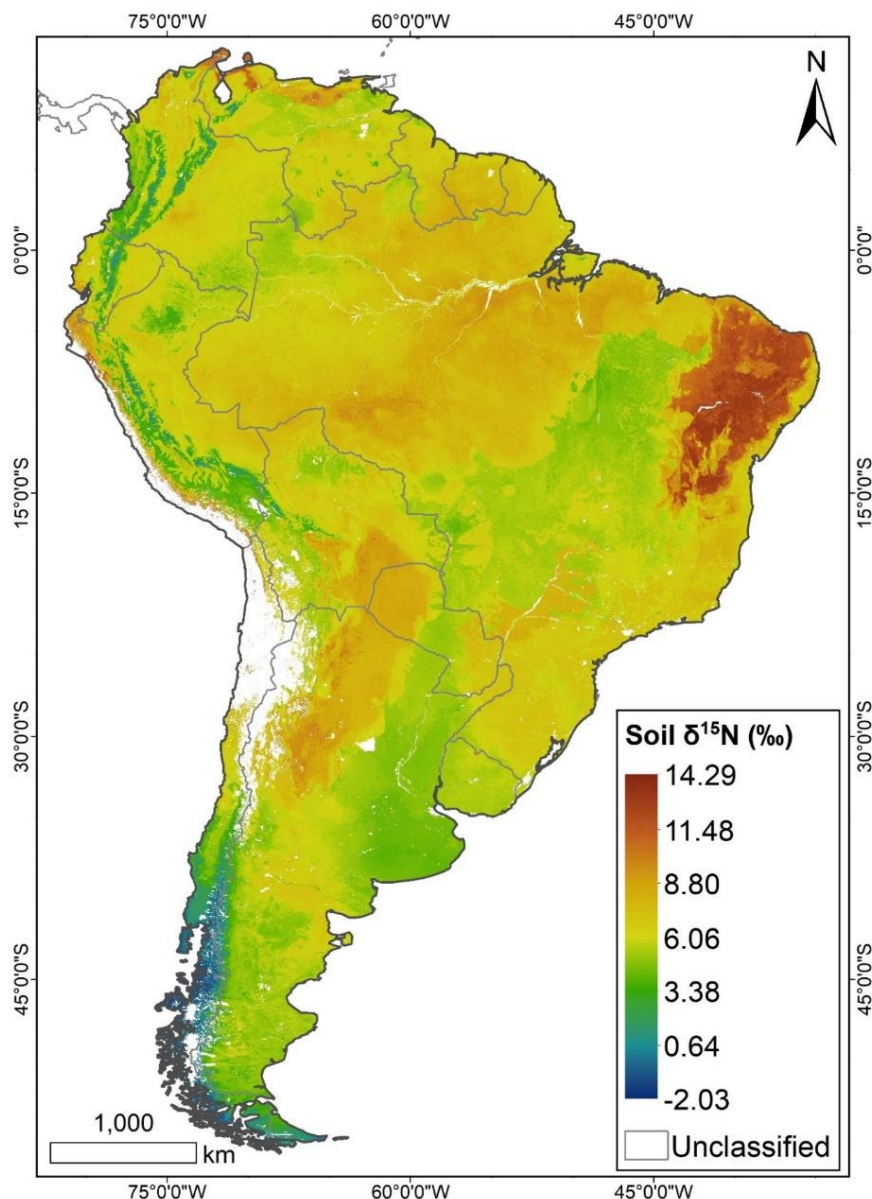


Figure 2.8. Isoscape of soil $\delta^{15}\text{N}$ (0 - 20 cm) for South America. The unclassified correspond to areas without vegetation, mainly ice covered, water and deserts.

Discussion

Source of uncertainty and model performance

The machine learning approach was capable of reconstructing patterns of soil $\delta^{15}\text{N}$ for the South American continent, provided an improved prediction of observed soil $\delta^{15}\text{N}$ variation (down to 20 cm) compared to previous regression-based approaches (Amundson et al., 2003). This result is consistent with the development of machine learning algorithms in digital soil mapping and biogeochemical predictions (Hengl et al., 2017, Bataille et al., 2018, Gomes et al., 2019). Among machine learning approaches, the RF model performed best, followed by the Cubist and GBM algorithms. Upon 10-fold cross-validation, the RF model produced an $R^2 = 0.64$ vs. observed soil $\delta^{15}\text{N}$ data. This significant correlation was roughly similar to our validation with the subset of data not used in the RF model (i.e., $R^2 = 0.62$ vs. the testing subset), indicating that the model was not significantly affected by overfitting.

That RF yielded the most efficient algorithm in our study was consistent with previous RF applications to mapping of different soil variables (Nawar and Mouazen, 2017, Gomes et al. 2019). Similarly, in an attempt to map strontium isoscape to central Europe, Bataille et al. (2018) compared the efficiency of several methods besides the GBM and Cubist algorithms, among them ordinary kriging, neural network, and the generalized linear model, and also found that RF had the best performance.

The highest CV values are concentrated in areas with limited data in our study. This pattern agrees with the assumption that spatial gaps in the dataset are the primary sources of error in the modeling of any soil variable (Malone et al., 2018). In particular, areas between the central and southern regions of South America are the most underrepresented among soil $\delta^{15}\text{N}$ observations. Filling these spatial gaps can further improve the accuracy of models using RF (Hengl et al., 2018).

Soil $\delta^{15}\text{N}$ spatial distribution in South America

Our study identified biome-type as the most essential factor for understanding spatial patterns of soil $\delta^{15}\text{N}$ at regional to continental scales. Highest soil $\delta^{15}\text{N}$ was modeled for areas of xeric shrublands in northeastern Brazil. This pattern is consistent with isotopic fractionation during ammonia volatilization, leaving residual soil $^{15}\text{N}/^{14}\text{N}$ pools considerably elevated in areas with water deficits and high pH soils (Högberg et al., 1997, Menezes et al., 2012). The same mechanisms are likely to explain the elevated soil

$\delta^{15}\text{N}$ (between 10 and 12 ‰) predicted for the Atacama Desert region (Ehleringer et al., 1992) and in the semiarid areas of northwestern Argentina and Paraguay.

Conversely, the lowest predicted soil $\delta^{15}\text{N}$ is apparent in temperate climates and along the mountainous Andes region in the northwest of South America. Temperate ecosystems have a slower rate of soil organic matter decomposition and N mineralization rates, which reduces isotopic fractionation in the surface soil, resulting in soil $\delta^{15}\text{N}$ convergence to litter inputs from plants (Martinelli et al., 1999). Further, N gaseous losses are relatively low compared to tropical forests, leading to lower isotopic fractionation during gaseous N losses. Peri et al. (2012) found similar $\delta^{15}\text{N}$ of surface soil and leaves along a precipitation gradient in the Patagonia region of Argentina, indicating that there is small isotopic fractionation during organic matter decomposition in the surface soil.

In tropical rainforests areas, the RF algorithm was capable of capturing finer (regional) scale soil $\delta^{15}\text{N}$ variation than regression models based on climate alone. Such improved capacity was seen along a tropical gradient, mainly in the Amazon forest, where the predicted soil $\delta^{15}\text{N}$ decreased from east to west. This gradient of $\delta^{15}\text{N}$ has been widely observed in previous empirical studies (Nardoto et al., 2008, 2014). The systematic decline in soil $\delta^{15}\text{N}$ within the Amazon is also apparent in partial dependence plots with MAP, where a decrease in the modeled $\delta^{15}\text{N}$ occurs between MAP 2000 mm to 2500 mm. In the eastern Amazonian region isotopically fractionating denitrification losses is probably the main drive of the increase of soil $\delta^{15}\text{N}$ (Houlton et al., 2006, Pérez et al., 2006).

These correlations were probably accentuated by the extreme positive $\delta^{15}\text{N}$ values in the semiarid areas, where there is a low quantity of soil organic carbon, and negative values in temperate forests, with largest amounts of organic carbon. However, soil organic carbon was unable to explain the spatial distribution of the intermediate values of soil $\delta^{15}\text{N}$ in South America (from 3 to 7 ‰), which appear mainly in the tropical and temperate savanna areas of the model. Those three large patterns described above are partially (though not wholly) captured in the global trends found by Craine et al. (2015b), in which latitudinal gradients of soil $\delta^{15}\text{N}$ were shown to be indirectly related to the MAP and MAT, which in turn influenced clay content and soil organic carbon. Craine et al. (2015b) suggested that in the hot and/or dry regions there is a higher amount of mineral organic matter, enriched in ^{15}N , than less enriched non-mineral organic matter. This explains the high influence of the organic carbon model on the prediction of soil $\delta^{15}\text{N}$, with the lowest values of organic carbon related to the highest predicted values of soil $\delta^{15}\text{N}$.

Savannas from South America have been substantially under-represented in previous $\delta^{15}\text{N}$ soil models (Amundson et al., 2003, Craine et al., 2015b). Our study adds an array of new data, thereby making it possible to examine correlations with soil $\delta^{15}\text{N}$ in this biome. The partial dependence plot shows that within the savanna's precipitation range (between 1000 and 2000 mm), predicted soil $\delta^{15}\text{N}$ decreases considerably, followed by increasing soil $\delta^{15}\text{N} > 2000$ mm. Low predicted soil $\delta^{15}\text{N}$ in savannas compared to semi-arid and forest regions are consistent with observations in the central region of Brazil (Bustamante et al., 2004). Savannas of South America have low N availability compared to tropical rainforests, but with less severe water deficit than tropical semi-arid regions. Particularly, the savannas of Central Brazil present low decomposition rates due to high C:N ratios (~ 60:1), low net N mineralization, although with high NH_4^+ production in the soil (Nardoto and Bustamante, 2003, Bustamante et al., 2006). This low N availability in the plant-soil system seemed to have been captured by low soil $\delta^{15}\text{N}$ that the model presented here.

Spatial variation of soil $\delta^{15}\text{N}$ is scale-dependent, given the difficulties encountered by global models in explaining important patterns at some regional scales (Cheng et al., 2009, Chen et al., 2018, Freitas et al., 2010). Even so, the Amundson et al. (2003) model has proven useful in several global-scale studies of soil and plant $\delta^{15}\text{N}$. The difficulty in representing spatial regions arises from the regional geographic or ecosystem limits have not been included in the analysis. Studies show that even in global biogeochemical models, the boundaries of biomes or climatic regions are important auxiliary variables (Terzer et al., 2013). When comparing our model with Amundson's et al. (2003), the importance of regional boundaries for future modeling of $\delta^{15}\text{N}$ was evident (Figure 2.9). Our model was able to delimit a large amplitude of soil $\delta^{15}\text{N}$ variation, showing spatial patterns of nonlinear correlation with MAP (Figure 2.9A). On the other hand, Amundson's global model captured a smaller amplitude of variation of $\delta^{15}\text{N}$ compared to our model (Figure 2.9B).

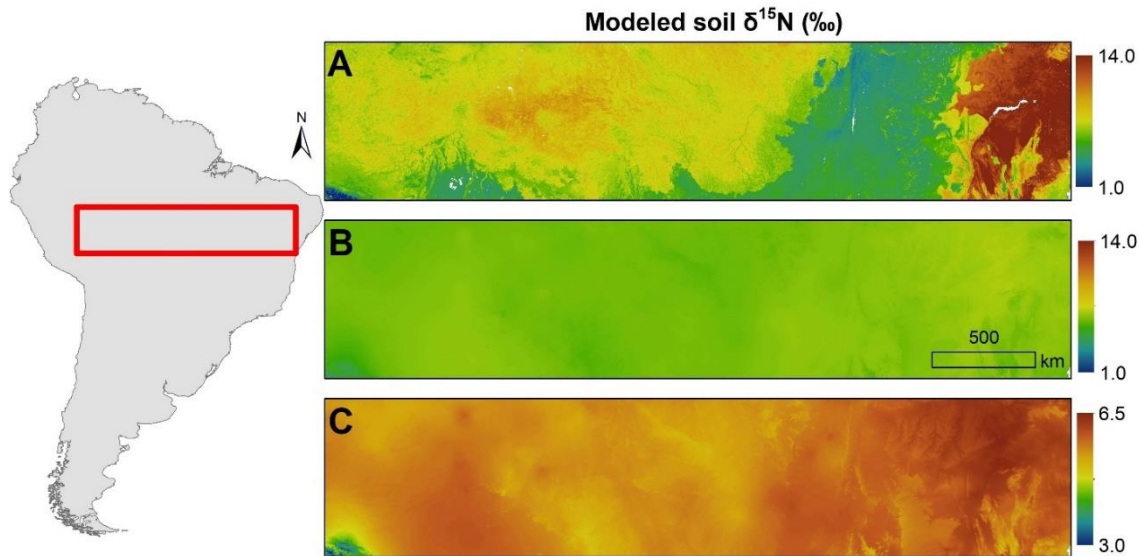


Figure 2.9. Comparison between the model of the present study (A) and the model from Amundson et al (2003) for 10 cm soil: B. Amundson's et al. model with the legend showing the same range of our model, C. Amundson's et al. model with the legend adapted to the own range of soil $\delta^{15}\text{N}$. The model for comparison was generated by the application of equation ($\delta^{15}\text{N}_{\text{soil}} = 0.2048 * \text{MAT} - 0.0012 * \text{MAP} + 4.3266$, $R^2 = 0.32$, $n = 29$) (Amundson et al., 2003) using the climatic dataset from WorldClim. The red rectangle over South America on the left indicates the spatial clipping used in the model comparison.

Applicability of the machine-learning soil $\delta^{15}\text{N}$ isoscape model

Spatial models of soil $\delta^{15}\text{N}$ have been identified as an essential benchmarking tool for improving N-carbon forecasts in global climate change (Houlton et al., 2015). Soil $\delta^{15}\text{N}$ isoscapes at large scales aggregate information on N balance and loss to the atmosphere from the soil-plant system (Brenner et al., 2001, Houlton and Bai, 2009). Our model, therefore, offers a more robust constraint on models and for understanding local to global biogeochemical fluxes. Bai et al. (2012) demonstrated the strength of spatial models of soil $\delta^{15}\text{N}$, adapting the equation proposed by Amundson et al. (2003) to estimate the gaseous N losses of terrestrial ecosystems. The authors identified high NO emissions in Africa and high N₂ emissions in the southeastern United States, where there are few N emission measurements (Bai et al., 2012). The addition of the regional factor and the increase in the accuracy of the base models as presented here will increase the power of these predictions.

Soil $\delta^{15}\text{N}$ isoscapes also hold demonstrated utility for conservation studies, providing a pathway for tracking wild animal movement (Hobson et al., 2012, García-Pérez and Hobson, 2014). These studies generally have a multi-isotopic approach, aggregating oxygen and hydrogen stable isotopes from water together with stable isotopes

over the animal's trophic niche, such as carbon and nitrogen. By relating these isoscapes to the animal tissue isotopic ratios it is possible to create probability maps of origin (García-Pérez and Hobson, 2014). The isoscape presented here has the potential to reduce the probability area of assignment studies since it accessed regional aspects of the variation of $\delta^{15}\text{N}$. This same principle applies to the use of the model in forensic investigations (Chesson et al., 2018), marking our approach of global cross-disciplinary importance.

Literature Cited

- Adhikari, K., Hartemink, A.E., Minasny, B., Bou Kheir, R., Greve, M.B., and Greve, M.H., 2014. Digital mapping of soil organic carbon contents and stocks in Denmark. PLoS ONE, 9.
- Amundson, R., Austin, A.T., Schuur, E.A.G., Yoo, K., Matzek, V., Kendall, C., Uebersax, A., Brenner, D., Baisden, W.T., 2003. Global patterns of the isotopic composition of soil and plant nitrogen. Global Biogeochem. Cycles 17, 1031. <https://doi.org/10.1029/2002GB001903>
- Bai, E., Boutton, T., Liu, F., Wu, X., Archer, S., 2013. N isoscapes in a subtropical savanna parkland : spatial-temporal perspectives. Ecosphere 4, 1–17. <https://doi.org/10.1890/ES12-00187.1>
- Bai, E., Houlton, B.Z., Wang, Y.P., 2012. Isotopic identification of nitrogen hotspots across natural terrestrial ecosystems. Biogeosciences 9, 3287–3304. <https://doi.org/10.5194/bg-9-3287-2012>
- Bataille, C.P., von Holstein, I.C.C., Laffoon, J.E., Willmes, M., Liu, X.M., Davies, G.R., 2018. A bioavailable strontium isoscape for Western Europe: A machine learning approach. PLoS One 13, 1–27. <https://doi.org/10.1371/journal.pone.0197386>
- Bowen, G.J., 2010. Isoscapes : Spatial Pattern in Isotopic Biogeochemistry. Annu. Rev. Earth Planet. Sci. 161–187. <https://doi.org/10.1146/annurev-earth-040809-152429>
- Brenner, D.L., Amundson, R., Baisden, W.T., Kendall, C., Harden, J., 2001. Soil N and ^{15}N variation with time in a California annual grassland ecosystem. Geochim. Cosmochim. Acta 65, 4171–4186.
- Bustamante, M.M.C., Martinelli, L. a., Silva, D. a., Camargo, P.B., Klink, C. a., Domingues, T.F., Santos, R. V., 2004. ^{15}N Natural Abundance in Woody Plants and Soils of Central Brazilian Savannas (Cerrado). Ecol. Appl. 14, 200–213. <https://doi.org/10.1890/01-6013>
- Bustamante, M.M.C., Medina, E., Asner, G.P., Nardoto, G.B., Garcia-Montiel, D.C., 2006. Nitrogen cycling in tropical and temperate savannas. Biogeochemistry 79, 209–237. <https://doi.org/10.1007/s10533-006-9006-x>
- Chen, C., Jia, Y., Chen, Y., Mahmood, I., Fang, Y., Wang, G., 2018. Nitrogen isotopic composition of plants and soil in an arid mountainous terrain: South slope versus north slope. Biogeosciences 15, 369–377. <https://doi.org/10.5194/bg-15-369-2018>
- Cheng, W., Chen, Q., Xu, Y., Han, X., Li, L., 2009. Climate and ecosystem ^{15}N natural

abundance along a transect of Inner Mongolian grasslands: Contrasting regional patterns and global patterns. *Global Biogeochem. Cycles* 23, 1–11.
<https://doi.org/10.1029/2008GB003315>

Chesson, L.A., Barnette, J.E., Bowen, G.J., Brooks, J.R., Casale, J.F., Cerling, T.E., Cook, C.S., Douthitt, C.B., Howa, J.D., Hurley, J.M., Kreuzer, H.W., Lott, M.J., Martinelli, L.A., O’Grady, S.P., Podlesak, D.W., Tipple, B.J., Valenzuela, L.O., West, J.B., 2018. Applying the principles of isotope analysis in plant and animal ecology to forensic science in the Americas. *Oecologia* 187, 1077–1094.
<https://doi.org/10.1007/s00442-018-4188-1>

Conen, F., Zimmermann, M., Leifeld, J., Seth, B., Alewell, C., 2008. Relative stability of soil carbon revealed by shifts in ^{15}N and C: N ratio. *Biogeosciences* 4, 2915–2928.

Craine, J.M., Brookshire, E.N.J., Cramer, M.D., Hasselquist, N.J., Koba, K., Marin-Spiotta, E., Wang, L., 2015a. Ecological interpretations of nitrogen isotope ratios of terrestrial plants and soils. *Plant Soil*. <https://doi.org/10.1007/s11104-015-2542-1>

Craine, J.M., Elmore, A.J., Wang, L., Augusto, L., Baisden, W.T., Brookshire, E.N.J., Cramer, M.D., Hasselquist, N.J., Hobbie, E.A., Kahmen, A., Koba, K., Kranabetter, J.M., Mack, M.C., Marin-Spiotta, E., Mayor, J.R., McLauchlan, K.K., Michelsen, A., Nardoto, G.B., Oliveira, R.S., Perakis, S.S., Peri, P.L., Quesada, C.A., Richter, A., Schipper, L.A., Stevenson, B. a., Turner, B.L., Viani, R.A.G., Wanek, W., Zeller, B., 2015b. Convergence of soil nitrogen isotopes across global climate gradients. *Sci. Rep.* 5, 8280. <https://doi.org/10.1038/srep08280>

Denk, T.R.A., Mohn, J., Decock, C., Lewicka-szczebak, D., Harris, E., Butterbach-bahl, K., Kiese, R., Wolf, B., 2017. Soil Biology & Biochemistry The nitrogen cycle : A review of isotope effects and isotope modeling approaches. *Soil Biol. Biochem.* 105, 121–137. <https://doi.org/10.1016/j.soilbio.2016.11.015>

Ehleringer, J.R., Mooneyt, H.A., Rundel, P.W., Evans, R.D., Palma, B., Delatorrell, J., 1992. Lack of nitrogen cycling in the Atacama Desert. *Nature* 359, 316–318.

ESRI., 2016. ArcGIS desktop, release 10.3.1. Environmental Systems Research Institute, Redlands, California, USA.

Freitas, A.D.S., de Sa Barreto Sampaio, E.V., Menezes, R.S.C., Tiessen, H., 2010. ^{15}N natural abundance of non-fixing woody species in the Brazilian dry forest (caatinga). *Isotopes Environ. Health Stud.* 46, 210–8.
<https://doi.org/10.1080/10256016.2010.488805>

Friedman, J.H., 2001. Greedy function approximation: A gradient boosting machine. *Annals of statistics* 29, 1189–1232.

Friedman, J.H., 2002. Stochastic gradient boosting. *Comput. Stat. Data Anal.* 38, 367–378.

Garcia-Perez, B., Hobson, K.A., 2014. A multi-isotope (d^2H , d^{13}C , d^{15}N) approach to establishing migratory connectivity of Barn Swallow (*Hirundo rustica*). *Ecosphere* 5, 1–12.

Gomes, L.C., Faria, R.M., de Souza, E., Veloso, G.V., Schaefer, C.E.G.R., Filho, E.I.F., 2019. Modelling and mapping soil organic carbon stocks in Brazil. *Geoderma* 1–14. <https://doi.org/10.1016/j.geoderma.2019.01.007>

- Gray, J.M., Bishop, T.F.A. Yang, X., 2015. Pragmatic models for the prediction and digital mapping of soil properties in eastern Australia. *Soil Res.* 53, 24-42.
- Greenwell, B., Boehmke, B. Cunningham J., 2019. gbm: Generalized Boosted Regression Models. R Package Version 2.1.5.
- Hengl, T., Jesus, J.M. De, Heuvelink, G.B.M., Ruiperez, M., Kilibarda, M., Blagoti, A., Shangguan, W., Wright, M.N., Geng, X., Bauer-marschallinger, B., Guevara, M.A., Vargas, R., Macmillan, R.A., Batjes, N.H., Leenaars, J.G.B., Ribeiro, E., Wheeler, I., Mantel, S., Kempen, B., 2017a. SoilGrids250m : Global gridded soil information based on machine learning. *PLoS One* 1–40. <https://doi.org/10.1371/journal.pone.0169748>
- Hengl, T., Leenaars, J.G.B., Shepherd, K.D., Walsh, M.G., Heuvelink, G.B.M., Mamo, T., Tilahun, H., Berkhout, E., Cooper, M., Fegraus, E., Wheeler, I., Kwabena, N.A., 2017b. Soil nutrient maps of Sub-Saharan Africa: assessment of soil nutrient content at 250 m spatial resolution using machine learning. *Nutr. Cycl. Agroecosystems* 109, 1–26. <https://doi.org/10.1007/s10705-017-9870-x>
- Hengl, T., Nussbaum, M., Wright, M.N., Heuvelink, G.B.M., Gräler, B., 2018. Random forest as a generic framework for predictive modeling of spatial and spatio-temporal variables. *PeerJ* 6, e5518. <https://doi.org/10.7717/peerj.5518>
- Hijmans, R.J., Cameron, S.E., Parra, J.L., Jones, P.G., Jarvis, A., 2005. Very high resolution interpolated climate surfaces for global land areas. *Int. J. Climatol.* 25, 1965–1978. <https://doi.org/10.1002/joc.1276>
- Hobbie, E.A., Macko, S.A., Williams, M., 2000. Correlations between foliar d15N and nitrogen concentrations may indicate plant–mycorrhizal interactions. *Oecologia* 122, 273–283.
- Hobson, K.A., van Wilgenburg, S.L., Wassenaar, L.I., Powell, R., Still, C.J., Craine, J.M., 2012. A multi-isotope (d13C, d15N, d2H) feather isoscape to assign Afrotropical migrant birds to origins. *Ecosphere* 3, 1–20.
- Högberg, P., 1997. ¹⁵N natural abundance in soil-plant systems. *New Phytol.* 137, 179–203.
- Houlton, B.Z., Bai, E., 2009. Imprint of denitrifying bacteria on the global terrestrial biosphere. *Proc. Natl. Acad. Sci.* 106, 21713–21716. <https://doi.org/10.1073/pnas.0912111106>
- Houlton, B.Z., Marklein, A.R., Bai, E., 2015. Representation of nitrogen in climate change forecasts. *Nat. Publ. Gr.* 5, 398–401. <https://doi.org/10.1038/nclimate2538>
- Houlton, B.Z., Sigman, D.M., Hedin, L.O., 2006. Isotopic evidence for large gaseous nitrogen losses from tropical rainforests. *Proc. Natl. Acad. Sci.* 103, 8745–8750. <https://doi.org/10.1073/pnas.0510185103>
- Hounkpatin, O.K.L., Hipt, F.O., Bossa, A.R.Y., Welp, G., Amelung, W., 2018. Soil organic carbon stocks and their determining factors in the Dano catchment (Southwest Burkina Faso). *Catena* 166, 298–309.
- Jarvis, A., Reuter, H.I., Nelson, A., Guevara, E., 2008. Hole-filled SRTM for the globe Version 4, available from the CGIAR-CSI SRTM 90m. <http://srtm.cgiar.org>.
- Kuhn, M., 2008. Building predictive models in R using the caret Package. *J. Stat. Softw.* 28, 1–26. <https://doi.org/10.1053/j.sodo.2009.03.002>

- Kuhn, M., Quinlan, R., 2018. Cubist: Rule- and instance-based regression modeling. R package version 0.2.2. <https://CRAN.R-project.org/package=Cubist>
- Liaw, A., Wiener, M. 2002. Classification and Regression by randomForest. *R News* 2(3), 18–22.
- Malone, B.P., Odgars, N.P., Stockmann, U., Minasny, B., McBratney, A.B., 2018. Digital mapping of soil classes and continuous soil properties. In: *Pedometrics*, Springer, Dordrecht, Netherlands. pp 373–413.
- Martinelli, L.A., Piccolo, M.C., Townsend, A.R., Vitousek, P. M., Cuevas, E., McDowell, W., Robertson, G.P., Santos O.C., Treseder K., 1999. Nitrogen stable isotopic composition of leaves and soil: Tropical versus temperate forests. *Biogeochemistry* 46, 45–65.
- Menezes, R.S.C., Sampaio, E.V.S.B., Giongo, V., Pérez-Marin, a M., 2012. Biogeochemical cycling in terrestrial ecosystems of the Caatinga Biome. *Rev. Brasileira Biol.* 72, 643–53. <https://doi.org/10.1590/S1519-69842012000400004>
- Nardoto, G.B., Bustamante, M.M.D.C., 2003. Effects of fire on soil nitrogen dynamics and microbial biomass in savannas of Central Brazil. *Pesqui. Agropecu. Bras.* 38, 955–962. <https://doi.org/10.1590/S0100-204X2003000800008>
- Nardoto, G.B., Ometto, J.P.H.B., Ehleringer, J.R., Higuchi, N., Bustamante, M.M.D.C., Martinelli, L.A., 2008. Understanding the Influences of Spatial Patterns on N Availability Within the Brazilian Amazon Forest. *Ecosystems*. <https://doi.org/10.1007/s10021-008-9189-1>
- Nardoto, G.B., Quesada, C.A., Patiño, S., Saiz, G., Baker, T.R., Schwarz, M., Schrot, F., Feldpausch, T.R., Domingues, T.F., Marimon, B.S., Marimon Junior, B.-H., Vieira, I.C.G., Silveira, M., Bird, M.I., Phillips, O.L., Lloyd, J., Martinelli, L.A., 2014. Basin-wide variations in Amazon forest nitrogen-cycling characteristics as inferred from plant and soil ^{15}N : ^{14}N measurements. *Plant Ecol. Divers.* 7, 173–187. <https://doi.org/10.1080/17550874.2013.807524>
- Nawar, S., Mouazen, A.M., 2017. Comparison between Random Forests, Artificial Neural Networks and Gradient Boosted Machines Methods of On-Line Vis-NIR Spectroscopy Measurements of Soil Total Nitrogen and Total Carbon. *Sensors* 17, 1–22. <https://doi.org/10.3390/s17102428>
- Olson, D.M., Dinerstein, E., Wikramanayake, E.D., Burgess, N.D., Powell, G.V.N., Underwood, E.C., D'amico, J.A., Itoua, I., Strand, H.E., Morrison, J.C., Loucks, C.J., Allnutt, T.F., Ricketts, T.H., Kura, Y., Lamoreux, J.F., Wettengel, W.W., Hedao, P., Kassem, K.R., 2001. Terrestrial Ecoregions of the World: A New Map of Life on Earth. *Bioscience* 51, 933. [https://doi.org/10.1641/0006-3568\(2001\)051\[0933:TEOTWA\]2.0.CO;2](https://doi.org/10.1641/0006-3568(2001)051[0933:TEOTWA]2.0.CO;2)
- Pardo, L.H., Nadelhoffer, K.J., 2010. Using Nitrogen Isotope Ratios to Assess Terrestrial Ecosystems at Regional and Global Scales, in: *Isoscapes: Understanding Movement, Pattern, and Process on Earth Through Isotope Mapping*. pp. 221–249.
- Pérez, T., Garcia-Montiel, D., Trumbore, S., Tyler, S., Camargo, P. de, Moreira, M., Piccolo, M., Cerri, C., 2006. Nitrous Oxide Nitrification and Denitrification ^{15}N enrichment factors from Amazon Forest soils. *Ecol. Appl.* 16, 2153–2167.
- Peri, P.L., Ladd, B., Pepper, D.A., Bonser, S.P., Laffan, S.W., Amelung, W., 2012.

- Carbon ($\delta^{13}\text{C}$) and nitrogen ($\delta^{15}\text{N}$) stable isotope composition in plant and soil in Southern Patagonia's native forests. *Glob. Chang. Biol.* 18, 311–321.
<https://doi.org/10.1111/j.1365-2486.2011.02494.x>
- Rascher, K.G., Hellmann, C., Mágua, C., Werner, C., 2012. Community scale ^{15}N isoscapes: Tracing the spatial impact of an exotic N 2-fixing invader. *Ecol. Lett.* 15, 484–491. <https://doi.org/10.1111/j.1461-0248.2012.01761.x>
- Robinson, D., 2001. $\delta^{15}\text{N}$ as an integrator of the nitrogen. *Trends Ecol. Evol.* 16, 153–162. [https://doi.org/10.1016/s0169-5347\(00\)02098-x](https://doi.org/10.1016/s0169-5347(00)02098-x)
- Rohatgi, A., 2018. WebPlotDigitizer. Austin, Texas, USA.
<https://automeris.io/WebPlotDigitizer>
- Terzer, S., Wassenaar, L.I., Araguás-Araguás, L.J., Aggarwal, P.K., 2013. Global isoscapes for $\delta^{18}\text{O}$ and $\delta^2\text{H}$ in precipitation: Improved prediction using regionalized climatic regression models. *Hydrol. Earth Syst. Sci.* 17, 4713–4728.
<https://doi.org/10.5194/hess-17-4713-2013>
- Trabucco, A., Zomer, R.J., Bossio, D.A., van Straaten, O., Verchot, L. V., 2008. Climate change mitigation through afforestation/reforestation: A global analysis of hydrologic impacts with four case studies. *Agric. Ecosyst. Environ.* 126, 81–97.
<https://doi.org/10.1016/j.agee.2008.01.015>
- Viscarra Rossel, R.A., Brus, D.J., Lobsey, C., Shi, Z., McLachlan G., 2016. Baseline estimates of soil organic carbon by proximal sensing: Comparing design-based, model-assisted and model-based inference. *Geoderma* 265, 152–163.
- Yang, R.M., Zhang, G.L., Liu, F., Lu, Y.Y., Yang, F., Yang, F., Yang, M., Zhao, Y.G., Li, D.C., 2016. Comparison of boosted regression tree and random forest models for mapping topsoil organic carbon concentration in an alpine ecosystem. *Ecological Indicators* 60, 870–878.
- Zhao, M., Heinsch, F.A., Nemani, R.R., Running, S.W., 2005. Improvements of the MODIS terrestrial gross and net primary production global data set. *Remote Sens. Environ.* 95, 164–176. <https://doi.org/10.1016/j.rse.2004.12.011>
- Zomer, R.J., Trabucco, A., Bossio, D.A., Verchot, L. V., 2008. Climate change mitigation: A spatial analysis of global land suitability for clean development mechanism afforestation and reforestation. *Agric. Ecosyst. Environ.* 126, 67–80.
<https://doi.org/10.1016/j.agee.2008.01.014>

CAPÍTULO 3 – APLICAÇÃO DE MODELO ISOTÓPICO ESPACIAL DE $\delta^{15}\text{N}$ DO SOLO EM ESTIMATIVAS DE PERDAS DE NITROGÊNIO POR DESNITRIFICAÇÃO NOS ECOSISTEMAS NATURAIS DA AMÉRICA DO SUL

Resumo

O nitrogênio é um elemento limitante da produção primária dos ecossistemas terrestres. Modelos isotópicos de balanço de massa ajudam a entender os padrões de perdas de N ao longo dos ecossistemas. Neste contexto, o objetivo deste estudo foi estimar o fluxo de perdas de N por vias gasosas devido à desnitrificação e por vias de lixiviação em estado de equilíbrio nos ecossistemas naturais da América do Sul, usando um novo modelo isotópico espacial de $\delta^{15}\text{N}$ do solo (ver capítulo 2). Para isso, foram compilados modelos de fixação biológica de N (FBN) e deposição atmosférica de N para o continente. Esses modelos somados representam o total de entrada de N nos ecossistemas naturais. Depois foi calculada a fração de N perdida por vias gasosas (f_{gas}) com base nos modelos de $\delta^{15}\text{N}$ do solo e de entrada e no efeito do fracionamento isotópico da desnitrificação, lixiviação e volatilização da amônia. A partir desta etapa os fluxos de perdas de N por vias gasosas e por lixiviação foram calculados. Na sequência, todo o procedimento metodológico foi repetido, desta vez usando outra isoscape de $\delta^{15}\text{N}$ do solo, para posterior comparação entre os resultados das duas abordagens. As estimativas a partir da isoscape deste estudo indicam que 32,4% do N é perdido para a atmosfera via desnitrificação nos solos naturais da América do Sul. As estimativas de fluxo de N mostraram que $1,3 \pm 1,1 \text{ g N m}^{-2}\text{ano}^{-1}$ é perdido em média para atmosfera pelo processo de desnitrificação nos solos naturais do continente. Perdas por lixiviação são de $2,5 \pm 1,8 \text{ g N m}^{-2}\text{ano}^{-1}$. As principais diferenças entre os resultados das duas isoscapes testadas ocorreram nos ecossistemas de savanas, onde este estudo estimou valores significativamente menores em relação à isoscape comparada. As nossas estimativas são mais coerentes com observações empíricas, o que mostra a importância da precisão dos modelos de entrada na interpretação dos resultados do modelo isotópico de balanço de massa.

Palavras-chave: modelo isotópico; balanço de massa; fluxo de N;

Introdução

Perdas de nitrogênio (N) dos ecossistemas terrestres limitam o estoque de carbono, a produção primária líquida e influenciam a dinâmica do clima (Galloway et al., 2008). O N pode ser perdido dos ecossistemas terrestres por emissão de formas gasosas ou por lixiviação de N dissolvido. A razão isotópica de N do solo tem se mostrado uma importante ferramenta que integra informações de entrada e saída de N dos ecossistemas (Craine et al., 2015). Medidas de isótopos estáveis de N do solo são inseridas em modelos isotópicos de balanço de massa para estimar a fração relativa de N que deixa ecossistemas terrestres naturais por desnitrificação e lixiviação (Bai et al., 2012, Houlton et al., 2015a, 2006, Houlton and Bai, 2009, Weintraub et al., 2016). Os resultados desses estudos estão alinhados entre si. Houlton e Bai (2009) estimaram que aproximadamente 1/3 das perdas de N dos ecossistemas terrestres é causada pela ação microbiana. Bai et al. (2012), adaptando o modelo de Houton e Bai (2009), estimaram que 35% das perdas relativas de N são produto da desnitrificação na biosfera terrestre. Ambos são baseados no modelo isotópico espacial de Amundson et al. (2003), que apontou um gradiente do $\delta^{15}\text{N}$ do solo seguindo os padrões globais de média anual de precipitação (MAP) e temperatura (MAT). Com isso, as estimativas do modelo isotópico de balanço de massa conseguem acessar padrões regionais de fração de perdas e fluxos de N gasoso e dissolvido (Bai et al., 2012).

As maiores perdas relativas de N por desnitrificação ocorrem em ambientes secos, onde o potencial de evapotranspiração é maior que a precipitação na maior parte do ano (Galbally et al., 2008). No entanto, isso não se reflete no fluxo de N que é perdido para a atmosfera, visto que este nutriente é limitante desses ecossistemas (Freitas et al., 2010, Menezes et al., 2012). Por outro lado, a fração relativa de perdas gasosas diminui consideravelmente em ambientes de clima temperado, dando lugar ao predomínio de perdas por lixiviação (Seitzinger et al., 2006). A variação espacial das perdas de N por desnitrificação e lixiviação também está bem documentada nas áreas de florestas tropicais (Houlton et al., 2006, Nardoto et al., 2008, Pérez et al., 2006, Weintraub et al., 2016). Nessas regiões, áreas com grande aporte de precipitação ($> 4000 \text{ mm}$) têm a desnitrificação restrita devido à diminuição da atividade da enzima desnitrificante (DEA – sigla em inglês), que indica de forma quantitativa o processo biológico multi enzimático da redução de NO_3^- para N_2 (Nardoto et al., 2008). Além disso, o grande fluxo de água aumenta as perdas por lixiviação. Por outro lado, nas florestas tropicais com precipitação $< 3000 \text{ mm}$, existe uma maior disponibilidade de N que induz a um maior potencial de

nitrificação e desnitrificação, favorecendo as perdas de N por vias gasosas (Nardoto et al., 2008, Pérez et al., 2006).

Os modelos isotópicos de balanço de massa global foram capazes de estimar esses padrões nesses ambientes de maneira eficiente, com resultados coerentes com observações empíricas (Houlton and Bai 2009, Bai et al., 2012). No entanto, Bai et al. (2012) superestimaram os fluxos de N_2O ($0,15 - 0,40 \text{ g N m}^{-2} \text{ ano}^{-1}$) quando comparado com observações empíricas (Dalal and Allen, 2008, de Carvalho et al., 2017). Os autores interpretaram que a ausência de informações sobre o regime de fogo nas savanas podem ter aumentado a estimativa de N_2O . Porém, em áreas de savana tropical, existe o predomínio de NH_4^+ no solo em relação ao NO_3^- , o que restringe as emissões acumuladas por desnitrificação (Bustamante et al. 2006).

Outra explicação possível para essa incongruência é a isoscape usada no modelo de Bai et al. (2012). Esse modelo é baseado em regressões lineares múltiplas entre dados de $\delta^{15}\text{N}$ no solo e MAP e MAT apresentadas por Amundson et al. (2003). Embora a isoscape de Amundson et al. (2003) seja eficiente para mostrar padrões de variação global, ela apresenta inconsistências na representação dos padrões regionais devido à falta de pontos amostrais em alguns ecossistemas como, por exemplo, as savanas tropicais. Portanto, é possível que as incertezas presentes na isoscape se reflita nos resultados do modelo de Bai et al. (2012), podendo levar a interpretações equivocadas. Craine et al. (2015) sugeriram que antes de aplicar modelos de $\delta^{15}\text{N}$ em estimativas e previsões do ciclo do N, é preciso expandir as bases de dados de $\delta^{15}\text{N}$. Para os autores, relações não-lineares tornam-se evidentes conforme aumenta a base de dados de $\delta^{15}\text{N}$, o que pode afetar as interpolações do ciclo do nitrogênio em ecossistemas pouco representados (Craine et al., 2015).

Neste contexto, o objetivo deste estudo foi estimar o fluxo de perdas de N gasoso e dissolvido em ecossistemas terrestres naturais da América do Sul. Para tanto, foi incorporada a nova isoscape de $\delta^{15}\text{N}$ do solo para a América do sul no modelo proposto por Bai et al. (2012). Esta nova isoscape foi gerada com a incorporação de dados empíricos coletados em áreas com déficit de amostragem na América do Sul. Além disso, foi baseada em relações não lineares entre $\delta^{15}\text{N}$ do solo e múltiplas covariáveis climáticas, pedológicas e biofísicas (Sena-Souza et al., 2019 em revisão – ver capítulo 2).

Material e Métodos

Área de estudo

A modelagem foi realizada para o continente da América do Sul. Este continente contém nove grandes biomas em seu território segundo a classificação de Olson et al. (2001) (Figura 3.1). Além disso, existem seis importantes *hotspots* de conservação da biodiversidade no continente: Mata Atlântica, Cerrado, Floresta de Valdívia, Andes Tropical e a região de Tumbes-Chacó-Magdalena (Phoenix et al., 2006).

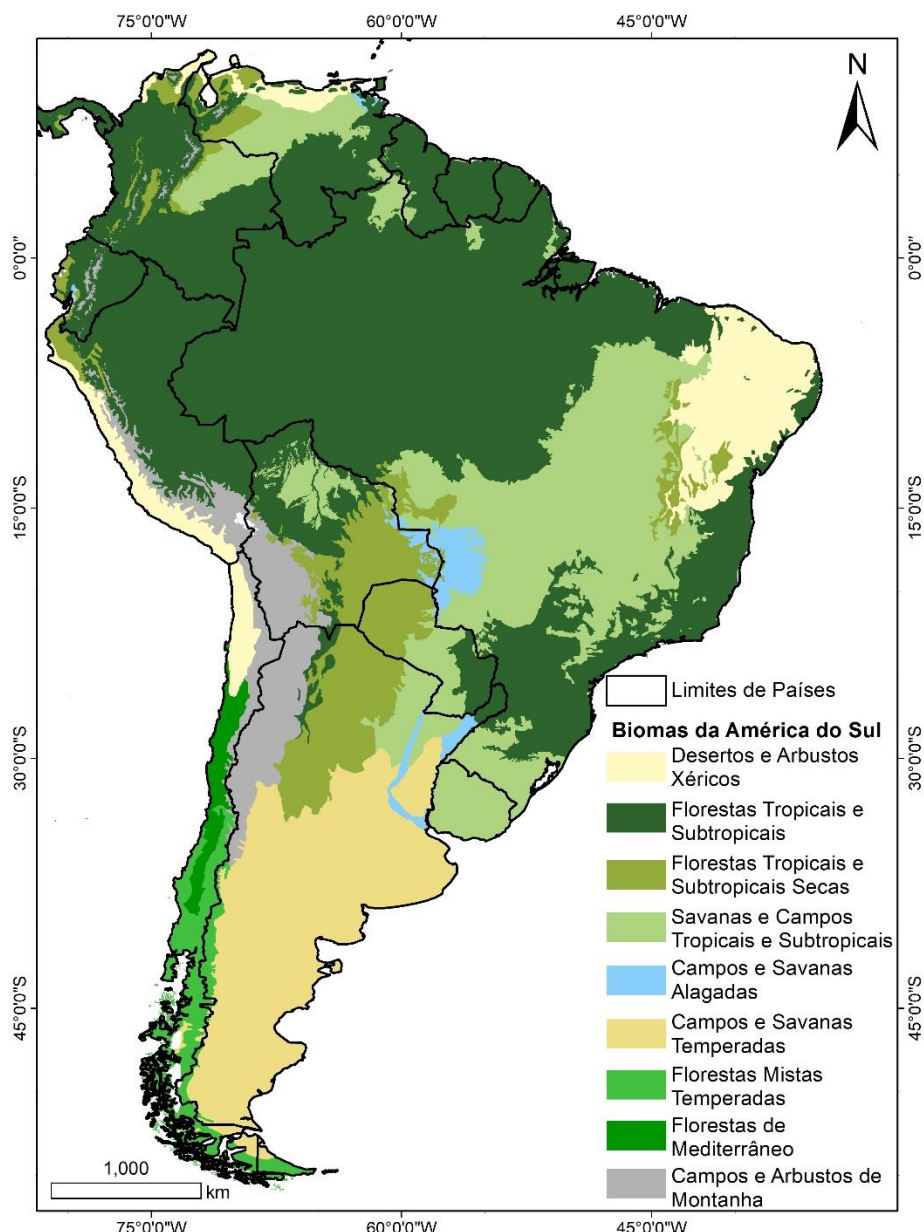


Figura 3.1. Mapa da América do Sul mostrando os biomas segundo a classificação de Olson et al. (2001).

Abordagem metodológica

A abordagem deste estudo é baseada no trabalho de Bai et al. (2012). A primeira etapa do trabalho consistiu em usar dados secundários de fixação de N (Wang and Houlton, 2009) e de deposição de N (Lelieveld and Dentener, 2000) para estimar a massa total de entrada de N dos ecossistemas terrestres da América do Sul. Posteriormente, uma isoscape de $\delta^{15}\text{N}$ do solo gerada a partir de aplicação de algoritmo de floresta randômica (ver capítulo anterior) foi aplicada ao modelo para estimar a proporção de perda de N por pela desnitrificação e pela lixiviação. Por fim, a isoscape de $\delta^{15}\text{N}$ do solo gerada pela equação de Amundson (2003), amplamente utilizada na literatura, foi aplicada ao mesmo modelo de Bai et al. (2012). Esta etapa nos permite apontar as principais diferenças entre os dois modelos isotópicos espaciais na estimativa de saídas de N dos ecossistemas. Por fim, nós estimamos a incerteza do modelo. Os dados de entrada do modelo se encontram em diferentes resoluções espaciais, havendo então a necessidade de padronização. Portanto, nós padronizamos a resolução espacial em $0.5^\circ \times 0.5^\circ$.

Evolução do modelo isotópico de balanço de massa

O modelo isotópico utilizado neste estudo é baseado em um modelo conceitual apresentado por Houlton et al. (2006). Este modelo considera o pressuposto de estado de equilíbrio dos ecossistemas. Isso significa que, de modo geral, a quantidade de N que entra no ecossistema terrestre por deposição e fixação biológica de N é a mesma que é perdida por emissões de N gasoso e por lixiviação de N dissolvido. Ou seja, a fração de N que se perde por vias gasosas ($f_{gastotal}$) e somado à fração que sai por lixiviação ($f_{lixiviação}$) é igual ao total de N perdido (Eq. 1).

$$f_{gastotal} + f_{lixiviação} = 1 \quad (1)$$

Embora uma parte do N que entra fique retido no solo em forma de NO_3^- ou associado aos minerais, essa parcela de N é mínima e não apresenta um efeito significativo no balanço de N do sistema. O estado de equilíbrio vem sendo reportado em matemáticos anteriores (Amundson et al., 2003, Brenner et al., 2001, Houlton et al., 2006, Houlton and Bai, 2009), bem como por observações empíricas em diversos ecossistemas ao redor da Terra (Houlton et al., 2006, Houlton and Bai, 2009). Ou seja, os processos do ciclo interno de N não afetam o $\delta^{15}\text{N}$ do solo total. Assim, assumimos que o $\delta^{15}\text{N}$ do solo se dá pela seguinte equação (Eq. 2):

$$\delta^{15}N_{solo} = \delta^{15}N_I + f_{gastotal} \times \varepsilon_{gastotal} + f_{lixiviação} \times \varepsilon_L \quad (2)$$

Onde:

$\delta^{15}N_{solo}$ é o valor da razão isotópica do solo,

$\delta^{15}N_I$ é a razão isotópica do N que entra no ecossistema (deposição ou FBN – fixação biológica de N),

$f_{gastotal}$ é a fração de N do sistema que se perde por vias gasosas (incluindo nitrificação/desnitrificação e volatilização de NH_3),

$f_{lixiviação}$ é a fração de N que se perde por lixiviação,

$\varepsilon_{gastotal}$ é o fator de enriquecimento isotópico das perdas de N por vias gasosas,

ε_L é o fator de enriquecimento isotópico das perdas de N por lixiviação.

No modelo de Bai et al. (2012), no qual este estudo é baseado, todas as formas de desnitrificação são consideradas juntas, uma vez que os diferentes grupos de bactérias levam a um fracionamento isotópico similar nesse processo (Sutka et al. 2006). Entretanto, a fração das perdas por volatilização do NH_3 (f_{NH_3}) foi contabilizada a partir do fluxo médio em solos naturais calculado por bioma na escala global (Bouwman et al. 1997) e separada da perda gasosa total, com o intuito de estimar apenas as perdas de N gasoso provenientes de processos biológicos (Eq. 3).

$$f_{gastotal} = f_{gas} + f_{NH_3} \quad (3)$$

Assim, o f_{NH_3} foi inserido no modelo de f_{gas} . Portanto, f_{gas} se refere à perda de N gasoso pelo processo de desnitrificação. Tendo o novo modelo isotópico espacial de $\delta^{15}N_{solo}$ (ver capítulo 2), é possível adaptar a equação Eq. 2 isolando f_{gas} e inserindo f_{NH_3} para estimar a fração de N que se perde por vias gasosas da desnitrificação (Eq. 4):

$$f_{gas} = \frac{\delta^{15}N_{solo} - \delta^{15}N_I - (\varepsilon_{NH_3} - \varepsilon_L) \times f_{NH_3} - \varepsilon_L}{\varepsilon_G - \varepsilon_L} \quad (4)$$

A conversão de f_{gas} em fluxo de N gasoso (N_{gas}) em estado de equilíbrio foi realizada inserindo modelos espaciais de entrada de N (Eq. 5):

$$N_{gas} = (N_{fixação} + N_{deposição}) \times f_{gas} \quad (5)$$

Os modelos espaciais de entrada de N foram os mesmos modelos usados por Bai et al. (2012), para posterior comparação entre os resultados obtidos. Os modelos foram disponibilizados por Edith Bai via comunicação pessoal. $N_{fixação}$ é a combinação do

modelo global de fixação simbiótica de N₂, gerado pelo modelo CASA CNP) (Wang et al., 2010, 2007, Wang and Houlton, 2009) e um modelo de fixação assimbiótica de N₂, baseado na média por bioma (Cleveland et al., 1999) e na classificação no modelo CASA CNP (Wang et al. 2007, Wang et al. 2010). O modelo de $N_{depo\acute{s}ito}$ é um modelo tridimensional de transporte químico de Lelieveld e Dentener (2000).

Parametrização do modelo

Os valores atribuídos a cada parâmetro do modelo de f_{gas} foram definidos com base em observações empíricas. O $\delta^{15}\text{N}$ dos compostos de N que entram nos ecossistemas fica próximo de 0‰. Isso ocorre tanto para entradas por fixação biológica de N (Boddey et al., 2000, Yoneyama et al., 1993), quanto por deposição atmosférica (Handley et al., 1999). Esses valores ocorrem porque a amostra padrão para medidas isotópicas é a razão isotópica do ar atmosférico. Portanto, para o $\delta^{15}\text{N}_I$ foi usado um modelo espacial com valores entre -1,5‰ e 0‰ (Bai et al. 2012).

Cada caminho de perda de N gera um efeito de fracionamento distinto devido à discriminação isotópica que deixa o substrato enriquecido em ^{15}N . A volatilização do NH₃ é o processo que causa o maior efeito de fracionamento (ε_{NH_3}). Neste estudo foi considerado um ε_{NH_3} de 29‰, de acordo com a média observada por Höglberg (1997). Para o efeito do fracionamento isotópico causado pelas perdas via emissão de gases da desnitrificação (ε_G) em áreas naturais foi considerado o valor de 16‰ (Houlton and Bai, 2009). Entre as vias pelas quais o N é perdido dos ecossistemas terrestres, caminhos de lixiviação de N dissolvido são os que causam menor discriminação isotópica (Feuerstein et al., 1997, Houlton et al., 2006). O valor de ε_L foi 1‰, o mesmo usado na parametrização de Bai et al. (2012).

Isoscapes de $\delta^{15}\text{N}$ do solo e comparação entre os modelos

A isoscape de $\delta^{15}\text{N}$ do solo usada neste estudo foi elaborada a partir de variáveis climáticas, pedológicas, de vegetação, bem como limites de ecorregiões e biomas (ver capítulo 2, Sena-Souza et al. 2019 em revisão). Essa isoscape foi elaborada a partir de uma abordagem de *machine learning* usando o algoritmo de floresta randômica, que apontou os limites dos biomas como a principal covariável na predição do $\delta^{15}\text{N}$ do solo, seguido pelo teor de carbono orgânico e pela média anual de precipitação. Essa abordagem permitiu aumentar a amplitude dos valores preditos de $\delta^{15}\text{N}$ do solo (-2‰ a 14,5‰) em comparação ao modelo de regressão linear múltiplo com dados climáticos de

precipitação (MAP) e temperatura (MAT) (Eq. 6) usada por Bai et al. (2012) no modelo isotópico de balanço de massa (-2,5‰ a 10,5‰) (Amundson et al. 2003).

$$\delta^{15}N_{\text{soil}} = 0.2048 \times \text{MAP} - 0.0012 \times \text{MAT} + 4.32 \quad (6)$$

A equação de Amundson et al (2003) foi aplicada aos dados climáticos de MAP e MAT da base de dados WorldClim medidos anualmente entre 1970 e 2000 (Hijmans et al., 2005) para representar o modelo de isoscape usado em Bai et al. (2012). As estimativas de fluxo de N gasoso geradas com base nas duas isoscapes foram comparados por meio do teste U não-paramétrico de Mann-Whitney Wilcoxon. A diferença estatística da distribuição dos valores de fluxo de N gasoso modelado foi medida considerando os biomas que apresentaram as maiores médias.

Resultados

Modelo f_{gas}

O modelo apresentado na Figura 3.2 mostra diferenças nos padrões regionais. O primeiro padrão espacial observado são as maiores perdas por fração gasosa de N na região nordeste do continente, e as menores seguindo o padrão regional da cordilheira dos Andes, ao longo da costa oeste da América do Sul. Áreas com valores baixos também podem ser observadas na região central do Brasil, onde se encontra grande parte das savanas tropicais do continente. O modelo também indica um gradiente de f_{gas} na região da floresta tropical úmida, com a fração de perdas de N por vias gasosas diminuindo de leste (Amazônia oriental) para oeste (Amazônia ocidental) (Figura 3.2). De modo geral, o modelo elaborado com base na nova isoscape de $\delta^{15}\text{N}$ do solo indicou que 32,4% do N que entra nos ecossistemas terrestres não fertilizados da América do Sul voltam para a atmosfera via desnitrificação a cada ano.

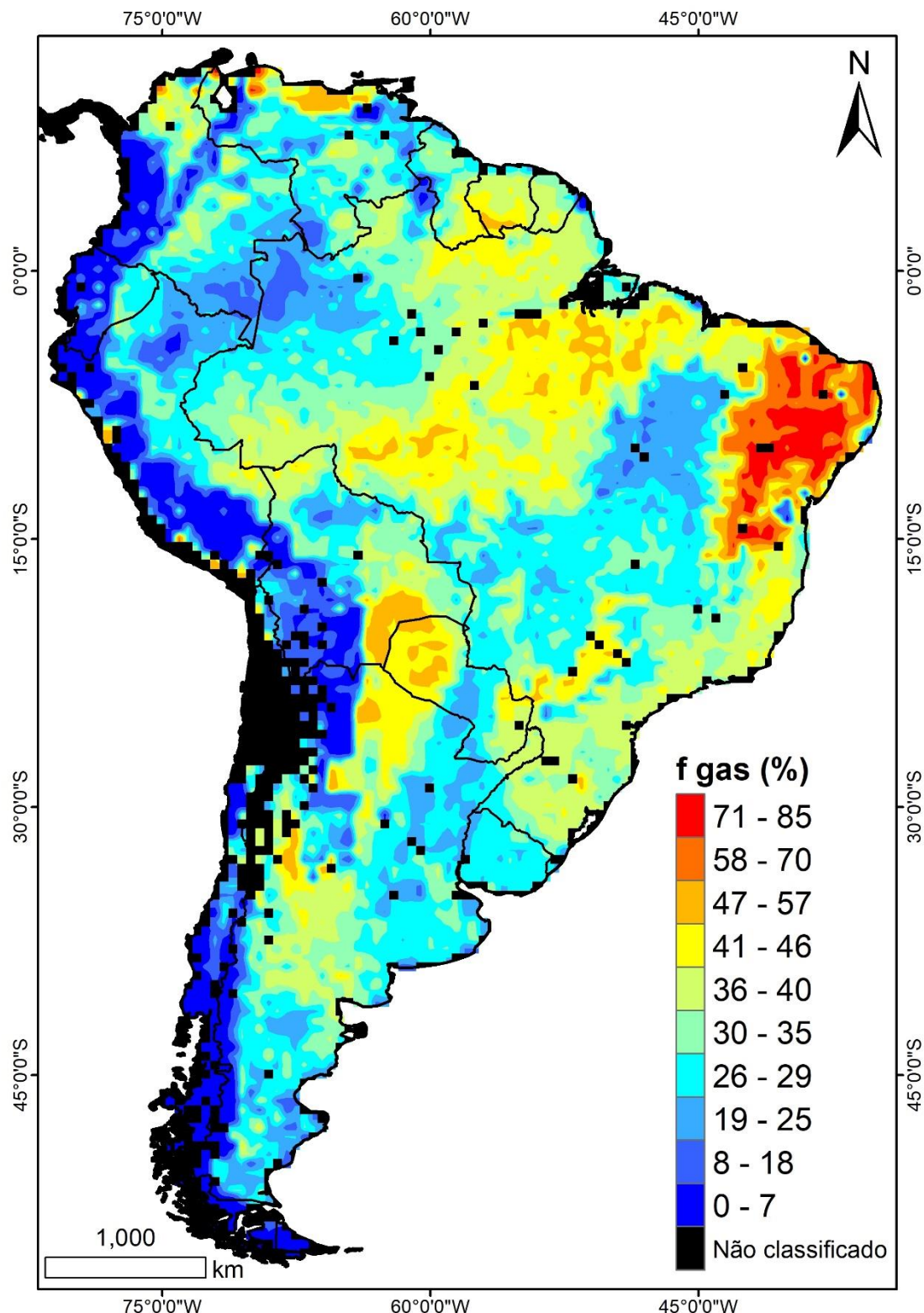


Figura 3.2. Resultado do modelo mostrando o padrão espacial da fração de perda de N que deixa o sistema em formas gasosas como produto da desnitrificação (f_{gas}).

Na região nordeste do continente, de clima semi-árido, 60,5% ($\pm 15,5\%$) do N sai pela desnitrificação. Por outro lado, as regiões de florestas mistas temperadas apresentaram a menor média de fração gasosa, com 11,2% ($\pm 7,1\%$) (Figura 3.3). Seguindo o padrão das savanas tropicais, a região de campos e savanas alagadas teve um f_{gas} médio calculado em 28,6% ($\pm 4,6\%$). Esses valores indicam que aproximadamente 71 % do N que entra na região de savanas alagadas via deposição ou fixação biológica de N é perdido como N dissolvido via lixiviação. Esse padrão foi semelhante ao modelado para as áreas de savanas tropicais, onde 27,7% ($\pm 6,4\%$) do N volta para a atmosfera via desnitrificação, e para os campos de clima temperado (28,8% $\pm 7,1\%$). Nas regiões de floresta tropical úmida, a fração gasosa das perdas de N foi 32,9% ($\pm 9,3\%$).

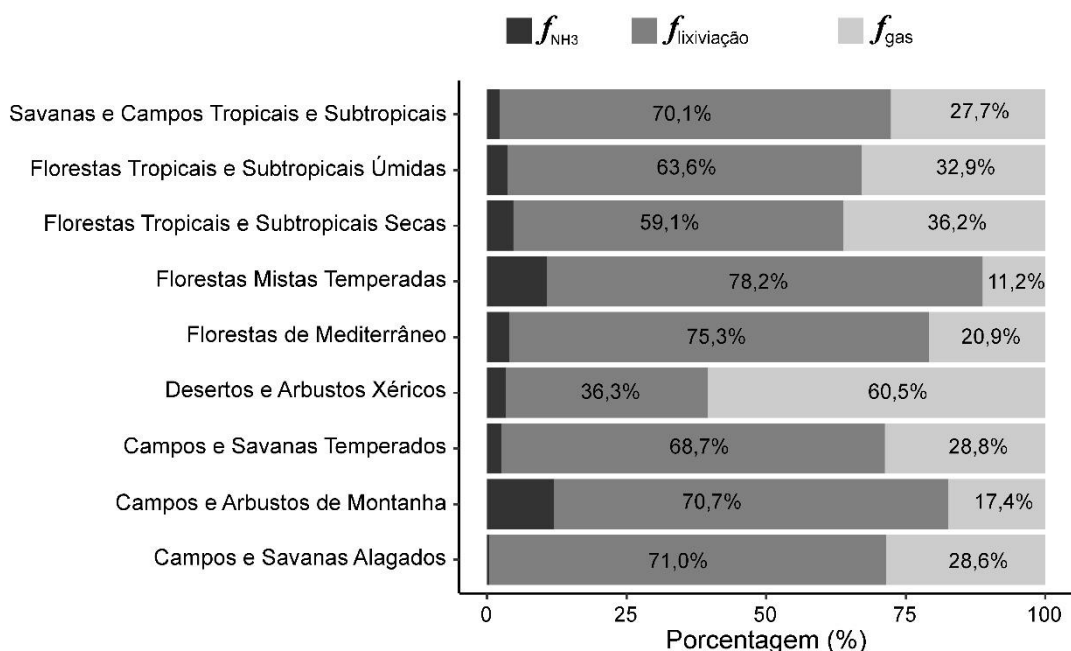


Figura 3.3. Proporção estimada da contribuição de cada caminho para a perda total de N dos principais biomas da América do Sul.

Fluxo de saída de N via lixiviação vs desnitrificação

As estimativas do modelo deste estudo mostram que $1,3 \pm 1,1 \text{ g N m}^{-2}\text{ano}^{-1}$ é perdido em média para atmosfera pelo processo de desnitrificação nos ecossistemas terrestres não fertilizados da América do Sul (Figura 3.4a). As maiores perdas estimadas são no território do Brasil, com exceção da região da Amazônia Ocidental e da porção norte do bioma Cerrado, onde os valores de fluxo de N da desnitrificação são baixos (Figura 3.4a). Valores altos de fluxo de N por vias gasosas também aparecem no sul da Bolívia e no Paraguai (Figura 3.4a). O modelo de fluxo de saída de N por lixiviação mostrou que $2,5 \pm 1,8 \text{ g N m}^{-2}\text{ano}^{-1}$ são perdidos dos ecossistemas terrestres naturais da

área de estudo como compostos de N dissolvido. As maiores perdas por lixiviação ocorrem nos ecossistemas de savanas tropicais no centro-oeste do Brasil, sudeste da Bolívia e Paraguai (Figura 3.4b).

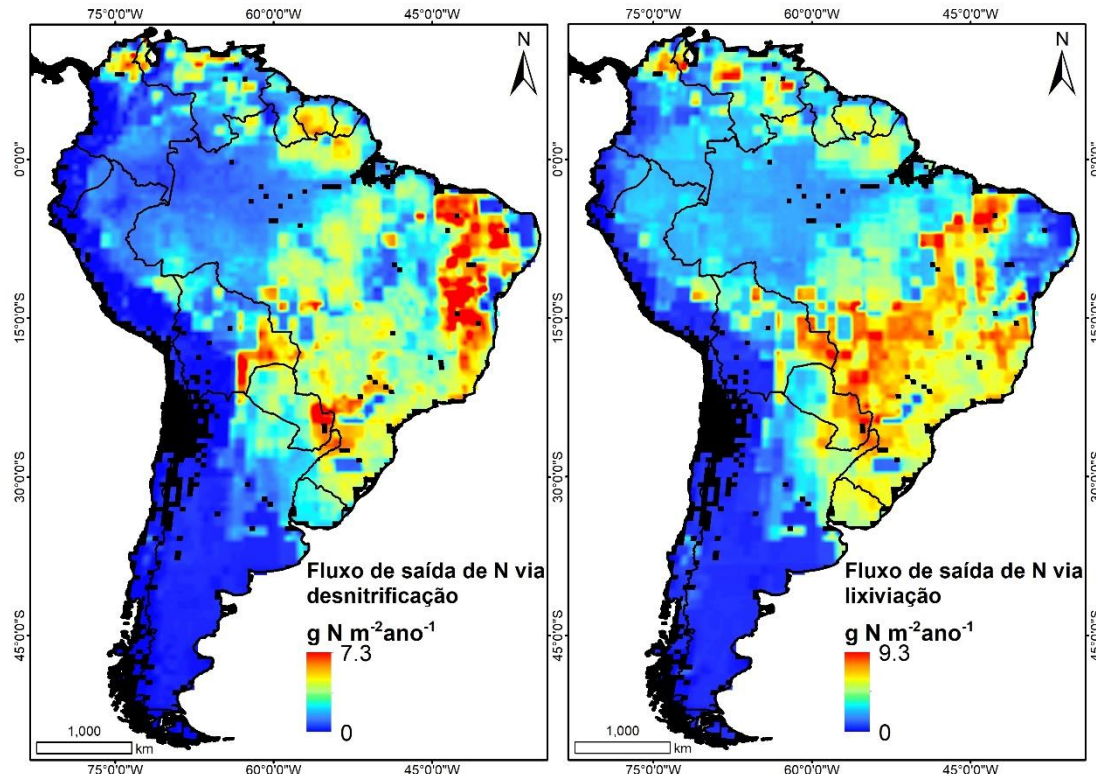


Figura 3.4. Resultados dos modelos de fluxo de N que se perde por desnitrificação (a) e por lixiviação (b).

Em relação aos padrões regionais de fluxo de N via desnitrificação, a região de desertos e arbustos xéricos tem a maior média de perda de N gasoso, de $2,6 \pm 1,8$ g N m⁻² ano⁻¹. A região do semi-árido é a única com as perdas gasosas maiores que as perdas por lixiviação nos ecossistemas naturais (Figura 3.3). Nessas áreas, as perdas de N dissolvido modelado é de $1,7 \pm 1,4$ g N m⁻² ano⁻¹ (Tabela 3.1). Por outro lado, as maiores perdas de N por lixiviação ocorrem nas áreas de savanas alagadas, $4,6 \pm 1,7$ g N m⁻² ano⁻¹, e nas savanas tropicais $4,2 \pm 1,7$ g N m⁻² ano⁻¹ (Tabela 3.1). As florestas tropicais úmidas perdem em média $1,3 \pm 1,0$ g N m⁻² ano⁻¹ por vias gasosas e $2,5 \pm 1,4$ g N m⁻² ano⁻¹ como N dissolvido. Esses padrões foram semelhantes ao modelado para as florestas secas, onde $1,5 \pm 1,4$ g N m⁻² ano⁻¹ são perdidos dos ecossistemas terrestres por via gasosa devido à atividade microbiana, enquanto que $2,5 \pm 1,9$ g N m⁻² ano⁻¹ são perdidos via lixiviação (Tabela 1). Outras regiões apresentaram um fluxo de saída de N muito baixo, como a

Patagônia e as tundras ao longo da Cordilheira dos Andes ($0,0 \pm 0,1$ g N m $^{-2}$ ano $^{-1}$ e $0,1 \pm 0,1$ g N m $^{-2}$ ano $^{-1}$, respectivamente).

Tabela 3.1. Resultados estimados de fluxo regional de saída de nitrogênio dos ecossistemas terrestres naturais dos principais biomas da América do Sul. Valores representam a média aritmética \pm desvio padrão.

Bioma	Área (10 ¹² m ²)	Saída de N do modelo (g N m ⁻² ano ⁻¹)	
		Desnitrificação	Lixiviação
Desertos e Arbustos Xéricos	0,85	$2,6 \pm 1,8$	$1,6 \pm 1,4$
Campos e Savanas Temperados	1,54	$0,3 \pm 0,3$	$0,7 \pm 0,9$
Florestas Tropicais e Subtropicais Secas	1,41	$1,5 \pm 1,4$	$2,4 \pm 1,9$
Florestas Tropicais e Subtropicais Úmidas	8,24	$1,3 \pm 1,0$	$2,4 \pm 1,4$
Florestas de Mediterrâneo	0,09	$0,1 \pm 0,1$	$0,5 \pm 0,5$
Campos e Savanas Alagados	0,26	$1,9 \pm 0,9$	$4,5 \pm 1,7$
Florestas Mistas Temperadas	0,18	$0,0 \pm 0,1$	$0,3 \pm 0,3$
Savanas e Campos Tropicais e Subtropicais	3,21	$1,7 \pm 0,9$	$4,1 \pm 1,7$
Campos e Arbustos de Montanha	0,52	$0,1 \pm 0,1$	$0,3 \pm 0,5$
Total (América do Sul)	16,3	$1,3 \pm 1,1$	$2,5 \pm 1,8$

Comparação com abordagens anteriores usando outras isoscapes de δ¹⁵N do solo

O modelo gerado neste estudo se difere de Bai et al. (2012) pela abordagem da elaboração da isoscape de δ¹⁵N do solo como dado de entrada. É possível observar as diferenças nos resultados no modelo final com base nas duas abordagens comparando os valores dos ecossistemas com maiores emissões de N gasoso via desnitrificação. Entre os principais ecossistemas testados, a área de desertos e arbustos xéricos foi a única na qual o modelo apresentado neste estudo teve valores significativamente maiores que os valores de desnitrificação de Bai et al. (2012) (teste de Wilcoxon, $W = 41958$, $p < 0,01$) (Figura 3.5). As áreas de florestas tropicais úmidas e florestas tropicais secas tiveram valores modelados menores que a abordagem de Bai et al. (2012) ($W = 3146400$, $p < 0,001$, $W = 104140$, $p < 0,01$, respectivamente). Entretanto, as maiores diferenças entre os dois modelos se encontram nos ecossistemas de savanas tropicais ($W = 273890$, $p < 0,001$) e nos campos e savanas alagadas ($W = 1576$, $p < 0,001$). Em ambos os ecossistemas os valores médios das perdas de N por atividade microbiológica foram significativamente inferiores ao modelo usado na comparação (Figura 3.5).

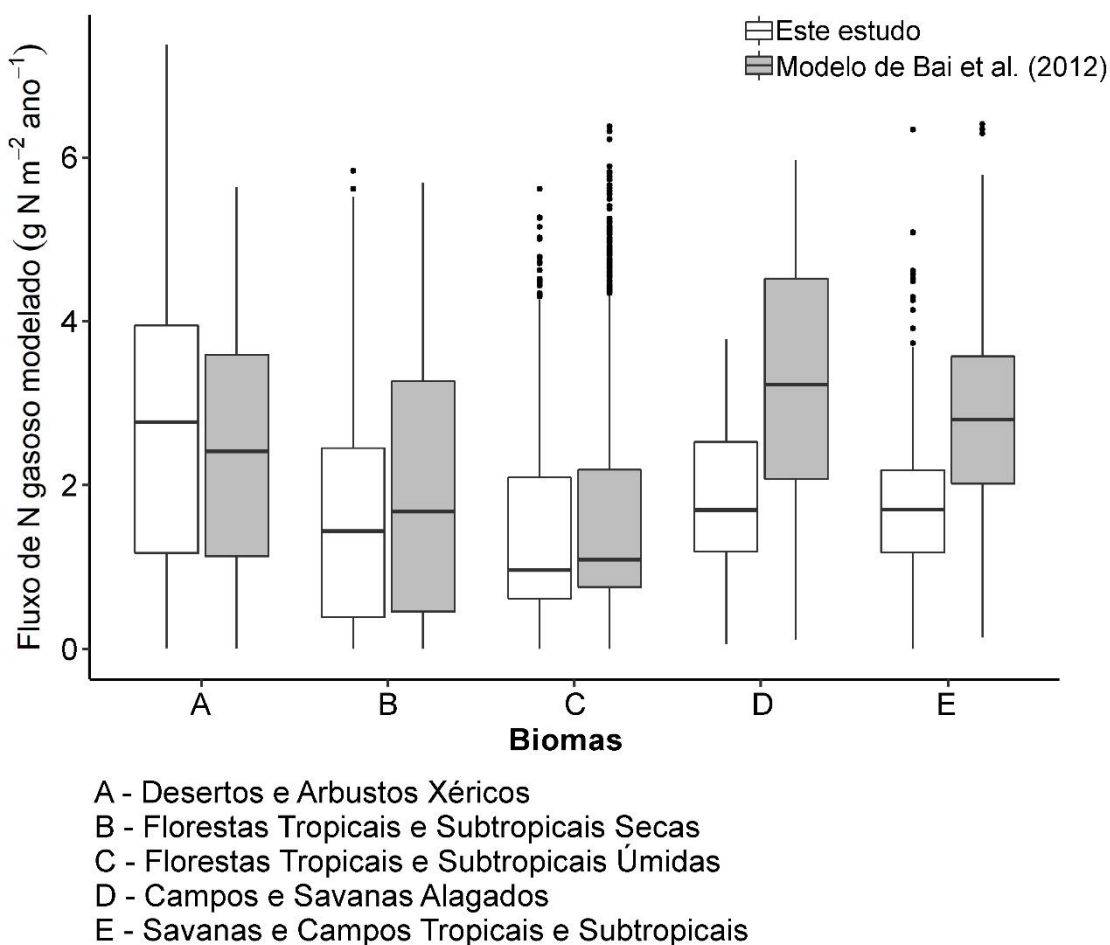


Figura 3.5. Boxplot mostrando as diferenças entre o fluxo de N que se perde pela desnitrificação nos biomas tropicais da América do Sul. As letras no eixo x correspondem aos biomas nomeados na legenda na parte inferior da figura. As barras brancas correspondem ao modelo baseado na isoscape do capítulo 2; as barras cinzas correspondem ao modelo baseado na isoscape de Amundson et al. (2003).

Discussão

Este novo modelo de $\delta^{15}\text{N}$ do solo foi usado para estimar as perdas de N gasoso em estado de equilíbrio para os ecossistemas naturais da América do Sul, em uma abordagem semelhante à outros estudos realizados em diversas escalas (Bai et al. 2012, Hilton et al. 2013, Houlton et al. 2015, Weintraub et al., 2016). A fração de perdas por desnitrificação modelada para a América do Sul (32,4%) foi semelhante à proporção 35% encontrada por Bai et al. (2012) para a escala global. Os resultados também concordam com o padrão encontrado por Houlton e Bai (2009), que apontam uma perda de aproximadamente 1/3 do N por desnitrificação de volta para a atmosfera. Entretanto, a

amplitude de fgas encontrada nesse estudo (0% a 84%) foi maior que a mapeada por Bai et al. (2012) (0% a 69%). Essa diferença pode ser explicada pela maior amplitude de valores de $\delta^{15}\text{N}$ do solo representada pela isoscape usada no presente estudo (Sena-Souza et al., 2019 em revisão – ver capítulo 2).

A variação espacial do modelo de f_{gas} mostra que as menores frações de perdas de N por vias gasosas ocorrem nos biomas de clima temperado, principalmente na área de floresta temperada e de campos de montanha, seguindo ao norte do continente ao longo da cordilheira dos Andes. Nessas áreas, o caminho de saída de N predominante é a lixiviação. Nessas regiões, a baixa temperatura provavelmente é um fator limitante da decomposição da matéria orgânica, o que faz com que o solo apresente baixa quantidade de nitrato, limitando assim a desnitrificação na maior parte do ano (Seitzinger et al., 2006). Por isso, as perdas por desnitrificação ficam restritas (menores que 20%). Essa proporção está concordando com estudos anteriores que indicaram uma perda expressiva de N dissolvido em comparação com o N gasoso em ecossistemas terrestres temperados (Seitzinger et al., 2006).

Nas florestas tropicais úmidas, embora a média de f_{gas} seja semelhante àquela calculada para a América do Sul, a distribuição espacial não é homogênea. Na região que corresponde à Amazônia ocidental, a fração de perda de N proveniente da desnitrificação fica entre 8% e 25% de acordo com o modelo. Tal valor está bem abaixo dos valores encontrados na porção leste que chegam à 58%. Esse padrão foi semelhante ao encontrado por Houlton et al. (2006) nas florestas tropicais úmidas do Havaí (de 24% a 53%). Weintraub et al. (2016), por sua vez, estimaram uma amplitude de 10% a 60% de perdas gasosas por desnitrificação em uma área de floresta tropical úmida de montanha na Costa Rica. Esse padrão segue a distribuição espacial da precipitação na região e já foi descrito em estudos sobre a desnitrificação em ambientes de floresta tropical úmida (Nardoto et al., 2008, Houlton et al., 2006, Pérez et al., 2006, Weintraub et al., 2016). Uma explicação proposta por Houlton et al. (2006) é que em condições específicas favoráveis pode ocorrer uma desnitrificação total, anulando o efeito do fracionamento isotópico, uma vez que todo o nitrato seria consumido. Neste caso, o modelo isotópico de balanço de massa aplicado neste estudo não seria capaz de estimar a fração de perdas por desnitrificação. Entretanto, o mais provável é o predomínio de perdas por lixiviação/erosão em áreas de grande aporte de precipitação (Hilton et al. 2013, Weintraub et al., 2016, Houlton and Bai, 2009). Em áreas tropicais montanhosas, as perdas por caminhos hidrológicos são acentuadas pela erosão causada por uma maior inclinação das vertentes (Hilton et al., 2013). Além disso,

a diminuição da temperatura com o aumento da elevação pode restringir o metabolismo microbiano, diminuindo assim a desnitrificação (Weintraub et al., 2016).

Na região que corresponde à Amazônia oriental, a maior fração de perdas por desnitrificação em comparação com a porção oeste do bioma já era esperado devido à uma maior atividade da enzima desnitrificante (Nardoto et al., 2008). Além disso, nas áreas com menor MAP das florestas tropicais úmidas há um maior potencial de mineralização líquida e nitrificação (Pérez et al., 2006). Esses padrões sugerem que nas florestas tropicais úmidas, as maiores perdas ocorrem onde há maior disponibilidade de N (Houlton et al., 2006, Martinelli et al., 1999, Nardoto et al., 2008).

A área dos desertos e arbustos xéricos apresentou a maior proporção de perdas de N por vias gasosas em relação à lixiviação. Nessas áreas, a evapotranspiração é muito maior que a precipitação, portanto a lixiviação tende a ser mais baixa. A volatilização de NH₃ é apontada como um dos principais caminhos de saída de N desses ecossistemas devido ao pH elevado associado ao déficit hídrico (Högberg 1997, Menezes et al., 2012). Embora a desnitrificação seja baixa nesses ecossistemas (Menezes et al. 2012), podem ocorrer picos de atividade microbiana depois de eventos de chuva, que contribuem para o efeito cumulativo do modelo isotópico de balanço de massa.

Nas savanas tropicais e savanas alagadas, a fração de N perdida por vias gasosas fica em torno de 28%. As savanas tropicais da América do Sul possuem um ciclo de N considerado fechado, onde as perdas por de N gasoso é mínimo (Bustamante et al., 2004, Högberg, 1997). Nas savanas tropicais ocorre um predomínio de NH₄⁺ no solo em relação ao NO₃⁻, o que causa as baixas taxas de desnitrificação (Bustamante et al., 2006). Além disso, há uma grande escassez de N nesses sistemas, o que restringe as perdas desse nutriente (Pinto et al., 2002).

A partir do modelo de f_{gas} , foi possível estimar o fluxo de N gasoso, considerando os modelos de FBN e deposição atmosférica (Bai et al., 2012). Os modelos de fluxo permitiram estimar a contribuição de um determinado território para o balanço total de N. Entretanto, por se tratar de um modelo restrito às áreas naturais, não é possível estimar o total de N emitido ou perdido por lixiviação sem informação espacial sobre o uso do solo. Ainda assim, as estimativas de fluxo de perda de N serviram para mostrar os padrões espaciais do efeito cumulativo da desnitrificação em cada bioma.

A comparação entre o modelo de fluxo de N deste estudo com o de Bai et al. (2012) teve como objetivo apontar a importância e as inconsistências decorrentes da precisão da isoscape de $\delta^{15}\text{N}$ do solo. O submodelo de desnitrificação de Bai et al. (2012)

superestimou perdas de N₂O em relação à estudos anteriores, tanto em modelos (Potter et al. 1996) quanto em observações empíricas (Dalal and Allen, 2008). Os autores interpretaram que isso ocorreu devido à não inclusão do fogo como variável do modelo. No entanto, o presente estudo estimou valores muito menores de fluxo de N gasoso nas áreas de savanas tropicais e savanas alagadas quando comparado com os valores estimados com base na isoscape usada por Bai et al. (2012).

A aplicação de uma nova isoscape de $\delta^{15}\text{N}$ do solo para a América do sul (Sena-Souza et al. 2019 em revisão – ver capítulo 2) no modelo de Bai et al. (2012) levou à estimativas de perdas de N dos sistemas terrestres mais coerentes com dados empíricos de estudos anteriores, o que reforça a importância da precisão dos modelos de entrada na interpretação dos resultados do modelo final.

Referências Bibliográficas

- Amundson, R., Austin, A.T., Schuur, E.A.G., Yoo, K., Matzek, V., Kendall, C., Uebersax, A., Brenner, D., Baisden, W.T., 2003. Global patterns of the isotopic composition of soil and plant nitrogen. *Global Biogeochem. Cycles* 17, 1031. <https://doi.org/10.1029/2002GB001903>
- Bai, E., Houlton, B.Z., Wang, Y.P., 2012. Isotopic identification of nitrogen hotspots across natural terrestrial ecosystems. *Biogeosciences* 9, 3287–3304. <https://doi.org/10.5194/bg-9-3287-2012>
- Boddey, R.M., Peoples, M.B., Palmer, B., Dart, P.J., 2000. Use of the ^{15}N natural abundance technique to quantify biological nitrogen fixation by woody perennials. *Nutrient Cycling in Agroecosystems*.
- Brenner, D.L., Amundson, R., Baisden, W.T., Kendall, C., Harden, J., 2001. Soil N and ^{15}N variation with time in a California annual grassland ecosystem. *Geochim. Cosmochim. Acta* 65, 4171–4186.
- Bustamante, M.M.C., Martinelli, L.A., Silva, D.A., Camargo, P.B., Klink, C.A., Domingues, T.F., Santos, R. V, 2004. ^{15}N natural abundance in woody plants and soils of central Brazilian savannas (Cerrado). *Ecol. Appl.* 14, 200–213. <https://doi.org/10.1890/01-6013>
- Bustamante, M.M.C., Medina, E., Asner, G.P., Nardoto, G.B., Garcia-Montiel, D.C., 2006. Nitrogen cycling in tropical and temperate savannas. *Biogeochemistry* 79, 209–237. <https://doi.org/10.1007/s10533-006-9006-x>
- Cleveland, C.C., Townsend, A.R., Schimel, D.S., Fischer, C. Von, Fisher, H., Howarth, R.W., Hedin, L.O., Perakis, S.S., Latty, E.F., Fischer, S.C. Von, Elseroad, A., Wasson, M.F., 1999. Global patterns of terrestrial biological nitrogen (Nz). *Global Biogeochem. Cycles* 13, 623–645.
- Craine, J.M., Elmore, A.J., Wang, L., Augusto, L., Baisden, W.T., Brookshire, E.N.J.,

- Cramer, M.D., Hasselquist, N.J., Hobbie, E. a., Kahmen, A., Koba, K., Kranabetter, J.M., Mack, M.C., Marin-Spiotta, E., Mayor, J.R., McLauchlan, K.K., Michelsen, A., Nardoto, G.B., Oliveira, R.S., Perakis, S.S., Peri, P.L., Quesada, C. a., Richter, A., Schipper, L. a., Stevenson, B. a., Turner, B.L., Viani, R. a. G., Wanek, W., Zeller, B., 2015. Convergence of soil nitrogen isotopes across global climate gradients. *Sci. Rep.* 5, 8280. <https://doi.org/10.1038/srep08280>
- Dalal, R.C., Allen, D.E., 2008. Greenhouse gas fluxes from natural ecosystems. *Aust. J. Bot.* 1, 369–407.
- de Carvalho, A.M., de Oliveira, W.R.D., Ramos, M.L.G., Coser, T.R., de Oliveira, A.D., Pulrolnik, K., Souza, K.W., Vilela, L., Marchão, R.L., 2017. Soil N₂O fluxes in integrated production systems, continuous pasture and Cerrado. *Nutr. Cycl. Agroecosystems* 108, 69–83. <https://doi.org/10.1007/s10705-017-9823-4>
- Feuerstein, T.P., Ostrom, P.H., Ostrom, N.E., 1997. Isotopic biogeochemistry of dissolved organic nitrogen: A new technique and application. *Org. Geochem.* 27, 363–370. [https://doi.org/10.1016/S0146-6380\(97\)00071-5](https://doi.org/10.1016/S0146-6380(97)00071-5)
- Freitas, A.D.S., de Sa Barreto Sampaio, E.V., Menezes, R.S.C., Tiessen, H., 2010. 15N natural abundance of non-fixing woody species in the Brazilian dry forest (caatinga). *Isotopes Environ. Health Stud.* 46, 210–8. <https://doi.org/10.1080/10256016.2010.488805>
- Galloway, J.N., Townsend, A.R., Erisman, J.W., Bekunda, M., Cai, Z., Freney, J.R., Martinelli, L.A., Seitzinger, S.P., Sutton, M.A., 2008. Transformation of the nitrogen cycle: Recent trends, questions, and potential solutions. *Science* (80-.). 320, 889–892. <https://doi.org/10.1126/science.1136674>
- Handley, L.L., Austin, A.T., Robinson, D., Scrimgeour, C.M., Raven, J.A., Heaton, T.H.E., Schmidt, S., Stewart, G.R., 1999. The 15 N natural abundance (δ 15 N) of ecosystem samples reflects measures of water availability. *Aust. J. Plant Physiol.* 26, 185–199. <https://doi.org/10.1071/PP98146>
- Hijmans, R.J., Cameron, S.E., Parra, J.L., Jones, P.G., Jarvis, A., 2005. Very high resolution interpolated climate surfaces for global land areas. *Int. J. Climatol.* 25, 1965–1978. <https://doi.org/10.1002/joc.1276>
- Hilton, R.G., Galy, A., West, A.J., Hovius, N., Roberts, G.G., 2013. Geomorphic control on the d15N of mountain forests. *Biogeosciences* 10, 1693–1705. <https://doi.org/10.5194/bg-10-1693-2013>
- Högberg, P., 1997. 15N natural abundance in soil-plant systems. *New Phytol.* 137, 179–203. <https://doi.org/10.1046/j.1469-8137.1997.00808.x>
- Houlton, B.Z., Bai, E., 2009. Imprint of denitrifying bacteria on the global terrestrial biosphere. *Proc. Natl. Acad. Sci.* 106, 21713–21716. <https://doi.org/10.1073/pnas.0912111106>
- Houlton, B.Z., Marklein, A.R., Bai, E., 2015. Representation of nitrogen in climate change forecasts. *Nat. Publ. Gr.* 5, 398–401. <https://doi.org/10.1038/nclimate2538>
- Houlton, B.Z., Sigman, D.M., Hedin, L.O., 2006. Isotopic evidence for large gaseous nitrogen losses from tropical rainforests. *Proc. Natl. Acad. Sci.* 103, 8745–8750. <https://doi.org/10.1073/pnas.0510185103>
- Lelieveld, J., Dentener, F.J., 2000. What controls tropospheric ozone? *J. Geophys. Res. Atmos.* 105, 3531–3551. <https://doi.org/10.1029/1999JD901011>

- Martinelli, L. a., Piccolo, M.C., Townsend, a. R., Vitousek, P.M., Cuevas, E., McDowell, W., Robertson, G.P., Santos, O.C., Treseder, K., 1999. Nitrogen stable isotopic composition of leaves and soil: Tropical versus temperate forests. *Biogeochemistry* 46, 45–65. <https://doi.org/10.1007/BF01007573>
- Menezes, R.S.C., Sampaio, E.V.S.B., Giongo, V., Pérez-Marin, a M., 2012. Biogeochemical cycling in terrestrial ecosystems of the Caatinga Biome. Rev. Brasileira Biol. 72, 643–53. <https://doi.org/10.1590/S1519-69842012000400004>
- Nardoto, G.B., Ometto, J.P.H.B., Ehleringer, J.R., Higuchi, N., Bustamante, M.M.D.C., Martinelli, L.A., 2008. Understanding the influences of spatial patterns on N availability within the Brazilian Amazon forest. *Ecosystems* 11, 1234–1246. <https://doi.org/10.1007/s10021-008-9189-1>
- Olson, D.M., Dinerstein, E., Wikramanayake, E.D., Burgess, N.D., Powell, G.V.N., Underwood, E.C., D'amico, J.A., Itoua, I., Strand, H.E., Morrison, J.C., Loucks, C.J., Allnutt, T.F., Ricketts, T.H., Kura, Y., Lamoreux, J.F., Wettenberg, W.W., Hedao, P., Kassem, K.R., 2001. Terrestrial Ecoregions of the World: A New Map of Life on Earth. *Bioscience* 51, 933. [https://doi.org/10.1641/0006-3568\(2001\)051\[0933:TEOTWA\]2.0.CO;2](https://doi.org/10.1641/0006-3568(2001)051[0933:TEOTWA]2.0.CO;2)
- Pérez, T., Garcia-Montiel, D., Trumbore, S., Tyler, S., Camargo, P. de, Moreira, M., Piccolo, M., Cerri, C., 2006. Nitrous Oxide Nitrification and Denitrification 15N enrichment factors from Amazon Forest soils. *Ecol. Appl.* 16, 2153–2167.
- Phoenix, G.K., Hicks, W.K., Cinderby, S., Kuyljenstierna, J.C.I., Stock, W.D., Dentener, F.J., Giller, K.E., Austin, A.T., Lefroy, R.D.B., Gimeno, B.S., Ashmore, M.R., Ineson, P., 2006. Atmospheric nitrogen deposition in world biodiversity hotspots: The need for a greater global perspective in assessing N deposition impacts. *Glob. Chang. Biol.* 12, 470–476. <https://doi.org/10.1111/j.1365-2486.2006.01104.x>
- Pinto, A. de S., Bustamante, M.M.D.C., Kisselle, K., Burke, R., Zepp, R., Viana, L.T., Varella, R.F., Molina, M., 2002. Soil emissions of N₂O, NO, and CO₂ in Brazilian Savannas: Effects of vegetation type, seasonality, and prescribed fires. *J. Geophys. Res.* 107, 1–9. <https://doi.org/10.1029/2001jd000342>
- Seitzinger, S., Harrison, J.A., Böhlke, J.K., Bouwman, A.F., Lowrance, R., Peterson, B., Tobias, C., Drecht, G. V., 2006. Denitrification across Landscapes and Waterscapes: A synthesis. *Ecol. Appl.* 16, 2064–2090. [https://doi.org/10.1890/1051-0761\(2006\)016\[2064:DALAWA\]2.0.CO;2](https://doi.org/10.1890/1051-0761(2006)016[2064:DALAWA]2.0.CO;2)
- Wang, Y.P., Houlton, B.Z., 2009. Nitrogen constraints on terrestrial carbon uptake: Implications for the global carbon-climate feedback. *Geophys. Res. Lett.* 36. <https://doi.org/10.1029/2009GL041009>
- Wang, Y.P., Houlton, B.Z., Field, C.B., 2007. A model of biogeochemical cycles of carbon, nitrogen, and phosphorus including symbiotic nitrogen fixation and phosphatase production. *Global Biogeochem. Cycles* 21, 1–15. <https://doi.org/10.1029/2006GB002797>
- Wang, Y.P., Law, R.M., Pak, B., 2010. A global model of carbon, nitrogen and phosphorus cycles for the terrestrial biosphere. *Biogeosciences* 7, 2261–2282. <https://doi.org/10.5194/bg-7-2261-2010>
- Weintraub, S.R., Cole, R.J., Schmitt, C.G., All, J.D., 2016. Climatic controls on the isotopic composition and availability of soil nitrogen across mountainous tropical

- forest. *Ecosphere* 7, 1–13. <https://doi.org/10.1002/ecs2.1412/supinfo>
- Yoneyama, T., Muraoka, T., Murakami, T., Boonkerd, N., 1993. Natural abundance of ^{15}N in tropical plants with emphasis on tree legumes. *Plant Soil* 153, 295–304.

ANEXO A

Base de dados usada na modeladem do $\delta^{15}\text{N}$ do solo do Capítulo 2. Esta tabela foi submetida como material suplementar do artigo referente ao Capítulo 2 para apreciação da revista *Ecosphere* e está em processo de revisão.

Table S1. Compilation of soil $\delta^{15}\text{N}$ data from literature, unpublished data from partnerships, and original data from field work. Lat and Long are the geographic coordinates (latitude and longitude in WGS-84 coordinate system).

Lat	Long	Observed $\delta^{15}\text{N}$	Reference
-2.81667	-47.35000	10.72	Piccolo et al. 1996
-3.30000	-47.16667	8.76	Piccolo et al. 1996
-2.50000	-60.16667	8.60	Piccolo et al. 1996
-9.18333	-63.11667	10.05	Piccolo et al. 1996
-12.86667	-60.05000	11.18	Piccolo et al. 1996
-10.28333	-62.86667	9.84	Piccolo et al. 1996
-10.15000	-62.81667	12.00	Piccolo et al. 1996
-10.70000	-62.20000	10.93	Piccolo et al. 1996
-2.20000	-47.36667	8.64	Davidson et al. 2007
-1.16750	-47.75222	5.81	Davidson et al. 2007
-2.42472	-54.70417	9.30	Nardoto 2005
-2.37000	-60.09000	9.44	Nardoto 2005
0.41667	-65.85917	6.75	Nardoto 2005
-15.15000	-47.51000	4.36	Nardoto 2005
-24.28333	-48.41667	8.40	Silva 2005
-22.60000	-52.23333	8.15	Silva 2005
-15.25087	-61.24528	5.70	Nardoto et al. 2014
-3.74099	-70.30551	5.70	Nardoto et al. 2014
-3.74124	-70.30251	5.60	Nardoto et al. 2014
-9.60050	-55.93720	8.70	Nardoto et al. 2014
-9.57838	-55.91762	7.40	Nardoto et al. 2014
-3.94778	-73.43570	6.10	Nardoto et al. 2014
-3.95295	-73.43740	3.90	Nardoto et al. 2014
-3.95126	-73.43894	6.30	Nardoto et al. 2014
-3.95437	-73.42577	4.20	Nardoto et al. 2014
-2.62750	-60.15306	9.30	Nardoto et al. 2014
-0.69852	-76.48218	6.30	Nardoto et al. 2014
-0.69792	-76.47380	6.50	Nardoto et al. 2014
-1.73673	-51.46291	9.20	Nardoto et al. 2014
-1.73571	-51.46198	10.60	Nardoto et al. 2014
-1.71583	-51.45722	10.30	Nardoto et al. 2014
-14.38556	-61.14778	6.20	Nardoto et al. 2014
-2.19103	-47.32779	8.50	Nardoto et al. 2014
-12.49967	-68.96296	4.80	Nardoto et al. 2014
-10.56640	-68.31148	8.50	Nardoto et al. 2014
-10.55611	-68.30103	7.80	Nardoto et al. 2014

6.10212	-61.40337	6.80	Nardoto et al. 2014
-12.81297	-51.85372	5.10	Nardoto et al. 2014
-14.56083	-60.74861	5.70	Nardoto et al. 2014
-14.56750	-60.74778	6.70	Nardoto et al. 2014
-1.06833	-77.61528	7.30	Nardoto et al. 2014
-1.07750	-77.60950	6.90	Nardoto et al. 2014
-1.07353	-77.61222	6.60	Nardoto et al. 2014
-1.06167	-77.62167	7.00	Nardoto et al. 2014
-0.89444	-52.19028	8.30	Nardoto et al. 2014
-8.88395	-72.78992	5.30	Nardoto et al. 2014
-14.55669	-60.92789	5.30	Nardoto et al. 2014
-14.57719	-60.83178	6.20	Nardoto et al. 2014
-3.05624	-69.99071	6.20	Nardoto et al. 2014
-3.05760	-69.99303	6.70	Nardoto et al. 2014
-14.40814	-61.14027	7.10	Nardoto et al. 2014
-14.40828	-61.13837	5.30	Nardoto et al. 2014
-2.60861	-60.21417	4.80	Nardoto et al. 2014
-2.60944	-60.21611	7.80	Nardoto et al. 2014
-2.60694	-60.20889	5.80	Nardoto et al. 2014
-1.45000	-48.45000	7.70	Nardoto et al. 2014
-16.39101	-61.21244	9.00	Nardoto et al. 2014
8.11361	-61.69222	6.30	Nardoto et al. 2014
-9.04368	-72.26743	7.40	Nardoto et al. 2014
1.93284	-67.02168	3.10	Nardoto et al. 2014
1.93000	-67.03828	2.40	Nardoto et al. 2014
-11.41120	-55.32470	8.80	Nardoto et al. 2014
-3.25211	-72.90744	7.90	Nardoto et al. 2014
-3.25114	-72.90359	8.00	Nardoto et al. 2014
-12.84411	-69.28838	6.90	Nardoto et al. 2014
-12.83475	-69.28608	7.00	Nardoto et al. 2014
-12.83647	-69.27829	7.10	Nardoto et al. 2014
-12.83029	-69.27053	7.20	Nardoto et al. 2014
-12.83850	-69.29601	5.80	Nardoto et al. 2014
-12.82568	-69.26103	6.70	Nardoto et al. 2014
-12.92125	-52.37311	5.10	Nardoto et al. 2014
-2.85111	-54.95472	10.50	Nardoto et al. 2014
-3.30963	-54.94185	10.40	Nardoto et al. 2014
-0.63888	-76.15462	6.60	Nardoto et al. 2014
-0.63778	-76.14358	7.30	Nardoto et al. 2014
-18.52448	-60.81249	11.00	Nardoto et al. 2014
-14.83074	-52.15983	6.70	Nardoto et al. 2014
-14.83194	-52.16904	5.80	Nardoto et al. 2014
-3.43955	-72.84581	5.50	Nardoto et al. 2014
-2.64000	-54.59000	10.25	Pérez et al. 2006
-10.20500	-62.79167	11.10	Pérez et al. 2006
-51.77047	-71.74956	6.41	Peri et al. 2012
-51.61756	-71.99131	-1.17	Peri et al. 2012
-51.31486	-72.18289	5.93	Peri et al. 2012
-50.30647	-72.78956	4.96	Peri et al. 2012
-48.36897	-72.13956	2.51	Peri et al. 2012

-51.83281	-71.70972	2.33	Peri et al. 2012
-48.37181	-72.05328	4.11	Peri et al. 2012
-51.22258	-72.26392	3.27	Peri et al. 2012
-46.05675	-71.68636	-1.21	Peri et al. 2012
-46.88283	-71.88208	5.73	Peri et al. 2012
-50.52453	-72.78164	2.30	Peri et al. 2012
-50.55350	-72.84200	2.37	Peri et al. 2012
-50.46197	-73.02353	-1.33	Peri et al. 2012
-50.46553	-73.02869	-0.93	Peri et al. 2012
-49.23800	-72.90292	-2.34	Peri et al. 2012
-50.47278	-72.99375	-0.22	Peri et al. 2012
-49.28444	-72.88864	1.00	Peri et al. 2012
-49.17772	-72.94831	-3.74	Peri et al. 2012
-46.86667	-71.86667	4.18	Peri et al. 2012
-49.21111	-72.95672	2.33	Peri et al. 2012
-51.56519	-72.35569	5.59	Peri et al. 2012
-51.57392	-72.00519	2.60	Peri et al. 2012
-48.32914	-72.18819	4.67	Peri et al. 2012
-51.22258	-72.27903	2.75	Peri et al. 2012
-48.42717	-71.82842	5.91	Peri et al. 2012
-51.61931	-71.99283	-1.63	Peri et al. 2012
-51.57256	-72.30975	3.95	Peri et al. 2012
-48.44706	-71.83836	4.59	Peri et al. 2012
-51.53361	-72.14081	-0.60	Peri et al. 2012
-50.43119	-72.75664	2.30	Peri et al. 2012
-50.46197	-73.02353	-1.33	Peri et al. 2012
-49.14633	-72.94378	-1.23	Peri et al. 2012
-49.08108	-72.88903	-4.83	Peri et al. 2012
-23.31000	-51.16277	10.90	Yoneyama et al. 1993
-19.31083	-46.04888	5.10	Yoneyama et al. 2003
-7.65194	-40.14888	14.00	Mendonça et al. 2010
-22.58333	-50.38333	4.12	Viani et al. 2011
-22.40000	-49.70000	4.94	Viani et al. 2011
-72.85000	-40.11670	0.49	Boeckx et al. 2005
-72.20000	-40.78330	-3.34	Boeckx et al. 2005
-73.43330	-40.20000	-0.76	Boeckx et al. 2005
-38.75000	-63.75000	3.75	Harris et al. 2007
-8.42505	-36.46672	13.54	Unpublished data
-8.49124	-36.37979	9.93	Unpublished data
-8.94167	-36.69444	4.18	Unpublished data
-7.66417	-40.17056	16.47	Unpublished data
-7.57933	-40.11325	13.62	Unpublished data
-7.66120	-39.96356	8.85	Unpublished data
-8.23111	-37.78250	13.95	Unpublished data
-7.39001	-37.24269	8.33	Unpublished data
-8.03156	-37.68216	17.28	Unpublished data
-7.40444	-35.18602	6.45	Unpublished data
-7.53142	-35.47194	8.89	Unpublished data
-8.20717	-35.34781	9.21	Unpublished data
-14.10654	-47.70449	6.41	This paper

-14.10823	-47.71358	3.33	This paper
-14.10992	-47.72267	4.64	This paper
-14.11161	-47.73176	5.27	This paper
-14.10484	-47.69540	5.22	This paper
-14.11541	-47.70275	5.86	This paper
-14.11710	-47.71184	4.94	This paper
-14.11879	-47.72094	4.45	This paper
-14.12048	-47.73003	4.64	This paper
-14.11371	-47.69366	4.78	This paper
-15.71088	-48.00071	6.47	This paper
-15.70659	-48.00916	6.09	This paper
-15.70195	-48.01726	6.19	This paper
-15.69713	-48.02517	6.93	This paper
-15.71481	-47.99232	6.89	This paper
-15.71832	-48.00654	5.61	This paper
-15.71261	-48.01607	7.83	This paper
-15.70886	-48.02261	6.28	This paper
-15.70440	-48.03023	6.86	This paper
-15.72320	-47.99839	4.57	This paper
-13.62138	-46.28055	4.60	This paper
-13.62132	-46.28975	3.76	This paper
-13.61229	-46.28042	3.75	This paper
-13.61232	-46.28970	3.79	This paper
-13.58517	-46.28038	4.10	This paper
-13.58497	-46.28916	5.44	This paper
-19.49358	-44.18600	7.00	This paper
-21.01853	-44.21764	5.96	This paper
-20.99339	-44.17175	7.42	This paper
-21.97725	-47.85489	7.94	This paper
-22.83392	-51.71447	9.29	This paper
-24.02217	-53.74383	11.30	This paper
-23.80806	-53.59033	8.01	This paper
-24.10525	-52.35953	4.35	This paper
-24.30278	-52.70217	7.54	This paper
-25.11192	-50.06375	7.59	This paper
-30.10178	-51.69947	7.72	This paper
-28.93008	-54.34131	6.11	This paper
-29.45872	-54.81883	8.24	This paper
-31.36694	-54.00792	6.51	This paper
-31.83267	-52.47725	6.10	This paper
-28.22503	-52.40664	8.09	This paper
-20.51700	-51.57925	4.92	This paper
-22.29040	-54.80983	7.36	This paper
-12.36972	-52.22472	6.34	This paper
-14.62782	-52.38396	5.60	This paper
-14.99756	-52.27928	6.26	This paper
-19.27961	-48.74947	4.54	This paper
-19.17450	-48.16778	4.77	This paper
-10.45811	-37.19958	5.80	This paper
-10.56300	-37.16378	4.62	This paper

-10.21856	-37.32625	9.46	This paper
-9.29878	-40.58572	12.26	This paper
-7.46522	-40.41953	14.24	This paper
-8.50567	-40.71058	14.72	This paper
-6.80656	-45.41111	4.06	This paper
-9.21047	-45.14831	4.73	This paper
-11.44547	-45.60819	4.08	This paper
-6.92052	-47.46605	8.22	This paper
-6.92910	-47.46286	4.38	This paper
-6.96815	-47.44832	6.29	This paper
-6.89567	-47.47145	3.09	This paper
-6.87196	-47.47439	3.96	This paper
-7.12638	-47.42354	2.53	This paper
-7.13119	-47.42381	7.36	This paper
-7.02410	-47.45400	5.08	This paper
-7.09685	-47.43169	7.08	This paper
-7.14772	-47.42100	6.42	This paper
-7.14705	-47.42006	6.52	This paper
-7.20652	-47.42820	8.99	This paper
-7.12943	-47.42609	3.56	This paper
-7.13496	-47.43163	8.99	This paper
-7.42543	-46.71829	4.38	This paper
-7.42606	-46.71771	4.35	This paper
-7.42185	-46.75515	4.68	This paper
-7.42843	-46.78996	3.22	This paper
-7.40781	-46.86922	7.52	This paper
-7.40982	-47.01145	4.57	This paper
-7.41237	-47.09483	3.43	This paper
-7.41210	-47.17249	3.88	This paper
-7.01889	-47.34185	4.59	This paper
-7.01985	-47.34900	4.72	This paper
-7.02244	-47.36904	4.65	This paper
-7.02384	-47.37851	3.66	This paper
-7.00444	-47.43544	3.66	This paper
-7.43370	-47.68360	3.14	This paper
-7.48897	-47.90043	4.78	This paper
-7.33061	-48.31003	2.09	This paper
-7.37251	-48.34777	4.82	This paper
-7.54405	-48.41346	2.75	This paper
-8.22993	-48.46457	2.17	This paper
-8.69426	-48.50610	4.75	This paper
-8.93422	-48.51350	3.94	This paper
-9.55206	-48.52731	4.91	This paper
-9.56725	-48.45456	3.00	This paper
-9.68493	-48.38568	5.61	This paper
-10.47119	-48.32361	5.63	This paper
-10.94020	-48.31576	6.06	This paper
-11.33574	-48.15365	5.56	This paper
-13.24969	-46.85802	5.38	This paper
-13.42064	-47.13083	4.75	This paper

-14.73529	-47.54877	6.73	This paper
-7.14349	-47.42025	4.66	This paper
-18.18194	-52.84940	6.75	This paper
-18.11782	-52.91604	6.49	This paper
-18.16912	-53.01470	6.08	This paper
-18.11243	-53.05221	6.32	This paper
-18.08683	-52.98852	6.56	This paper
-18.05547	-52.93580	7.98	This paper
-18.28968	-52.93276	6.48	This paper
-17.99081	-52.98946	6.46	This paper
-17.91041	-52.95040	5.86	This paper
-17.66747	-52.94248	4.90	This paper
-17.63239	-52.37346	4.27	This paper
-17.81855	-52.00443	6.59	This paper
-18.30761	-52.75886	7.19	This paper
-17.91083	-51.78262	7.45	This paper
-17.86900	-51.57569	2.63	This paper
-17.81795	-51.17541	5.83	This paper
-17.61341	-50.75222	7.45	This paper
-17.46895	-50.43630	5.13	This paper
-17.17051	-50.05078	5.71	This paper
-18.28796	-52.83817	6.31	This paper
-18.23273	-52.87928	5.37	This paper
-15.78928	-56.36761	6.02	This paper
-15.79902	-56.37106	6.46	This paper
-15.83390	-56.37457	5.95	This paper
-15.84207	-56.40832	9.57	This paper
-16.03676	-56.52023	6.73	This paper
-16.10984	-56.59380	7.03	This paper
-16.46195	-56.40325	5.01	This paper
-16.30293	-56.56216	6.78	This paper
-16.39379	-56.62712	6.33	This paper
-16.38514	-56.60916	5.40	This paper
-16.38835	-56.59649	5.63	This paper
-17.19216	-56.92213	4.65	This paper
-17.04856	-56.95485	1.37	This paper
-16.78085	-56.85061	4.86	This paper
-16.76447	-56.85211	4.64	This paper
-16.61496	-56.74804	7.11	This paper
-16.51508	-56.70249	4.49	This paper
-16.39400	-56.63688	4.21	This paper
-16.39490	-56.62492	4.59	This paper

References

Boeckx, P., L. Paulino, C. Oyarzún, O. van Cleemput, and R. Godoy. 2005. Soil $\delta^{15}\text{N}$ patterns in old-growth forests of southern Chile as integrator for N-cycling. *Isotopes. Environ. Health. Stud.* 41:249–259.

- Davidson, E. A., C. J. R. de Carvalho, A. M. Figueira, F. Y. Ishida, J. P. H. B. Ometto, G. B. Nardoto, R. T. Saba, S. N. Hayashi, E. C. Leal, I. C. G. Vieira, and L. A. Martinelli. 2007. Recuperation of nitrogen cycling in Amazonian forests following agricultural abandonment. *Nature* 447:995–998.
- Harris, W. N., A. S. Moretto, R. A. Distel, T. W. Boutton, and R. M. Bóo. 2007. Fire and grazing in grasslands of the Argentine Caldenal: Effects on plant and soil carbon and nitrogen. *Acta Oecologica* 32:207–214.
- Mendonça, L., H. Frischkorn, M. Snatiago, P. B. Camargo, J. O. G. Lima, J. Mendes Filho. 2010. Identificação de mudanças florestais por $\delta^{13}\text{C}$ e $\delta^{15}\text{N}$ dos solos da Chapada do Araripe, Ceará. *Revista Brasileira de Engenharia Agrícola Ambiental* 14:314–319
- Nardoto, G. B. 2005. Abundância natural de ^{15}N na Amazônia e Cerrado - implicações para a ciclagem de nitrogênio. University of São Paulo, São Paulo, Brazil.
- Nardoto, G. B., C. A. Quesada, S. Patiño, G. Saiz, T. R. Baker, M. Schwarz, F. Schrodte, T. R. Feldpausch, T. F. Domingues, B. S. Marimon, B.-H. Marimon Junior, I. C. G. Vieira, M. Silveira, M. I. Bird, O. L. Phillips, J. Lloyd, and L. A. Martinelli. 2014. Basin-wide variations in Amazon forest nitrogen-cycling characteristics as inferred from plant and soil ^{15}N : ^{14}N measurements. *Plant Ecology & Diversity* 7:173–187.
- Pérez, T., D. Garcia-Montiel, S. Trumbore, S. Tyler, P. de Camargo, M. Moreira, M. Piccolo, and C. Cerri. 2006. Nitrous Oxide Nitrification and Denitrification ^{15}N enrichment factors from Amazon Forest soils. *Ecol. Appl.* 16:2153–2167.
- Peri, P. L., B. Ladd, D. A. Pepper, S. P. Bonser, S. W. Laffan, and W. Amelung. 2012. Carbon ($\delta^{13}\text{C}$) and nitrogen ($\delta^{15}\text{N}$) stable isotope composition in plant and soil in Southern Patagonia's native forests. *Global Change Biology* 18:311–321.
- Piccolo, M. C., C. Neill, J. M. Melillo, C. C. Cerri, and P. A. Steudler. 1996. ^{15}N natural abundance in forest and pasture soils of the Brazilian Amazon Basin. *Plant and Soil* 182:249–258.
- Silva, D. M. L. 2005. Dinâmica de nitrogênio em três microbacias do Estado de São Paulo. Dissertation. University of São Paulo, São Paulo, Brazil.
- Viani, R. A. G., R. R. Rodrigues, T. E. Dawson, and R. S. Oliveira. 2011. Functional differences between woodland savannas and seasonally dry forests from south-eastern Brazil: Evidence from ^{15}N natural abundance studies. *Austral Ecology* 36:974–982.
- Yoneyama, T., T. Muraoka, T. Murakami, and N. Boonkerd. 1993. Natural abundance of ^{15}N in tropical plants with emphasis on tree legumes. *Plant and Soil* 153:295–304.

ANEXO B

Script adaptado para o mapeamento da isoscape de $\delta^{15}\text{N}$ do solo do Capítulo 2.

```
#####DEFINIR DIRETÓRIO#####
setwd("D:\\R\\endereço\\")
memory.limit(size=100000)

#####CARREGAR PACOTES#####
library(dplyr);library(nlme);library(raster);library(rgdal);library(sp);library(ncdf4);library(readxl);library(car);library(gstat);library(randomForest);library(GSIF);library(ranger);library(ModelMap);library(caret);library(corrplot);library(devtools);library(randomForestCI);library(dplyr);library(randomForest);library(ggplot2);require(GGally); library(rattle);library(rpart.plot); library(base);library(Cubist);library(automap);library(extratrees);library(rworldma);library(ggmap);library(mapproj);library(corrplot); library(vSURF); library(MVN);library(mvnormtest); library(ggplot2);library(pdp);library(ggplot2);library(Rmisc)

##### ABRIR BANCO DE DADOS E AGREGAR LOCAIS POR DISTÂNCIA (0.01) #####
d15n.orig <- read.table("dados_15n_0-20.txt", header = T)
y.red<-round(d15n.orig$y, digits = 2)
x.red<-round(d15n.orig$x, digits = 2)
coord<-data.frame(x.red,y.red)
d15n.orig<-data.frame(d15n.orig,coord)

d15n.agg <- aggregate(d15n.orig[, "d15n.obs", drop=F], d15n.orig[,4:5], mean)
colnames(d15n.agg)<-c("x", "y", "d15n.obs")
d15n_spatial <- SpatialPointsDataFrame(d15n.agg[,c("x","y")], d15n.agg)

#####CARREGAR RASTERS DE VARIÁVEIS PREDITORAS#####
## Os rasters foram cortados para a América do Sul no ArcGis 10.3 e organizados em uma pasta

ai_yr = raster("D:\\pasta com rasters\\ai.tif")
pet_yr = raster("D:\\pasta com rasters\\pet_yr.tif")
bulk_5 = raster("D:\\pasta com rasters\\bulk_5_1km.tif")
cec_5 = raster("D:\\pasta com rasters\\cec_5_1km.tif")
clay_5 = raster("D:\\pasta com rasters\\clay_5_1km.tif")
orc_5 = raster("D:\\pasta com rasters\\orc_5_1km.tif")
phh2o_5 = raster("D:\\pasta com rasters\\phh2o_5_1km.tif")
phh2o_5 = phh2o_5*0.1
phkcl_5 = raster("D:\\pasta com rasters\\phkcl_5_1km.tif")
phkcl_5 = phkcl_5*0.1
silt_5 = raster("D:\\pasta com rasters\\silt_5_1km.tif")
sand_5 = raster("D:\\pasta com rasters\\sand_5_1km.tif")
#soiltax_wrb = raster("D:\\pasta com rasters\\soiltax_wrb_1km.tif")
#gpp = raster("D:\\pasta com rasters\\gpp.tif")
npp = raster("D:\\pasta com rasters\\npp_certo.tif")
tmp_wc = raster("D:\\pasta com rasters\\tmp_wc.tif")
tmp_wc = tmp_wc*0.1 ## transforming temperature data
pre_wc = raster("D:\\pasta com rasters\\pre_wc.tif")
alt = raster("D:\\pasta com rasters\\alt.tif")
eco_tnc = raster("D:\\pasta com rasters\\eco_tnc.tif")
biome = raster("D:\\pasta com rasters\\biome_wwf.tif")

##### Deixar todos com o mesmo tamanho e quantidade de pixels antes de fazer o stack #####
biome<-resample(biome,alt) ### resample para padronizar os tamanhos dos rasters para o stack()
npp<-resample(npp,alt)
ai_yr<-resample(ai_yr,alt)
pet_yr<-resample(pet_yr,alt)
eco_tnc<-resample(eco_tnc,alt) ### resample para padronizar os tamanhos dos rasters para o stack()

#####Extraindo valores dos pixels para os pontos#####

```

```

altxy<-extract(altxy, d15n_spatial, method='bilinear',
                 buffer=NULL,na.rm=TRUE)
ai_yrxy<-extract(ai_yr, d15n_spatial, method='bilinear',
                 buffer=NULL,na.rm=TRUE)
pet_yrxy<-extract(pet_yr, d15n_spatial, method='bilinear',
                 buffer=NULL,na.rm=TRUE)
bulk_5xy<-extract(bulk_5, d15n_spatial, method='bilinear',
                 buffer=NULL,na.rm=TRUE)
cec_5xy<-extract(cec_5, d15n_spatial, method='bilinear',
                 buffer=NULL,na.rm=TRUE)
clay_5xy<-extract(clay_5, d15n_spatial, method='bilinear',
                 buffer=NULL,na.rm=TRUE)
orc_5xy<-extract(orc_5, d15n_spatial, method='bilinear',
                 buffer=NULL,na.rm=TRUE)
phh2o_5xy<-extract(phh2o_5, d15n_spatial, method='bilinear',
                 buffer=NULL,na.rm=TRUE)
phkcl_5xy<-extract(phkcl_5, d15n_spatial, method='bilinear',
                 buffer=NULL,na.rm=TRUE)
silt_5xy<-extract(silt_5, d15n_spatial, method='bilinear',
                 buffer=NULL,na.rm=TRUE)
sand_5xy<-extract(sand_5, d15n_spatial, method='bilinear',
                 buffer=NULL,na.rm=TRUE)
nppxy<-extract(npp, d15n_spatial, method='bilinear',
                 buffer=NULL,na.rm=TRUE)
tmp_wcxy<-extract(tmp_wc, d15n_spatial, method='bilinear',
                 buffer=NULL,na.rm=TRUE)
pre_wcxy<-extract(pre_wc, d15n_spatial, method='bilinear',
                 buffer=NULL,na.rm=TRUE)
eco_tncxy<-extract(eco_tnc, d15n_spatial, method='simple',
                 buffer=NULL,na.rm=TRUE)
biome_wwfxy<-extract(biome, d15n_spatial, method='simple',
                 buffer=NULL,na.rm=TRUE)

### Combinando os data frames para criar a matriz de regressão #####
d15n_proj_xy <- data.frame(d15n_spatial,altxy,bulk_5xy,cec_5xy,clay_5xy,
                           orc_5xy, phh2o_5xy,phkcl_5xy,silt_5xy,sand_5xy,
                           ai_yrxy,pet_yrxy,nppxy,tmp_wcxy,pre_wcxy,
                           eco_tncxy,biome_wwfxy)

### Removendo linhas com NA #####
d15n_proj_xy <- na.omit(d15n_proj_xy)

write.csv(d15n_proj_xy,file="d15n_proj_xy_as.csv")
d15n_proj_xy <-read.csv("d15n_proj_xy_as.csv", header = T)
d15n_proj_xy$biome

### Criando a matriz de regressão Final com casos completos #####
d15n_proj_set <- subset(d15n_proj_xy,select=c("y","x","d15n.obs",
"altxy","bulk_5xy",
"cec_5xy","clay_5xy","orc_5xy","phh2o_5xy","phkcl_5xy",
"silt_5xy", "sand_5xy",
"ai_yrxy","pet_yrxy",
"nppxy","tmp_wcxy","pre_wcxy","eco_tncxy","biome_wwfxy"))

colnames(d15n_proj_set)<- c("y","x","d15n.obs","altxy","bulk_5xy","cec_5xy",
                           "clay_5xy","orc_5xy","phh2o_5xy","phkcl_5xy",
                           "silt_5xy", "sand_5xy",
                           "ai_yrxy","pet_yrxy",
                           "nppxy","tmp_wcxy","pre_wcxy","eco_tncxy","biome_wwfxy")

d15n_proj_set$biome<-as.integer(d15n_proj_set$biome)

##transformando dataset em SpatialPoint

d15n_clean<-SpatialPointsDataFrame(d15n_proj_set[,c("x","y")],
d15n_proj_set)## for log transformed data
proj4string(d15n_clean) <- CRS("+proj=longlat +ellps=WGS84")
plot(d15n_clean)
writeOGR(d15n_clean, ".", "d15n_clean_final", driver="ESRI Shapefile") #####
LEMBRAR DE ABRIR ESSA TABELA

#####PROCESSANDO OS DADOS#####

```

```

##### Aqui são separados 80% dos dados para treinar o modelo e outros 20% para testar

set.seed(123)
inTrain <- createDataPartition(y=d15n_proj_set$d15n.obs, p=0.80, list=FALSE)
training <- d15n_proj_set[inTrain,];
testing <- d15n_proj_set[-inTrain,];
hist(training$d15n.obs)
hist(testing$d15n.obs)
write.csv(training,file="training.csv")
write.csv(testing,file="testing.csv")

colnames(training)<-c("x","y","d15n.obs","alt","bulk_5","cec_5","clay_5",
                      "orc_5","phh2o_5","phkcl_5","silt_5","sand_5",
                      "ai_yr","pet_yr","npp","tmp_wc","pre_wc",
                      "eco_tnc","biome")
colnames(testing)<-c("x","y","d15n.obs","alt","bulk_5","cec_5","clay_5",
                      "orc_5","phh2o_5","phkcl_5","silt_5","sand_5",
                      "ai_yr","pet_yr","npp","tmp_wc","pre_wc",
                      "eco_tnc","biome")
train_p <- project(as.matrix(training[,c("x","y")]), "+proj=eck4 +lon_0=0
+x_0=0 +y_0=0 +ellps=WGS84 +units=m +no_defs")

### Preparando para a validação cruzada ###

?trainControl
fitControl <- trainControl## 10-fold crossvalidation
  method = "repeatedcv",
  number = 10,
  ## repeated ten times
  repeats = 5,
  verboseIter=FALSE,
  returnResamp="final",
  savePredictions="all"
# With parallel backend
#allowParallel=TRUE
)

#####Random forest
set.seed(123)
training<-training[,3:19]
bestmtry <- tuneRF(training, training$d15n.obs, stepFactor=3, improve=2,
ntree=500)
mtry <- 4
tunegrid <- expand.grid(.mtry=mtry)
RF1 <- train(d15n.obs ~ ., data = training, method = "rf",
tuneGrid=tunegrid,trControl= fitControl, importance = TRUE)
VarImp(RF1)

##### Calcular os quartis da floresta randomica para mapear incertezas usando
dados de teste
library(quantregForest)
testing<-testing[,-1:-2]
qrf1 <- train(d15n.obs ~ ., data = testing, method = "qrf",
tuneGrid=tunegrid,trControl= fitControl)
qrf1$pred

#####modelo Cubist
set.seed(123)
CUBIST<-train(d15n.obs ~ ., data = training, method = 'cubist', trControl=
fitControl)

#####modelo GBM
set.seed(123)
tunegrid <- expand.grid(n.trees = 500, interaction.depth = c(30), shrinkage =
c(0.1), n.minobsinnode=c(5))
GBM <- train(d15n.obs ~ ., data = training, method = "gbm", trControl=
fitControl,tuneGrid=tunegrid,metric='RMSE',maximize=FALSE)

#####SELECCIONAR MELHOR MODELO#####
x11()
results <- resamples(list(rf=RF1,cubist=CUBIST, gbm=GBM))
summary(results)

comp.result<-data.frame(results$values)

```

```

#### criando tabela de comparação para comparar modelos com gráficos ####
rf.performance<-comp.result[,2:4]
cubist.performance<-comp.result[,5:7]
gbm.performance<-comp.result[,8:10]
rf.performance["model"]<-c("RF")
cubist.performance["model"]<-c("CUBIST")
gbm.performance["model"]<-c("GBM")
colnames(rf.performance)<-c("MAE", "RMSE", "R2", "model")
colnames(cubist.performance)<-c("MAE", "RMSE", "R2", "model")
colnames(gbm.performance)<-c("MAE", "RMSE", "R2", "model")

comp.models<-rbind(rf.performance, cubist.performance, gbm.performance)

comp.models

RMSE1<-comp.models[1:50,]
mean(RMSE1$RMSE)

library(dplyr)

Data =
  mutate(comp.models,
    Group = factor(model, levels=unique(model)))
library(FSA)

Summarize(R2 ~ Group,
  data = Data)

kruskal.test(R2 ~ Group,
  data = Data)

#####
##### VISUALIZANDO MELHOR MODELO#####
##### Plotar importância das variáveis

imp<-varImp(RF1$finalModel)
imp$varnames <- rownames(imp) # row names to column
rownames(imp) <- NULL
imp$varnames<-c("alt","density","cec","clay",
  "orc","phh2o","phkc1","silt","sand",
  "ai","pet","npp","tmp","pre",
  "ecoreg","biome")

png("varimport.jpg", width = 3, height = 4, units = 'in', res = 300)
ggplot(imp, aes(x=reorder(varnames, Overall), y=Overall)) +
  geom_point() +
  geom_segment(aes(x=varnames,xend=varnames,y=0,yend=Overall)) +
  ylab("%IncMSE") +
  xlab("Variable Name") +
  coord_flip()+
  theme_bw()+
  theme(panel.grid = element_blank(),axis.title = element_text(size =
  14),axis.text = element_text(size = 12))
dev.off()

?train
#plot(RF$finalModel,main='Error vs No. of trees plot: Base Model')

##### Plotado os gráficos da correlação parcial de variáveis importantes

install.packages("pdp")
install.packages("Rmisc")

tapply(d15n_proj_set$d15n.obs, d15n_proj_set$biome, sd)
bio <- summarySE(d15n_proj_set, measurevar="d15n.obs", groupvars="biome")

plot.biome<-ggplot(bio, aes(x = as.factor(biome), y = d15n.obs)) +
  geom_point(stat="identity",colour="black", # use black outlines,
  size=2) + # Thinner lines
  geom_errorbar(aes(ymin=d15n.obs-sd, ymax=d15n.obs+sd),width = .3) +
  scale_y_continuous(limits=c(-2, 16)) +
  xlab("Biomes") + # adiciona descrição do eixo x+
  ylab(expression (Obs~delta^{15}~N~^{(\u2030)})) + # adiciona descrição do
eixo y ++
  ggtitle("A")

```

```

theme_bw()+
  theme(panel.grid = element_blank(), axis.title = element_text(size = 14),
        axis.text = element_text(size = 12),
        plot.title=element_text( hjust=.01, vjust=-1))

plot.orc <- partial(RF1, pred.var = c("orc_5"), chull = TRUE, rug = TRUE,
plot = TRUE,plot.engine = "ggplot2") +
  xlab(expression ("Organic carbon content")) + # adiciona descrição do eixo x
  ylab(expression (delta^{15}N~"(\u2030)"))+
  ggtitle("B")+
  theme_bw()+
  theme(panel.grid = element_blank(),axis.title = element_text(size = 14),
        axis.text = element_text(size = 12),
        plot.title=element_text( hjust=.01, vjust=-1))

plot.bulk <- partial(RF1, pred.var = c("bulk_5"), chull = TRUE, rug = TRUE,
plot = TRUE,plot.engine = "ggplot2") +
  xlab(expression ("Bulk density")) + # adiciona descrição do eixo x
  ylab(expression (delta^{15}N~"(\u2030)")) +
  ggtitle("E")+
  theme_bw()+
  theme(panel.grid = element_blank(),axis.title = element_text(size = 14),
        axis.text = element_text(size = 12),
        plot.title=element_text( hjust=.01, vjust=-1))

plot.ai <- partial(RF1, pred.var = c("ai_yr"), chull = TRUE, rug = TRUE, plot
= TRUE,plot.engine = "ggplot2") +
  xlab(expression ("Aridity index")) + # adiciona descrição do eixo x
  ylab(expression (delta^{15}N~"(\u2030)")) +
  ggtitle("D")+
  theme_bw()+
  theme(panel.grid = element_blank(),axis.title = element_text(size = 14),
        axis.text = element_text(size = 12),
        plot.title=element_text( hjust=.01, vjust=-1))

plot.pre <- partial(RF1, pred.var = c("pre_wc"), chull = TRUE, rug = TRUE,
plot = TRUE,plot.engine = "ggplot2") +
  xlab(expression ("Mean annual precipitation")) + # adiciona descrição do
eixo x
  ylab(expression (delta^{15}N~"(\u2030)")) +
  ggtitle("C")+
  theme_bw()+
  theme(panel.grid = element_blank(),axis.title = element_text(size = 14),
        axis.text = element_text(size = 12),
        plot.title=element_text( hjust=.01, vjust=-1))

plot.npp <- partial(RF1, pred.var = c("npp"), chull = TRUE, rug = TRUE, plot
= TRUE,plot.engine = "ggplot2") +
  xlab(expression ("Net primary production")) + # adiciona descrição do eixo x
  ylab(expression (delta^{15}N~"(\u2030)")) +
  ggtitle("F")+
  theme_bw()+
  theme(panel.grid = element_blank(),axis.title = element_text(size = 14),
        axis.text = element_text(size = 12),
        plot.title=element_text( hjust=.01, vjust=-1))

png("parplot.png", width = 6, height = 7, units = 'in', res = 300)
grid.arrange(plot.biome,plot.orc, plot.pre, plot.ai, plot.bulk, plot.npp)
dev.off()

##### Validando o modelo com training data#####

pred<-as.data.frame(predict(RF,training))
comp.obspre.rf<-data.frame(pred$ predict(RF, training),,training$d15n.obs)

lm1<-
lm(comp.obspre.rf$pred..predict.RF..training..~comp.obspre.rf$training.d15n.o
bs)
summary (lm1)
RMSE<-sqrt(mean(lm1$residual^2))
png("comp_RF.png", width = 3.5, height = 3, units = 'in', res = 300)
plot.training<-ggplot(comp.obspre.rf, aes(x = pred..predict.RF..training.., y
= training.d15n.obs)) + geom_point(alpha = 1/2) +
  geom_abline(intercept = 0, slope = 1, colour = "grey") +
  stat_smooth(method = lm, colour = "black", se = 1) +

```

```

scale_x_continuous(limits=c(-5, 17.5)) +
scale_y_continuous(limits=c(-5, 17.5)) +
xlab(expression (Predicted~delta^{15}N["soil"]~"\u2030")) + # adiciona
descrição do eixo x
ylab(expression (Observed~delta^{15}N["soil"]~"\u2030")) +
ggtitle("A")+
theme_classic()# adiciona tema "Black and White"
theme(panel.grid = element_blank(),axis.title = element_text(size = 14),
axis.text = element_text(size = 12),
plot.title=element_text( hjust=.01, vjust=-7))
dev.off()

##### validando o modelo com 10-fold cross-validation data

comp.10fold<-data.frame(RF$pred$pred,RF$pred$obs)
is.num <- sapply(comp.10fold, is.numeric)
comp.10fold[is.num] <- lapply(comp.10fold[is.num], round, 2)

##### Stack rasters for prediction #####
southamerica_stack<-stack(alt,bulk_5,cec_5,clay_5,
                           orc_5, phh2o_5,phkc1_5,silt_5,sand_5,
                           ai_yr,pet_yr,npp,tmp_wc,pre_wc,
                           eco_tnc,biome)

names(southamerica_stack)<-c("alt","bulk_5","cec_5","clay_5",
                           "orc_5", "phh2o_5","phkc1_5","silt_5","sand_5",
                           "ai_yr", "pet_yr", "npp", "tmp_wc", "pre_wc",
                           "eco_tnc", "biome")

#####CRIANDO GRID PARA APLICAR O MODELO - PREDIÇÃO
sa.grid<-alt/alt

####APLICANDO O MODELO ESPACIALMENTE
final.rf1 <- predict(southamerica_stack, RF1, ext=sa.grid, na.rm=TRUE,
overwrite=TRUE, progress='text')

plot(final.rf1)
writeRaster(final.rf1, filename="RF_final.tif", format="GTiff",
overwrite=TRUE)

##### PREDIÇÃO ESPACIAL DOS DADOS TOTAIS #####
d15n.final.model <- d15n_proj_set[,3:20]
d15n.final.model <- d15n.final.model[,-11]
colnames(d15n.final.model)<-c("d15n.obs", "alt", "bulk_5", "cec_5", "clay_5",
                           "orc_5", "phh2o_5", "phkc1_5", "silt_5", "sand_5",
                           "ai_yr", "pet_yr", "npp", "tmp_wc", "pre_wc",
                           "eco_tnc", "biome")

RF_final <- train(d15n.obs ~ ., data = d15n.final.model, method = "rf",
tuneGrid=tunegrid,trControl= fitControl, importance = TRUE)
varImp(RF_final)
final.rf.final <- predict(southamerica_stack, RF_final, ext=sa.grid,
na.rm=TRUE, overwrite=TRUE, progress='text')
final.rf.final3 <- predict(southamerica_stack, RF1, ext=sa.grid, na.rm=TRUE,
overwrite=TRUE, progress='text')

plot( final.rf.final)
writeRaster(final.rf.final3, filename="RF_final4.tif", format="GTiff",
overwrite=TRUE)

##### testing model with total dataset

d15n_xy<-extract(final.rf, d15n_clean, method='bilinear',
buffer=NULL,na.rm=TRUE)
comp<-data.frame(d15n_proj_set$d15n.obs, d15n_xy)
colnames(comp)<-c("observed", "predicted")
ggplot(comp, aes(x = predicted, y = observed)) + geom_point(alpha = 1/2) +
geom_abline(intercept = 0, slope = 1, colour = "grey") +
stat_smooth(method = lm, colour = "black", se = F) +
scale_x_continuous(limits=c(-5, 17.5)) +
scale_y_continuous(limits=c(-5, 17.5)) +
xlab(expression (Predicted~delta^{15}N["soil"]~"\u2030")) + # adiciona
descrição do eixo x
ylab(expression (Observed~delta^{15}N["soil"]~"\u2030")) + # adiciona
descrição do eixo y
theme_classic() # adiciona tema "Black and White"

```

```

1m4<-1m(comp$observed~comp$predicted)
summary(1m4)

residuals_final<-as.data.frame(1m4$residuals)
resid_final<-data.frame(d15n_proj_set[,1:2], residuals_final)
resid_final<-SpatialPointsDataFrame(resid_final[,c("x","y")], resid_final)####
for log transformed data
proj4string(resid_final) <- CRS("+proj=longlat +ellps=WGS84")
plot(resid_final)
writeOGR(resid_final, "resid_final", "resid_final", driver="ESRI Shapefile")

#####
##### GERANDO 20 PREDIÇÕES PARA CHEGAR NO MAPA DE COEFICIENTE DE
##### VARIAÇÃO, que indica as áreas com maior oscilação entre as previsões

RF_1 <- train(d15n.obs ~ ., data = d15n.final.model, method = "rf",
tuneGrid=tunegrid,trControl= fitControl, importance = TRUE)
RF_pred1 <- predict(southamerica_stack, RF_1, ext=sa.grid, na.rm=TRUE,
overwrite=TRUE, progress='text')
writeRaster(RF_pred1, filename="RF_pred1.tif", format="GTiff", overwrite=TRUE)

RF_2 <- train(d15n.obs ~ ., data = d15n.final.model, method = "rf",
tuneGrid=tunegrid,trControl= fitControl, importance = TRUE)
RF_pred2 <- predict(southamerica_stack, RF_2, ext=sa.grid, na.rm=TRUE,
overwrite=TRUE, progress='text')
writeRaster(RF_pred2, filename="RF_pred2.tif", format="GTiff", overwrite=TRUE)

RF_3 <- train(d15n.obs ~ ., data = d15n.final.model, method = "rf",
tuneGrid=tunegrid,trControl= fitControl, importance = TRUE)
RF_pred3 <- predict(southamerica_stack, RF_3, ext=sa.grid, na.rm=TRUE,
overwrite=TRUE, progress='text')
writeRaster(RF_pred3, filename="RF_pred3.tif", format="GTiff", overwrite=TRUE)

RF_4 <- train(d15n.obs ~ ., data = d15n.final.model, method = "rf",
tuneGrid=tunegrid,trControl= fitControl, importance = TRUE)
RF_pred4 <- predict(southamerica_stack, RF_4, ext=sa.grid, na.rm=TRUE,
overwrite=TRUE, progress='text')
writeRaster(RF_pred4, filename="RF_pred4.tif", format="GTiff", overwrite=TRUE)

RF_6 <- train(d15n.obs ~ ., data = d15n.final.model, method = "rf",
tuneGrid=tunegrid,trControl= fitControl, importance = TRUE)
RF_pred6 <- predict(southamerica_stack, RF_6, ext=sa.grid, na.rm=TRUE,
overwrite=TRUE, progress='text')
writeRaster(RF_pred6, filename="RF_pred6.tif", format="GTiff", overwrite=TRUE)

RF_7 <- train(d15n.obs ~ ., data = d15n.final.model, method = "rf",
tuneGrid=tunegrid,trControl= fitControl, importance = TRUE)
RF_pred7 <- predict(southamerica_stack, RF_7, ext=sa.grid, na.rm=TRUE,
overwrite=TRUE, progress='text')
writeRaster(RF_pred7, filename="RF_pred7.tif", format="GTiff", overwrite=TRUE)

RF_8 <- train(d15n.obs ~ ., data = d15n.final.model, method = "rf",
tuneGrid=tunegrid,trControl= fitControl, importance = TRUE)
RF_pred8 <- predict(southamerica_stack, RF_8, ext=sa.grid, na.rm=TRUE,
overwrite=TRUE, progress='text')
writeRaster(RF_pred8, filename="RF_pred8.tif", format="GTiff", overwrite=TRUE)

RF_9 <- train(d15n.obs ~ ., data = d15n.final.model, method = "rf",
tuneGrid=tunegrid,trControl= fitControl, importance = TRUE)
RF_pred9 <- predict(southamerica_stack, RF_9, ext=sa.grid, na.rm=TRUE,
overwrite=TRUE, progress='text')
writeRaster(RF_pred9, filename="RF_pred9.tif", format="GTiff", overwrite=TRUE)

RF_10 <- train(d15n.obs ~ ., data = d15n.final.model, method = "rf",
tuneGrid=tunegrid,trControl= fitControl, importance = TRUE)
RF_pred10 <- predict(southamerica_stack, RF_10, ext=sa.grid, na.rm=TRUE,
overwrite=TRUE, progress='text')
writeRaster(RF_pred10, filename="RF_pred10.tif", format="GTiff",
overwrite=TRUE)

RF_11 <- train(d15n.obs ~ ., data = d15n.final.model, method = "rf",
tuneGrid=tunegrid,trControl= fitControl, importance = TRUE)
RF_pred11 <- predict(southamerica_stack, RF_11, ext=sa.grid, na.rm=TRUE,
overwrite=TRUE, progress='text')

```

```

writeRaster(RF_pred11, filename="RF_pred11.tif", format="GTiff",
overwrite=TRUE)

RF_12 <- train(d15n.obs ~ ., data = d15n.final.model, method = "rf",
tuneGrid=tunegrid,trControl= fitControl, importance = TRUE)
RF_pred12 <- predict(southamerica_stack, RF_12, ext=sa.grid, na.rm=TRUE,
overwrite=TRUE, progress='text')
writeRaster(RF_pred12, filename="RF_pred12.tif", format="GTiff",
overwrite=TRUE)

RF_13 <- train(d15n.obs ~ ., data = d15n.final.model, method = "rf",
tuneGrid=tunegrid,trControl= fitControl, importance = TRUE)
RF_pred13 <- predict(southamerica_stack, RF_13, ext=sa.grid, na.rm=TRUE,
overwrite=TRUE, progress='text')
writeRaster(RF_pred13, filename="RF_pred13.tif", format="GTiff",
overwrite=TRUE)

RF_14 <- train(d15n.obs ~ ., data = d15n.final.model, method = "rf",
tuneGrid=tunegrid,trControl= fitControl, importance = TRUE)
RF_pred14 <- predict(southamerica_stack, RF_14, ext=sa.grid, na.rm=TRUE,
overwrite=TRUE, progress='text')
writeRaster(RF_pred14, filename="RF_pred14.tif", format="GTiff",
overwrite=TRUE)

RF_15 <- train(d15n.obs ~ ., data = d15n.final.model, method = "rf",
tuneGrid=tunegrid,trControl= fitControl, importance = TRUE)
RF_pred15 <- predict(southamerica_stack, RF_15, ext=sa.grid, na.rm=TRUE,
overwrite=TRUE, progress='text')
writeRaster(RF_pred15, filename="RF_pred15.tif", format="GTiff",
overwrite=TRUE)

RF_16 <- train(d15n.obs ~ ., data = d15n.final.model, method = "rf",
tuneGrid=tunegrid,trControl= fitControl, importance = TRUE)
RF_pred16 <- predict(southamerica_stack, RF_16, ext=sa.grid, na.rm=TRUE,
overwrite=TRUE, progress='text')
writeRaster(RF_pred16, filename="RF_pred16.tif", format="GTiff",
overwrite=TRUE)

RF_17 <- train(d15n.obs ~ ., data = d15n.final.model, method = "rf",
tuneGrid=tunegrid,trControl= fitControl, importance = TRUE)
RF_pred17 <- predict(southamerica_stack, RF_17, ext=sa.grid, na.rm=TRUE,
overwrite=TRUE, progress='text')
writeRaster(RF_pred17, filename="RF_pred17.tif", format="GTiff",
overwrite=TRUE)

RF_18 <- train(d15n.obs ~ ., data = d15n.final.model, method = "rf",
tuneGrid=tunegrid,trControl= fitControl, importance = TRUE)
RF_pred18 <- predict(southamerica_stack, RF_18, ext=sa.grid, na.rm=TRUE,
overwrite=TRUE, progress='text')
writeRaster(RF_pred18, filename="RF_pred18.tif", format="GTiff",
overwrite=TRUE)

RF_19 <- train(d15n.obs ~ ., data = d15n.final.model, method = "rf",
tuneGrid=tunegrid,trControl= fitControl, importance = TRUE)
RF_pred19 <- predict(southamerica_stack, RF_19, ext=sa.grid, na.rm=TRUE,
overwrite=TRUE, progress='text')
writeRaster(RF_pred19, filename="RF_pred19.tif", format="GTiff",
overwrite=TRUE)

RF_20 <- train(d15n.obs ~ ., data = d15n.final.model, method = "rf",
tuneGrid=tunegrid,trControl= fitControl, importance = TRUE)
RF_pred20 <- predict(southamerica_stack, RF_20, ext=sa.grid, na.rm=TRUE,
overwrite=TRUE, progress='text')
writeRaster(RF_pred20, filename="RF_pred20.tif", format="GTiff",
overwrite=TRUE)

##### ABRIR OS MODELOS PREDITOS E CALCULAR CV #####
RFpred1 <-raster("D:\\endereço dos modelos salvos\\RF_pred1.tif")
RFpred2 <-raster("D:\\endereço dos modelos salvos\\RF_pred2.tif")
RFpred3 <-raster("D:\\endereço dos modelos salvos\\RF_pred3.tif")
RFpred4 <-raster("D:\\endereço dos modelos salvos\\RF_pred4.tif")
RFpred5 <-raster("D:\\endereço dos modelos salvos\\RF_pred5.tif")
RFpred6 <-raster("D:\\endereço dos modelos salvos\\RF_pred6.tif")
RFpred7 <-raster("D:\\endereço dos modelos salvos\\RF_pred7.tif")

```

```

RFpred8 <-raster("D:\\endereço dos modelos salvos\\RF_pred8.tif")
RFpred9 <-raster("D:\\endereço dos modelos salvos\\RF_pred9.tif")
RFpred10 <-raster("D:\\endereço dos modelos salvos\\RF_pred10.tif")
RFpred11 <-raster("D:\\endereço dos modelos salvos\\RF_pred11.tif")
RFpred12 <-raster("D:\\endereço dos modelos salvos\\RF_pred12.tif")
RFpred13 <-raster("D:\\endereço dos modelos salvos\\RF_pred13.tif")
RFpred14 <-raster("D:\\endereço dos modelos salvos\\RF_pred14.tif")
RFpred15 <-raster("D:\\endereço dos modelos salvos\\RF_pred15.tif")
RFpred16 <-raster("D:\\endereço dos modelos salvos\\RF_pred16.tif")
RFpred17 <-raster("D:\\endereço dos modelos salvos\\RF_pred17.tif")
RFpred18 <-raster("D:\\endereço dos modelos salvos\\RF_pred18.tif")
RFpred19 <-raster("D:\\endereço dos modelos salvos\\RF_pred19.tif")
RFpred20 <-raster("D:\\endereço dos modelos salvos\\RF_pred20.tif")

RFpred.stack <- stack(RFpred1,RFpred2,RFpred3,RFpred4,RFpred5,
                      RFpred6,RFpred7,RFpred8,RFpred9,RFpred10,
                      RFpred11, RFpred12,RFpred13,RFpred14,RFpred15,
                      RFpred16,RFpred17,RFpred18,RFpred19,RFpred20)

RFpred.stack <- round(RFpred.stack, digits = 2)

rfpred_se <- calc(RFpred.stack, se)
?calc

rfpred_mean <- calc(RFpred.stack, mean)
rfpred_mean <- round(rfpred_mean, digits = 2)

rfpred_sd <- calc(RFpred.stack, sd)
rfpred_sd <- round(rfpred_sd, digits = 2)

rfpred_cv<-(rfpred_sd/abs(rfpred_mean))*100
plot(rfpred_cv)

qt_rfpred<-quantile(RFpred.stack, probs = c(0.25, 0.75), type=7,names = FALSE)

##### Salvando o modelo final calculado pela média dos 20 modelos randômicos -
salvando desvio padrão

writeRaster(rfpred_mean, filename="rfpred_mean.tif", format="GTiff",
overwrite=TRUE)
writeRaster(rfpred_sd, filename="rfpred_sd.tif", format="GTiff",
overwrite=TRUE)

##### Abrindo modelo final para calcular resíduos entre preditos e observados e
coeficiente de variação

RFFinal <-raster("D:\\endereço dos modelos salvos\\rfpred_mean.tif")
d15nxy<-extract(RFFinal, d15n_spatial, method='bilinear',
buffer=NULL,na.rm=TRUE)

d15n_resid<-data.frame(d15n.agg,d15nxy)
d15n_resid<-na.exclude(d15n_resid)
lm_comp<-lm(d15n_resid$d15n.obs~d15n_resid$d15nxy)
summary(lm_comp)
resid<-lm_comp$residuals
d15n_resid<-data.frame(d15n_resid,resid)

d15n_resid<-SpatialPointsDataFrame(d15n_resid[,c("x","y")], d15n_resid)
proj4string(d15n_resid) <- CRS("+proj=longlat +ellps=WGS84")
writeOGR(d15n_resid, ".", "d15n_resid_final", driver="ESRI Shapefile")

```